Design and Construction of Carbon NanoTubes (CNTs) Triggered Pseudospark Switch

by

Haitao Zhao

A dissertation submitted to the Graduate Faculty of
Auburn University
in partial fulfillment of the
requirements for the Degree of
Doctor of Philosophy

Auburn, Alabama
August 4, 2012

Keywords: Pseudospark switch, carbon nanotubes, hollow cathode effect, field emission, pulsed power

Approved by

Hulya Kirkici, Chair, Professor of Electrical and Computer Engineering
Bogdan Wilamowski, Professor of Electrical and Computer Engineering
Stuart Wentworth, Associate Professor of Electrical and Computer Engineering

Abstract

Pseudospark switches have been used as fast closing switches in pulsed power systems. Advantages include high hold off voltage of 10s kV, high conduction current of ~10^4 A, fast current rise time of 10^{11} A/s, low delay and jitter time approaching ns, and long lifetime. In general, pseudospark switches have hollow anode and hollow cathode geometry and can be triggered by several methods that increase the charge carrier density in the hollow cathode region. The efficiency of these charge carrier accumulation determines the performance of switch operation.

In the electron injection triggering where electrons emitted from cold cathode emitter, are accelerated in the electric field and initiate the switch closing. Therefore, cold cathode material is critical to this trigger method. Carbon nanotubes (CNTs) are known for their excellent field emission characteristics. This property makes them a good candidate for the cold cathode material in this application.

In this research work, pseudospark switch triggered by carbon nanotubes coated electrode is designed and constructed. The trigger electrode is fabricated by coating CNTs, either randomly aligned CNTs, vertically aligned CNTs or trench wall patterned CNTS on silicon in chemical vapor deposition method (CVD). The CNTs are synthesized under different growth conditions with varying sputtering time, oxidation time, and growth time. The patterned CNTs are fabricated using monolithic IC fabrication processes. The trigger electrode is then assembled and tested in a pseudospark switch

constructed in-house with a quartz vacuum tube, a hollow cathode and a planar anode. The switch test experiments are carried out in different background pressures, different trigger voltages, and trigger electrodes with different types of CNTs. Delay and jitter time of the pseudospark switch under different working conditions are studied. Hold off voltage, conduction current and current rise time are presented, and optimizations of the switch operating characteristics are discussed.

Acknowledgments

The author would like to express his special thanks to his advisor Dr. Hulya Kirkici for her commitment to this project, technical advice, and support through the duration of this study. It would have been impossible to complete this work without her support. He also appreciates her support not only in academic work but also in his life. She is more than an advisor and like a mother in life.

The author wishes to thank Dr. Bogdan Wilamowski, Dr. Stuart Wentworth for serving on his committee and Dr. Park for being the outside reader. Special thanks are extended to technical staff Linda Barresi and Calvin Cutshaw for the material support throughout the experiment.

The author wishes to thank Dr. Yu-chun (Brad) Chen for valuable training and help in his research and to thank the fellow lab mates Shaomao Li, Mark Lipham, Ramesh Bokka, Fang Li, Zhenhong Li, Huirong Li, Rogger Tsai, Ming Zhang, and Rujun Bai, and to thank Department of Electrical and Computer Engineering for providing support and a friendly environment.

Special acknowledgement and heartfelt gratitude must be given to author's parents, wife, and son for their love, support, and encourage.

[ξ] Work supported by a grant from AFOSR with a contract # AF-FA9550-08-10051

Style manual or journal used Graduate School: Guide to preparation and submission of thesis and dissertations

Computer software used Microsoft Office 2007

Table of Contents

List of Tables

List of Figures

Chapter 1

Introduction

In the modern pulsed power field, the power switch technology is challenged by new applications, such as electron/ion beam generators which require a high current density of 10^4 A/cm^2, pulsed modulators which generate a peak current up to 19 kA, and excimer-lasers which reach a maximum voltage of 32 kV [1]. The capability of high power up to 10^{12} W and low jitter time of 10^{-9} s is identified as a significant parameter in a switch design and fabrication for pulsed power applications. The conventional switches, for example high-voltage switch gears, are no longer sufficient to meet these stringent requirements. Other switch theories, such as the gaseous spark discharge and hollow cathode effect, as well as the hardware innovation are some of the attracting research topics.

The pseudospark switch, also known as cold-cathode thyratron, is one of the most studied devices to control high voltage and high current pulse discharges. It is characterized by a very rapid breakdown phase with high hold off voltages of several tens of kV and peak currents of 10s kA with pulse repetition of up to several kHz. These are attributed to the “hollow cathode effect” that allow glow discharge to operate at relatively lower voltage and higher current than traditional glow discharges. The discharge can be

operated at 100% current reversal without turning into a constricted arc [2]. In a complete pseudospark switch, the trigger mechanism that supplies the seed electrons for a breakdown is critical because it greatly affects the switch performance. Several trigger mechanisms have been reported in the literature [3, 4]. The first one is the surface discharge triggering that employs a dielectric material as part of the trigger. But the lifetime of the trigger section is rather short because of the surface erosion of the dielectric material. The second trigger method is pulsed low current glow discharge triggering. The disadvantage is that a fairly high pulsed voltage is needed to generate the glow for trigger. The third method is optical triggering, where stringent requirements on the light source (laser beam or UV flashlight) to generate photoelectrons for trigger, makes them remain in advanced research stage. Another problem of optical triggering is the difficulty in large scale development where another setup for the laser or UV-flash light system is needed. The last method is electron beam injection, or field emission triggering. One of the disadvantages of this method is that a third triggering electrode is needed, which greatly increased the hardware complexity. And also the performance of the switch is highly dependent on the emitter materials. Traditionally, a metal electrode is used for this but high turn-on electric field of these materials, to some extent, has limited the development of the pseudospark switch for compact pulsed power applications. Therefore, it is important to study and achieve innovations on both switch body design and emitter materials.

The primary objective of this work is to design and construct a pseudospark switch that is easy-to-construct, compact, and has the potential of use with high hold off voltage and low delay time with nanosecond jitter. Instead of a traditional metal electrode,

CNT coated cold electron emitters are considered. The switch is triggered by electron injection mechanism in which the CNTs coated silicon electrode is used as the trigger electrode. The performance of the switch is tested under different operating conditions and the switch optimization parameters are reported.

Chapter 2

Background

2.1 Pulsed Power Engineering

Pulsed power engineering is the science and technology of storing energy over a relatively long period of time (usually seconds or minutes) and releasing it to a load as electrical energy over a much shorter time (usually microseconds or nanoseconds). Normally, a pulsed power system consists of an energy storage stage, a pulse forming stage, and a load as shown in Figure 2.1. Energy can be stored in several forms: chemically, mechanically or electrically. By using appropriate switches, closing switch or opening switch, the high energy is transferred from energy storage stage to the load through pulse forming stage. Depending on the energy storage and load requirements, switches can be closing switch (capacitive) or opening switch (inductive). Highest energy and power that can be achieved in a single pulse are in the order of 100 MJ and 10 TW respectively [5]. The corresponding voltage is from 10^4 – 10^7 V, and the current is in the range of 10^3 to 10^7 A. Figure 2.1 shows a sketch of a typical pulse forming network representing a complete pulse power system, and Figure 2.2 shows a typical pulse shape across a load.

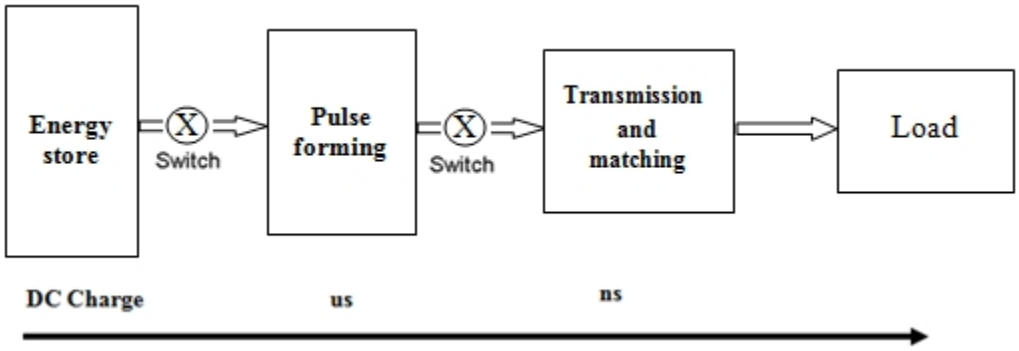

Figure 2.1 General scheme of a pulsed power system

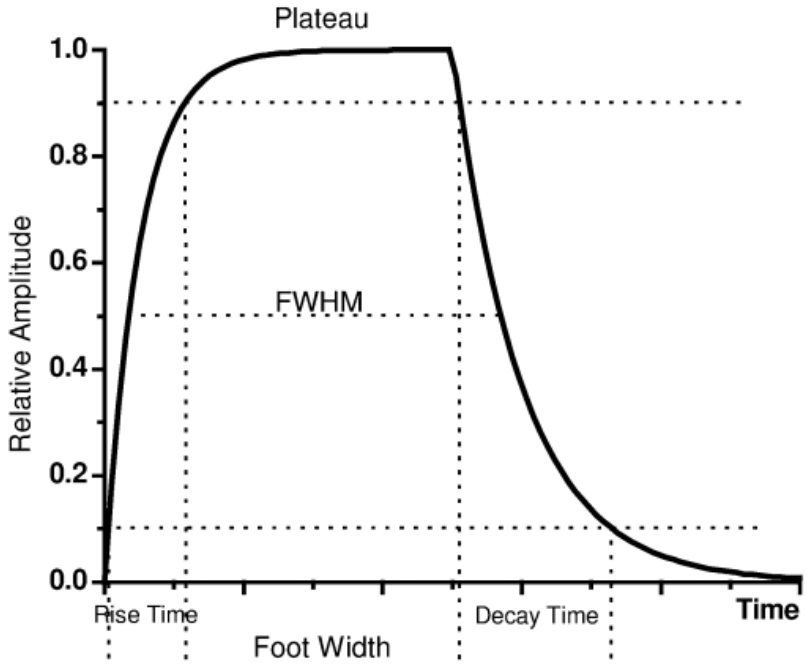

Figure 2.2 A typical pulse shape [5]

The important parameters of a pulsed power switch that delivers a pulse are listed and defined as follow:

Hold off Voltage: The maximum static voltage that can be applied to the switch before breakdown is triggered.

Rise Time: The time it takes for the voltage to rise from 10% to 90% of its peak voltage

Voltage Fall Time: After breakdown is initiated, the time interval during which the voltage drops from the value of hold off to that of the conduction voltage.

Pulse During: The full width between rise and decay times at half maximum of the pulse amplitude (FWHM).

Recover Time: The time interval during which the voltage reverses its polarity.

Repetition Rate: The rate at which the switch can be closed and opened without degradation of performance.

Conduction Drop: The voltage drop across the switch impedance during the conduction.

Peak Power: The maximum value of the product of voltage and current pulses which occur at the same time across the load.

Transfer Energy: The time integral of the product of voltage and current pulses.

Life Time: Under normal operating conditions, the total number of switching operations beyond which the switch can no longer function properly.

Reliability: A measure of the ratio between the numbers of success of operations to the total number of operations within the life time of the switch.

Delay time: The time interval between the trigger voltage and the switch breakdown.

Jitter time: The statistic standard deviation of delay times over successive closing/opening.

Requirements for the pulse length, average and peak energies, and the repetition rate are highly application specific. However, compactness, and portability are common driving forces in today's pulsed power systems [6]. Delay time and jitter are the most important parameters in terms of how efficiently the energy is transferred to the load.

2.2 Pseudospark Switches

Switches are important part of pulsed power system and stringent requirements imposed on them depending on applications. Based on the pressure, switches are classified into high pressure switch, such as spark gap, partial vacuum switch, such as thyratron and ignitron, and vacuum switch, such as vacuum spark gap, as shown in Figure 2.3.

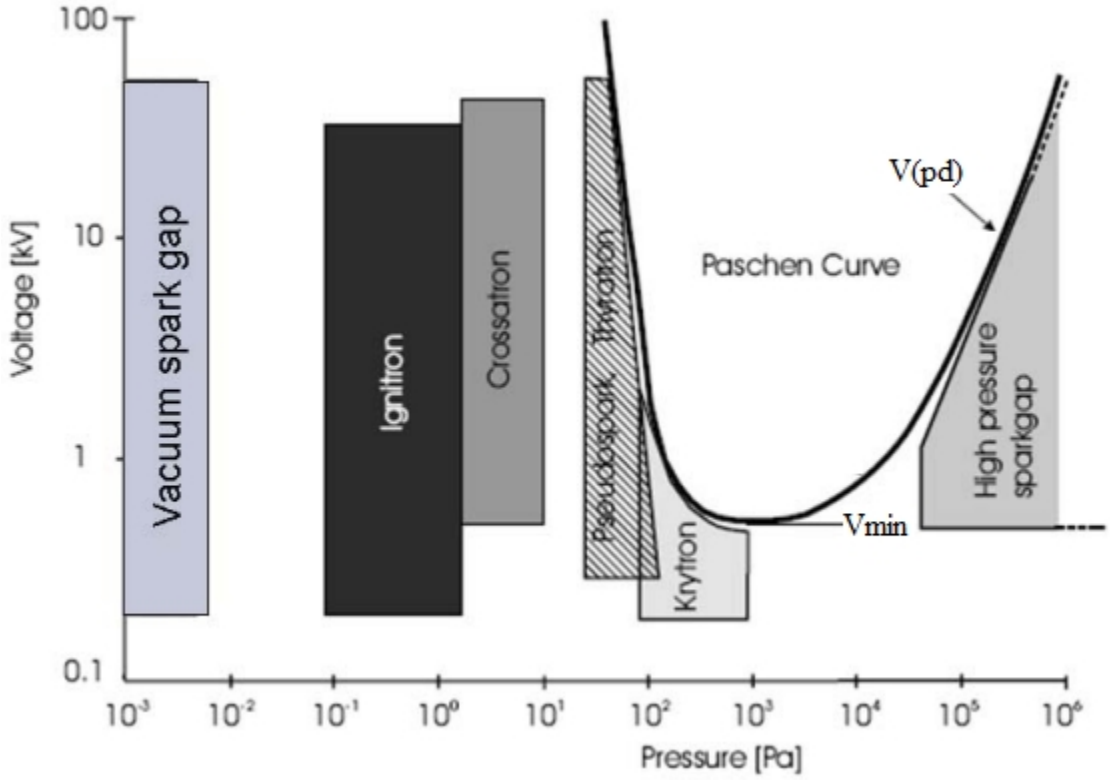

Figure 2.3 Typical operation regions of gaseous switch in relation to Paschen curve of breakdown [5]

Pseudospark switches, also known as cold cathode thyratron, are one type of partial vacuum switches with significant application prospect. It was first developed by Christiansen and Schultheib in 1978 as low-pressure, high-voltage plasma devices [7]. Great progress has been made in this area since then, including novel fabrication

techniques and advanced applications. Nowadays, pseudospark switch has been proven to be one of the most efficient closing switches in pulsed power system. It is capable of high power, high repetition rate and fast recovery time. The pseudospark switch has a special hollow cathode and hollow anode geometry. Typical operation pressure is around 1 to 10^3 mTorr. The geometry of pseudospark switch is very simple and suffers less electrode wear compared to other high pressure switches such as sparkgaps. Figure 2.4 is a basic schematic of the pseudospark switch.

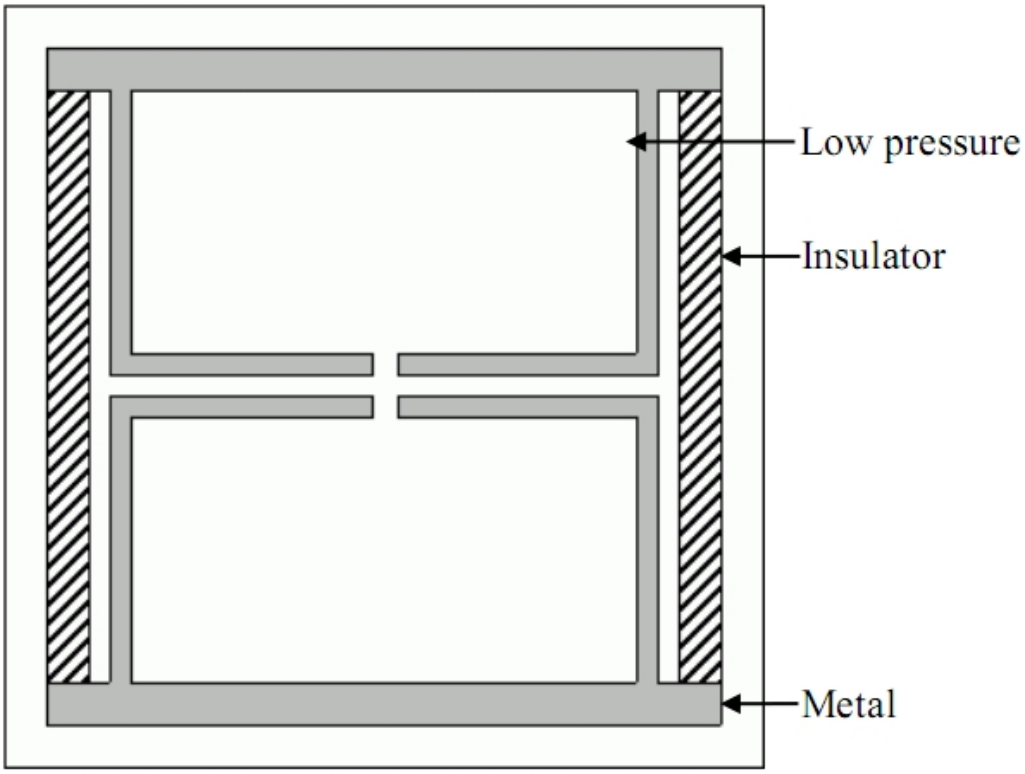

Figure 2.4 Schematic of pseudospark switch [1]

There are four phases in the pseudospark discharge: predischarge, hollow cathode discharge, super glow discharge, and decay of the discharge plasma [2]. The features for each phase are listed below and the first three phases are shown in Figure 2.5.

Predischarge (ignition of the pseudospark):

- Electrons are released from walls of cathode hole
- High avalanche occurs in cathode backspace (high α/p)
- Dense plasma forms in cathode hole and backspace

Hollow cathode discharge phase:

- Electrons from cathode backspace are extracted into electrode gap by virtual anode, and accelerated with almost no collisions
- Plasma goes into and shortens the electrode gap (2×10^6 m/s), then breakdown occurs.

Superdense glow discharge phase:

- Electron emission from backspace is limited
- Ions are accelerated by cathode fall (10^6 V/cm), collide with gas particle, bombard cathode surface, and induce field-enhanced thermionic electron emission (3000-4000 K in 30-100 ns)

Decay of the discharge plasma phase:

- Determined by external circuit
- No quenching phenomenon during current carrying phase
- Regain hold-off capability during current zero

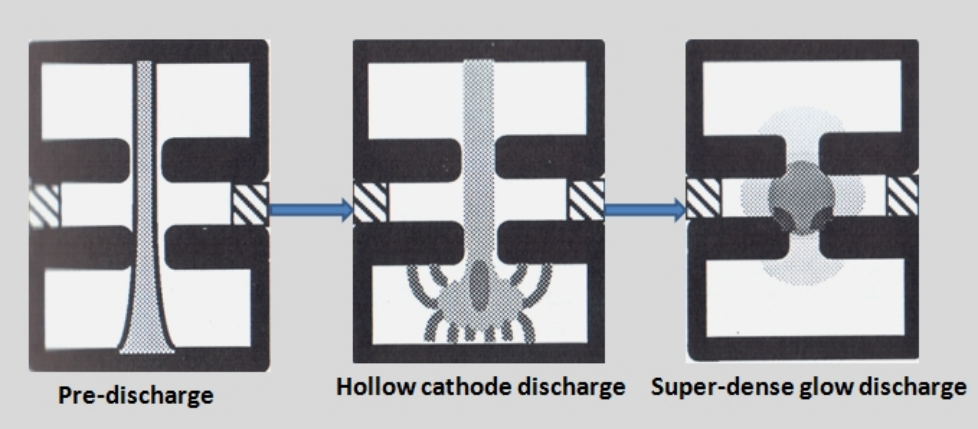

Figure 2.5 Phases of pseudospark discharge [2]

2.2.1 Gaseous breakdown and glow discharges

The glow discharge is a luminous low pressure discharge with applied voltage at 100 V to several kV through a gas. The simplest type of glow discharge is a direct-current glow discharge which consists of two electrodes in a cell held at low pressure about 0.1-10 Torr. If the applied voltage is increased to breakdown voltage, the gas will be ionized and a breakdown of the gas is observed, reaching the glow discharge regime. The glow discharge is a diffuse, steady discharge but if the applied voltage continues to increase, abnormal glow discharge begins. As the voltage is further increased to the point that the cathode glow covers the entire cathode, the current increases sharply and arc discharge begins.

The breakdown voltage of glow discharge is determined by the Paschen Law. It is a well-known plasma-physics law stating that the amount of potential difference required for a gas to breakdown is a function of pressure and gap distance. In the pseudospark discharge, it starts in the hollow cathode behind the borehole and expands to electrode gap.

2.2.2. Hollow cathode discharges

If a single plane cathode in glow discharge is replaced by a cathode with hollow structure, the current will be orders of magnitude larger at the same discharge voltage. The negative glow region of the discharge moves into the hollow structure resulting in higher ionization and excitation processes. This is called the hollow cathode effect and the hollow cathode structure is an important feature of the pseudospark switch [8]. The operation region of the hollow cathode discharge is 1 torr-cm < pD < 10 torr-cm, where p is pressure and D is a combination of electrode gap distance, hollow cathode diameter, and depth of the cathode cavity [9]. The *pd* in the Paschen breakdown curves determines that the switch operates at the "left side of the Paschen Curve" shown in Figure 2.3, whereas the PD determines the hollow cathode discharge development.

2.2.3 The hollow cathode effect

In a traditional high current pulsed power switch, an externally heated cathode must be used [2, 10]. The cathode needs to be preheated before the switch operation, in order to get sufficient electron emission. Thus external circuit unavoidably limits the reduction of the switch size where compact switches are needed. This led to the development of the pseudospark switches employing hollow cathode geometry. Due to the hollow cathode effect, the electron emission has been characterized as a super-emissive mode in which a quasi-uniform thermionic or field-enhanced thermionic emission dominates [11, 12]. Therefore, the sufficient electron emission is assured and the external circuit to heat the cathode can be removed.

The hollow cathode effect is mainly caused by pendulum electrons [13]. These special electrons emitted from the cathode surface float in the cathode cavity, reflecting

back and forth between the cathode sheaths, as shown in Figure 2.6. The movements of the pendulum electrons result in increased rate of ionizing collisions. The low weight electrons move fast towards the anode and the heavier ions stay in the cathode cavity, forming a virtual anode. Therefore, the electron emission rate increases due to the virtual anode. The cathode fall, defined as the distance between the virtual anode and the cathode sheaths, can be significantly thin in hollow cathode geometries leading to a extremely high electric field. Thus, the ion velocities and secondary electron emissions increase. Moreover, the newly emitted electrons further ionize the medium gas, generating more ions. The cathode fall becomes even thinner because of the expansion of the virtual cathode. In this way, the hollow cathode structure increases the probability of multiple processes and collisions for all particles, creating high current density plasma inside the hollow cathode cavity. Figure 2.7 indicates the formation of the cathode fall.

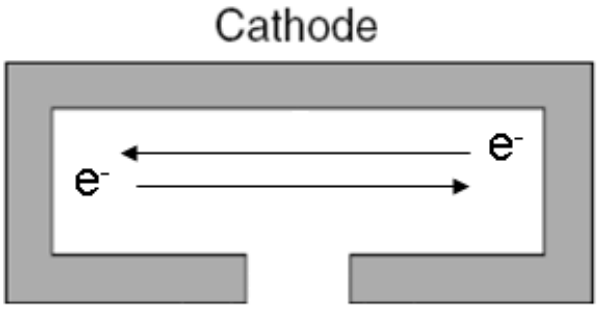

Figure 2.6 Movements of pendulum elecrons

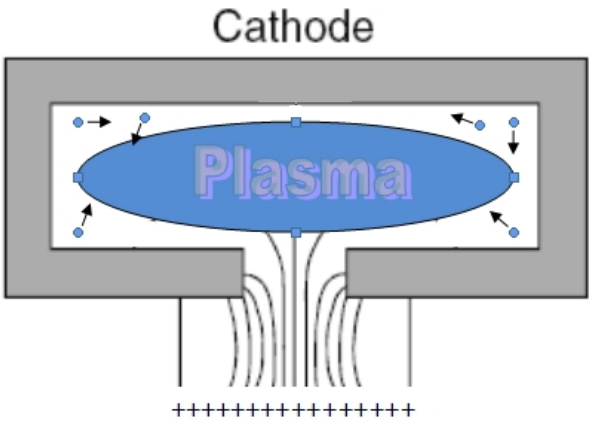

Figure 2.7 Formation of the cathode fall

2.2.4 Triggering mechanisms

Triggering system is the most important region of the pseudospark switch. At least 10^9 electrons are needed to initiate a low timing jitter breakdown [11]. Delay and jitter time are directly determined by trigger mechanisms. Four mechanisms, namely, surface discharge, low current glow discharge, optical triggering, and electron injection, are extensively studied in the literature and widely used in applications [1, 2, 10].

2.2.4.1 Surface discharge [10, 14, 15]

In the surface discharge triggering method, a trigger electrode located between two insulator discs, is inserted into the hollow cathode region of the main switch, as shown in Figure 2.8. A high voltage pulse is then applied to the trigger electrode for surface flashover discharge. This method is based on generating seed electron during the flashover across the insulator surface. Therefore, insulators are required to have low surface breakdown voltages and long lifetimes. High peak current can be provided in this method but the repeatability is low due to the limited life time of the insulator materials.

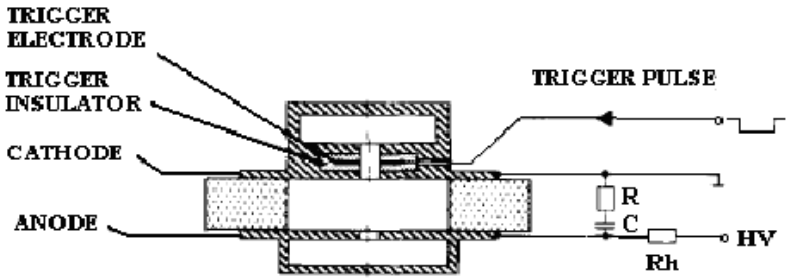

a

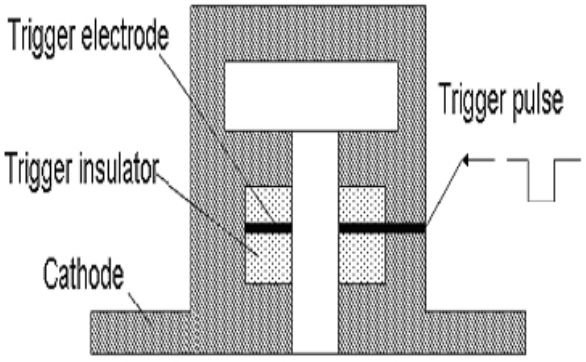

b

Figure 2.8 (a) Schematic drawing of pseudospark switch triggered by surface discharge (b) enlarge view of the trigger electrode [16]

2.2.4.2 Pulsed low-current glow discharge

In this method, the trigger module and main switch are separated by a third stage, normally a cylindrical cage forming another hollow cathode, as shown in Figure 2.9. A negative DC voltage is applied to the trigger electrode to generate a pulsed hollow cathode discharge inside the trigger module. The electrons generated here are driven to the main cathode by the help of auxiliary electrodes, and the breakdwon is initiated in the main switch by these electrons propogating through the small holes on the cage [5].

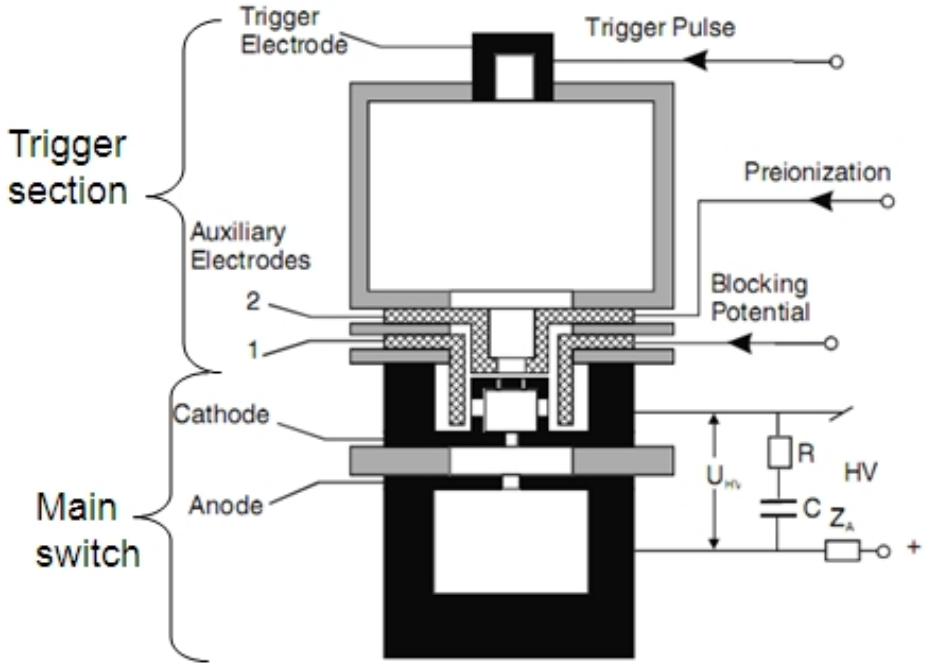

Figure 2.9 Pulsed low-current glow discharge triggered pseudospark switch [17]

2.2.4.3 Optical triggering

Pseudospark switch can also be triggered optically. A beam of light, either from a flash lamp, a radiation from a spark discharge, or a UV laser, such as XeCl at 308 nm and KrCl, impinges onto the cathode back space through a glass window and initiate the switch breakdown. This type of pseudospark switch is also called back lighted thyratron (BLT) and the structure can be super compact because the trigger region has been completely separated from the switch body. The operating characteristics of a BLT with a minimum dimension of approximately 20 mm with capability of 4 kA conduction current and 20 kV hold off voltage have been reported in [18] (see Figure 2.10 for a schematic of a BLT).

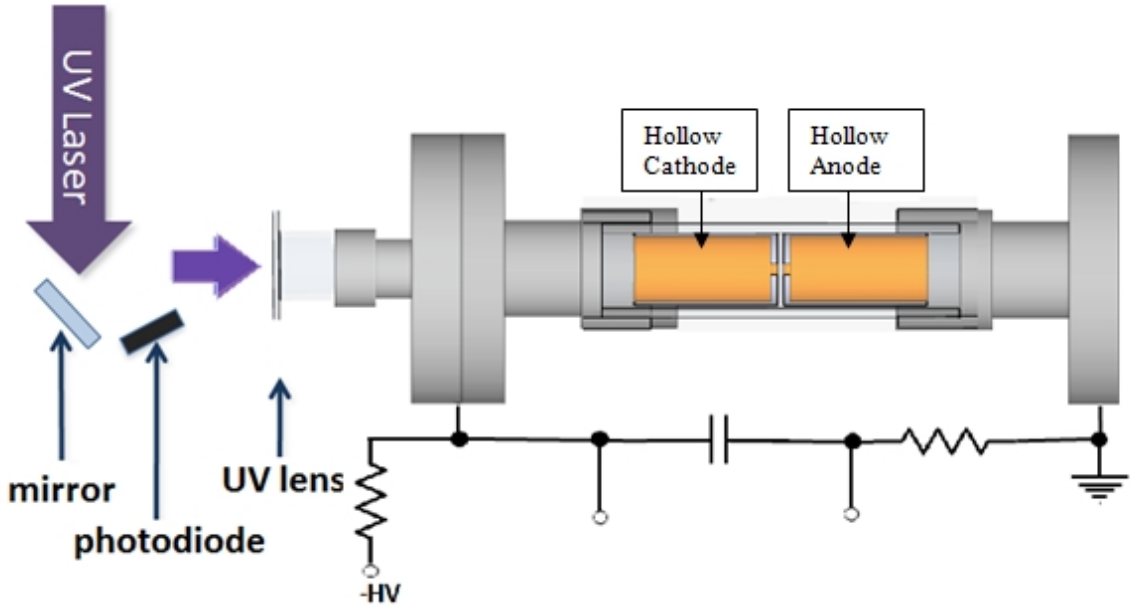

Figure 2.10 Back Lighted Thyratron [19]

2.2.4.4 Electron injection

Electron injection triggering operates very reliable with low jitter and delay time [20]. Electrons, normally from an electron beam or generated from a metal through field emission, enter the cathode cavity with relatively high energy, ionize the background gas by collisions, and initiate the switch breakdown. This method can be very efficient due to the fast velocity of electrons. But the electron source, for example the cold cathode electron emitter, is a key factor. It is necessary to use an emitter material with low turn-on field and high emission current. Electron beam system usually requires more complicated structure in peripheral circuitry.

2.3 Limitations of Pseudospark Switches

2.3.1 Life time limit

Although the life time and repetition rate of the pseudospark switch are dramatically improved, they still suffers from the electrode erosion because pseudospark

switches operate in high current mode [21]. During the superemissive phase, the face of the cathode, traditionally made from copper, is heated due to the high power density of the electron beam (10^9-10^{12} W/cm^3) which can evaporate the cathode material and cause rapid electrode degradation [22]. The erosion effect can be reduced by using other materials with higher melting point, such as molybdenum. The difficulties of the electrode machining and material cost are some of the limitations of these switches.

2.3.2 Hold off voltage limit.

The hold off voltage of pseudospark switch is the maximum voltage that the switch can withstand. As mentioned earlier, the pseudospark switches operate on the left side of Paschen curve, where "gap-distance" is much less than the mean free path as shown in Figure 2.11. Experiments have shown that the hold off voltage for a single gap pseudospark switch cannot comfortably exceed 32 kV without impairing the switch lifetime [23]. Attempts to overcome this limited hold off voltage led to the development of multiple-gap switch structures by stacking up multiple single-gap switches [23, 24]. For a reliable hold off voltage of 70 kV, at least three gaps are necessary. But two problems limit these structures. First, the switch size cannot be made as compact with multi-gap structure; Second, simultaneous triggering issue is challenging and impairing the delay time.

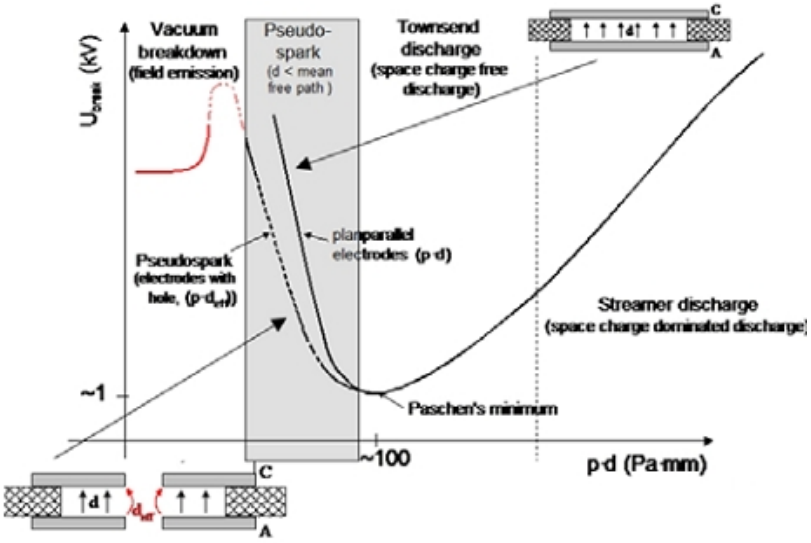

Figure 2.11 Paschen curve [25]

2.3.3 Conduction current limit

Pseudospark switches are designed for high conduction current. But, if the current exceeds 45 kA, interactions between cathode spots are enhanced, leading to buildup of high-erosive cathode spots and evaporate the cathode material rapidly. The resulting high electrode erosion therefore limits the switch applications as either a low current or a short–life device [26]. Multichannel operation is a way to solve this problem and has been widely studied [27, 28]. Multi-channels are distributed around a common hollow cathode. By this way, conduction current up to several 100 kA can be obtained. The limitations in this method are the complexity of the cathode structure and the cost of the materials.

2.3.4 Delay and jitter time limit

Delay time and jitter are determined by trigger mechanisms mentioned above. Each trigger method has its own advantages and disadvantages. For example, in the electron injection method, 10^9 to 10^{10} electrons are need for a reliable triggering. A lower

number of electrons results in high delay and jitter values or cannot initiate the discharge at all [29]. Therefore, the efficiency of trigger mechanism is another important factor that imposes limitation.

Chapter 3

Carbon Nanotubes

In order to improve the performance of the pseudospark switch, a proper cold cathode emitter material must be used to provide the seed electrons needed to initiate the hollow cathode discharge. Materials with high electric field emission rate are desired for a low delay and jitter time in a switch operation. Many materials have been studied and the results are reported in terms of turn-on field and emission current [30 - 34]. The turn-on field varies from 3 V/μm to 12 V/μm, and the emission current is around a few μA. Some high performance materials, such as carbon nanotubes (CNTs), rough polished copper, polycrystalline diamond and ZnO, have been tested and the turn-on fields are listed in Table 3.1 [35]. The results clearly show that CNTs have the lowest turn-on field. This property of carbon nanotubes makes them a good candidate for cold cathode emitter materials.

Table 3.1 Turn-on field of typical electron emitter materials

Material	**CNTs**	**Copper**	**Diamond**	**ZnO**
Turn-on field	0.9 V/μm	5 V/μm	2.2 V/μm	>10 V/μm
Saturation current density	1 mA/cm^2	0.1 mA/cm^2	0.1 mA/cm^2	1 mA/cm^2

3.1 Introduction

Carbon nanotubes are one of the pure forms of the carbon and have been of greatest interest since their discovery in 1991 by Iijima [36]. The name of the nanotube is derived from their size as the diameter of nanotube is in the order of nanometers and their lengths could be of several micrometers. CNTs are members of the fullerene structural family where the molecule is composed entirely of carbon in the forms of hollow spheres, ellipsoids, or tubes. CNTs have unique nano-structures with remarkable electrical, mechanical and chemical properties. They are one of the most diverse nano-scale materials leading to implementation of practical and commercial products in many aspects. For example, the high performance field effect transistors [37-39], single-electron transistors [40, 41], atomic force microscope tips [42], field emitters [43], and chemical/biochemical sensors [44]

3.2 Structure of CNTs

CNTs can be classified into many types: single wall carbon nanotubes (SWCNTs), multiwall carbon nanotubes (MWCNTs), randomly oriented CNTs and vertically aligned CNTs. Structures and properties vary from one type to another.

3.2.1 Single wall carbon nanotubes (SWCNTs)

A single wall carbon nanotube, nearly a one-dimension structure, is formed by rolling up a graphene sheet, which is assumed to be a single layer from a 3D graphite crystal, into a cylinder capping each end of the cylinder with half of fullerene molecule, as illustrated in Figure 3.1.

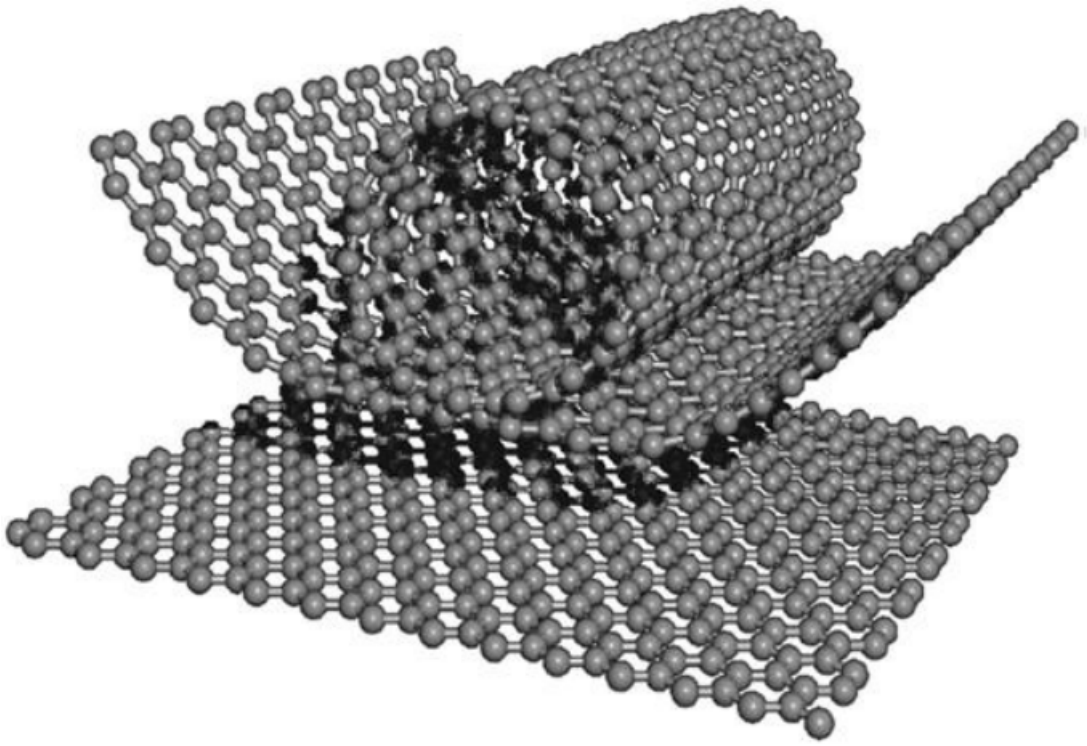

Figure 3.1 The formation of a SWCNT [45]

The structure of the SWCNTs is differentiated into two regions with different physical and chemical properties. The first one is the sidewall and the second one is the end cap of the tube. The symmetry and the electronic structures of the nanotubes change with directions, diameter and rolling of the graphene sheet. Figure 3.2 shows three different types of the SWCNTs structure.

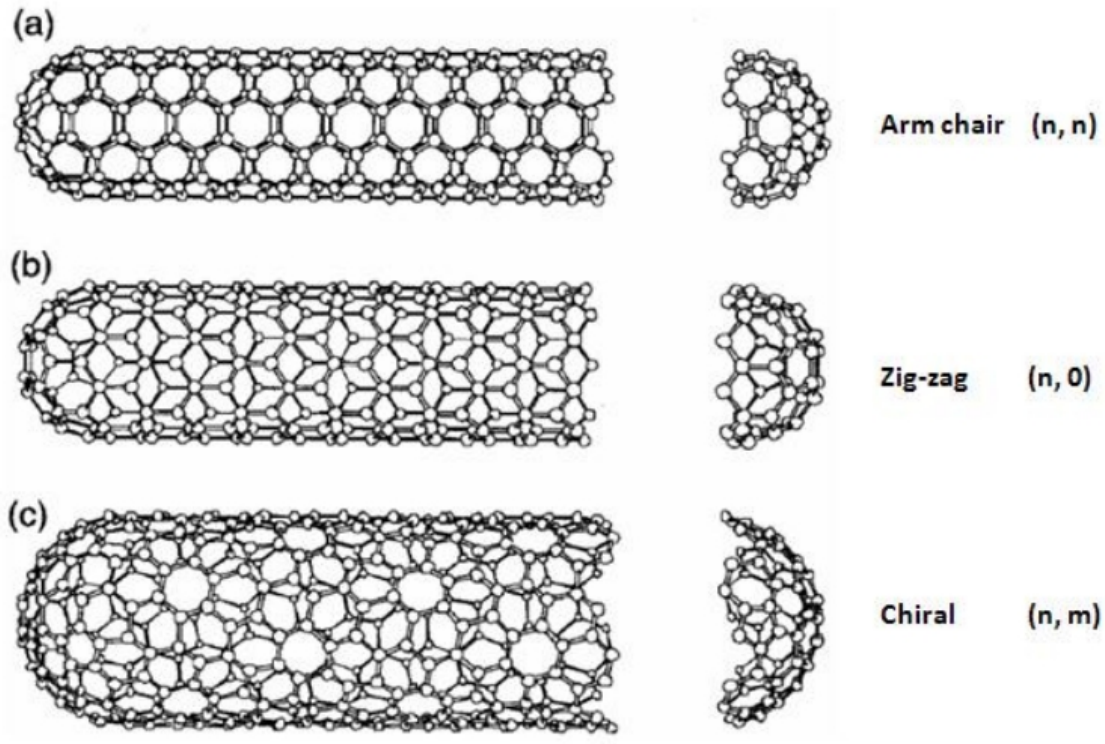

Figure 3.2 Classification of CNTs: (a) armchair (b) zigzag (c) chiral nanotubes [46]

The definition of each type can be explained from Figure 3.3. (n, m) is the chiral vector where integers n and m denote the number of unit vectors along the directions in the honeycomb crystal lattice of the grapheme [47].

3.2.2 Multi wall carbon nanotubes (MWCNTs)

Multi wall carbon nanotubes (MWCNTs) can be considered as a collection of concentric SWCNTs with different diameters, illustrated in Figure 3.3. Normally, the inner diameter is approximately 1-3 nm and the outer diameter is approximately 10 nm. Figure 3.4 shows TEM pictures of functional MWCNTs samples showing multi tube-walls with gap distance around 3.4 nm.

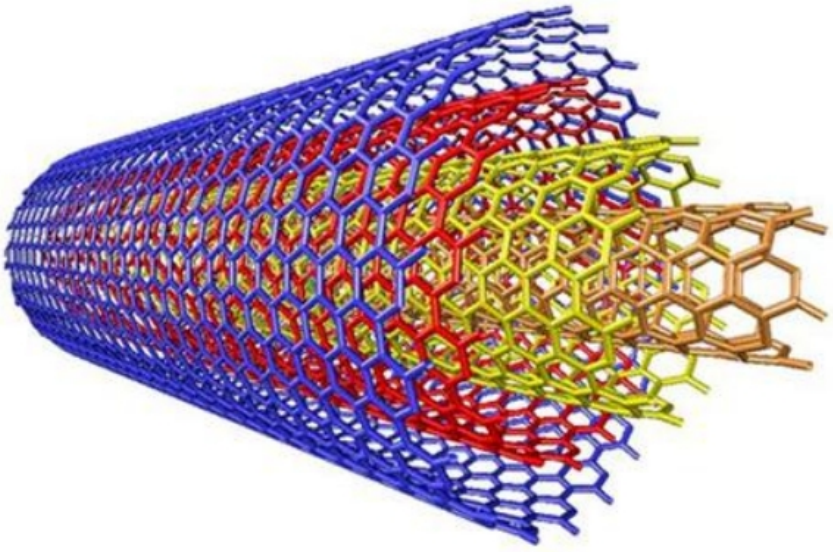

Figure 3.3 Structure of the Multi wall carbon nanotubes (MWCNTs) [48]

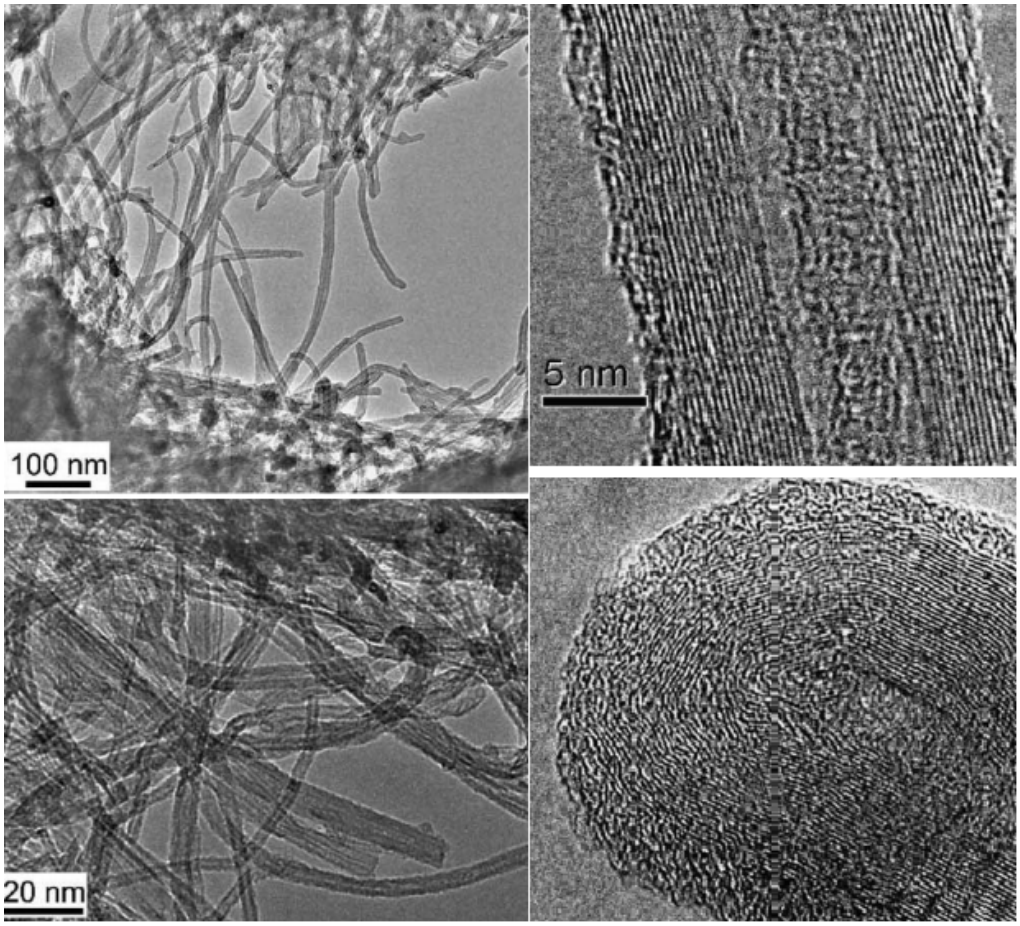

Figure 3.4 TEM pictures of MWCNTs [49]

3.2.3 Random and aligned oriented CNTs

From the orientation point of view, the CNTs can be divided into random CNTs and aligned CNTs. Aligned CNTs exhibit a unique feature that all tubes orient vertically in one direction. An ideal aligned CNT is just like a straight line with zero curvature. While in the random CNTs, tubes twine up freely. Aligned CNTs, with tube density around 10^9 tube/cm^2, are much denser than random CNTs. Both of them can be synthesized easily by chemical vapor deposition method (CVD). Figure 3.5 shows the SEM pictures of aligned and random CNTs.

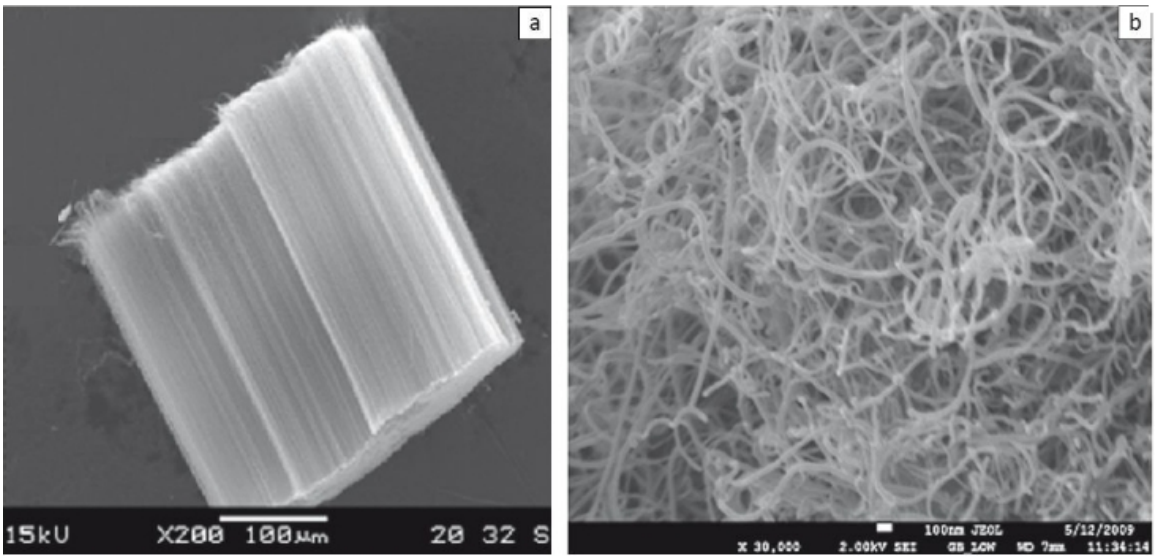

Figure 3.5 (a) aligned CNTs and (b) random CNTs [50]

3.3 Properties of CNTs

CNTs have many exceptional properties which motivated extensive research interests on their manufacturing and applications. They possess high intrinsic strength, stiffness, flexibility, high thermal and electrical conductivity. Furthermore, novel polymer composites are invented by incorporating CNTs to alter and improve the

material properties [51]. Three properties of CNTs, electrical, chemical, and mechanical, are the most important and have been widely studied in applications.

3.3.1 Electrical property

CNTs exhibit excellent electrical properties. Tested with four-probe measurement, the resistivity of different MWCNTs ranges from 5.1×10^{-6} to 1.2×10^{-4} Ωcm [52], and the resistivity of SWCNTs range from 3.4×10^{-7} to 1×10^{-6} Ωcm [53]. Both results are very low compared to other materials, showing that CNTs have unique electronic properties.

Due to the low resistivity and high thermal conductivity, CNTs have attracted interest for their applicability as very-large-scale integration (VLSI) interconnects [53]. Also, an isolated CNT can carry current densities in excess of 1000 MA/cm^2 without damage even at an elevated temperature of 250°C [54]. Recent modeling work has shown that the CNT bundle interconnects can potentially offer advantages over copper interconnect [55].

Recently, semiconducting CNTs have been used to fabricate field effect transistors (CNTFETs), which show great promise due to their superior electrical characteristics over silicon based MOSFETs. This device has been found to be superior in terms of subthreshold slope, a very important property for low power applications [56].

3.3.2 Chemical property

The Chemical property of CNTs is attributed to the curvature-induced local strain, which arises from pyramidalization of the sp^2-hybridlized carbon atoms and misalignment of π–or-bitals [57]. SWCNTs behave chemically inert due to the difficult covalent attachment of molecular species to fully sp^2-bonded carbon atoms on the

nanotube sidewalls. Adsorbing molecules to nanotubes via non-covalent forces, however, turns out to be facile and important, which leads to many potential applications [58].

CNTs also have promising applications in drug delivery and cancer therapy. Systems being used currently for drug delivery include dendrimers, polymers, and liposomes, but carbon nanotubes present the opportunity to work with effective structures that have high drug loading capacities and good cell penetration qualities. These nanotubes function with a larger inner volume to be used as the drug container, large aspect ratios for numerous functionalization attachments, and the ability to be readily taken up by cells [59]. Selective cancer cell destruction is achieved by functionalization of SWNT with a folate moiety, selective internalization of SWNTs inside cells labeled with folate receptor tumor markers, and NIR-triggered cell death, without harming receptor-free normal cells [60].

Biosensors are another application of CNTs. Carbon nanotube-plasma polymer-based amperometric biosensors for ultrasensitive glucose detection have been fabricated. The glucose biosensor showed ultrasensitivity (a sensitivity of 40 μA mM-1 cm-2, a correlation coefficient of 0.992, a linear response range of 0.025 –1.9 mM, a detection limit of 6.2 μM at S/N = 3, +0.8V vs Ag/AgCl), and a rapid response time (<4 seconds in reaching 95% of maximum response) [61]. The aligned carbon nanotube ultrasensitive biosensor for DNA detection is also reported [62]. Hybridization kinetics between complementary and target ssDNA nucleotide base pairs result in a local charge generation between base pairs that is injected into the SWCNTs resulting in a detectable change in SWCNT electrical conductance. This conductance change is amplified electrically and recorded. Based on previous Langmuir DNA kinetics calculations, the

projected sensitivity level of the SWCNT-DNA sensor is considerably higher than traditional fluorescent and hybridization assays [62].

3.3.3 Mechanical property

Carbon nanotube, with Young's modulus on the order of Tera-Pa and the tensile strength of 100 Giga-Pa, is one of the strongest materials in nature. Table 3.2 compares CNTs with other material. The defect free nanotubes are much stronger than the graphite because of the axial component of σ bonding. This component is greatly increased with rolling of graphite sheet into a seamless cylinder structure. The Young's modulus of MWCNTs is large compared to SWCNTs typically in the range of 1.1 to 1.3 TPa. This is because MWCNTs consist multiple layers of SWCNTs, and the highest Young's modulus of SWCNTs is considered along with the coaxial intertube coupling of van der walls force [63].

Table 3.2 Young's modulus, tensile strength, and density of carbon nantotubes compared with other materials reported in [64].

Material	Young's modulus(GPa	Tensile Strength(GPa)	Density(g/cm3)
MWNT	1200	150	2.6
Single-wall nanotube	1054	150	1.3
SWNT bundle	563	150	1.3
Graphite (in plane)	350	2.5	2.6
Steel	208	0.4	7.8
Epoxy	3.5	0.005	1.25
Wood	16	0.008	0.6

3.4 Synthesis of CNTs

3.4.1 Growth mechanism

Several CNTs growth mechanisms have been proposed, regarding to the generation of free carbon atoms and the precipitation of dissolved carbon from the catalyst particles. However, the growth mechanism is still not well understood, due to the diverse fabrication methods [65]. In general, the growth of CNTs is believed to be due to the decomposition of hydrocarbon gas mixtures, like acetylene and methane, with the presentence of catalyst, such as iron, molybdenum. Regardless of what mechanism occurs in the growth of CNTs, there are three stages common in the growth process as shown in Figure 3.6.

1. Metal catalyst particles formation on the substrate: this process is done normally by ion sputtering or e-beam evaporation. Different metals are used as catalyst based on the growth method such Fe, Co.

2. Free carbon atom formation and diffusion after catalyst formation: Free carbon atoms are generated in the hydrocarbon deposition process in high temperature and diffuse into the catalyst particles.

3. Carbon tubes growth: Rod-shaped carbon tubes grow out of the catalyst particles rapidly.

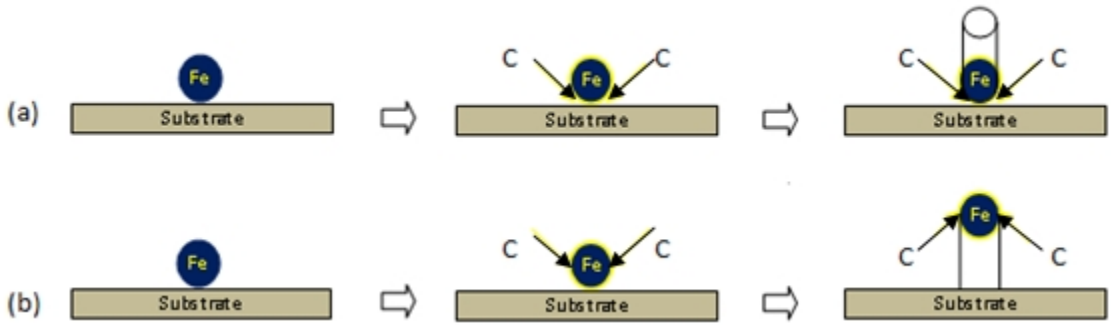

Figure 3.6 CNT growth stages (a) root growth (b) tip growth

There are two major theories of growth process, one is proposed by Baker and coworkers where the hydrocarbon is decomposed into C and H on the top surface of the metal catalyst [66]; then CNTs are grown when these carbon fragments diffuse into the metal particle and precipitate at the other end. The catalyst particle remains on the tip of the tube during the growth process until the leading catalytic particles is neutralized or the reaction is stopped due to the encapsulation of metal catalyst by a layer of carbon [66]. This is shown schematically in Figure 3.6 (a).

The other theory states that the catalytic metal particle always remains at the bottom of the filament or tube during the growth process [67]. The rapid diffusion of carbon species through the catalyst results in the growth of the filament from their bases, unlike the first model where the tubes are grown from their tips. CNTs based on these two theories is illustrated in Figure 3.7

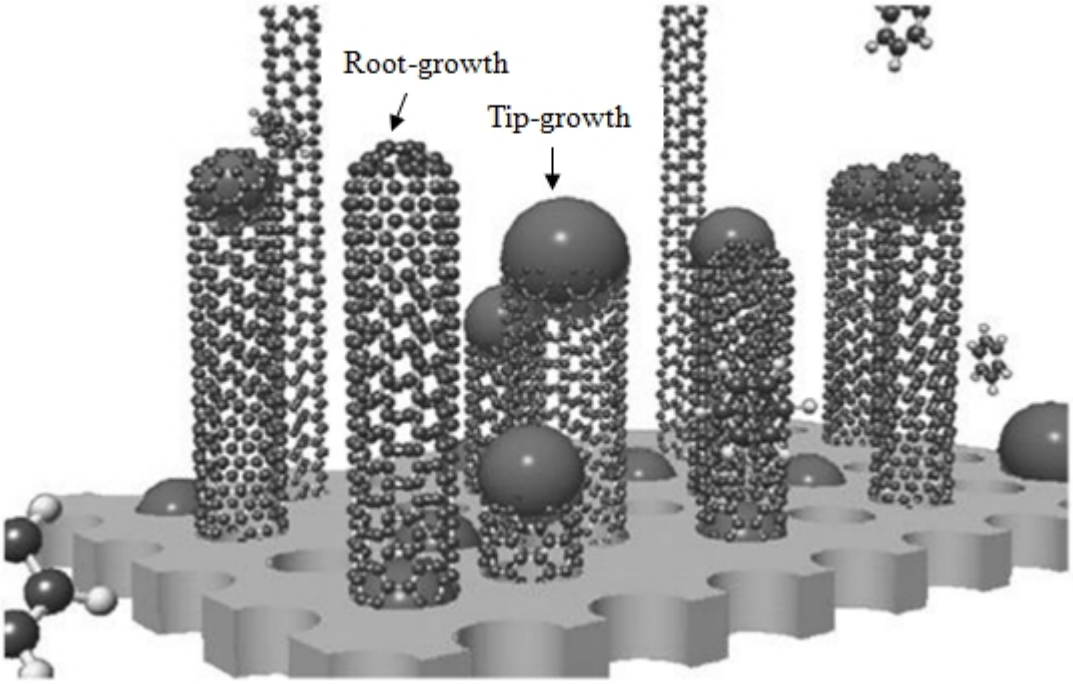

Figure 3.7 Schematic representation of two types of CNT growth mechanism [4]

A third theory, combing these two models together, has been proposed by Louchev [68]. Two important characteristic times in the diffusion process of carbon species are defined to explain the CNT growth mechanism. There are:

(1) The characteristic diffusion time of carbon through the catalytic metal nano-partcle to the nanotube growing point is defined as

$$t_d = R_p^2 / D_b$$

where R_p is the radius of catalytic metal particle and D_b is the diffusion coefficient.

(2) The surface saturation time of order is defined as

$$t_s = C^2 D_b / Q^2$$

Where C is the saturation concentration of carbon and Q is the impinging carbon flux. The surface saturation is defined as the increase of the carbon content to the saturation concentration level, which is responsible for triggering the carbon precipitation directly on the outer surface of the metal nanoparticles.

When $t_d << t_s$, the carbon diffuses through the metal particle body much faster researching the saturation point. Therefore, the carbon is precipitated at the bottom of the catalytic particles, lifting the particles during the growth process. This type of growth is defined as tip-growth. When $t_d >> t_s$, the carbon diffuses through the metal particle surface much faster researching the saturation point. The carbon is precipitated from the surface of the catalytic particles. Therefore, the tubes are grown out from the catalytic particle surface, leaving the catalytic particles at the bottom. This type of growth is defined as bottom-growth. This process is illustrated in Figure 3.8 [68].

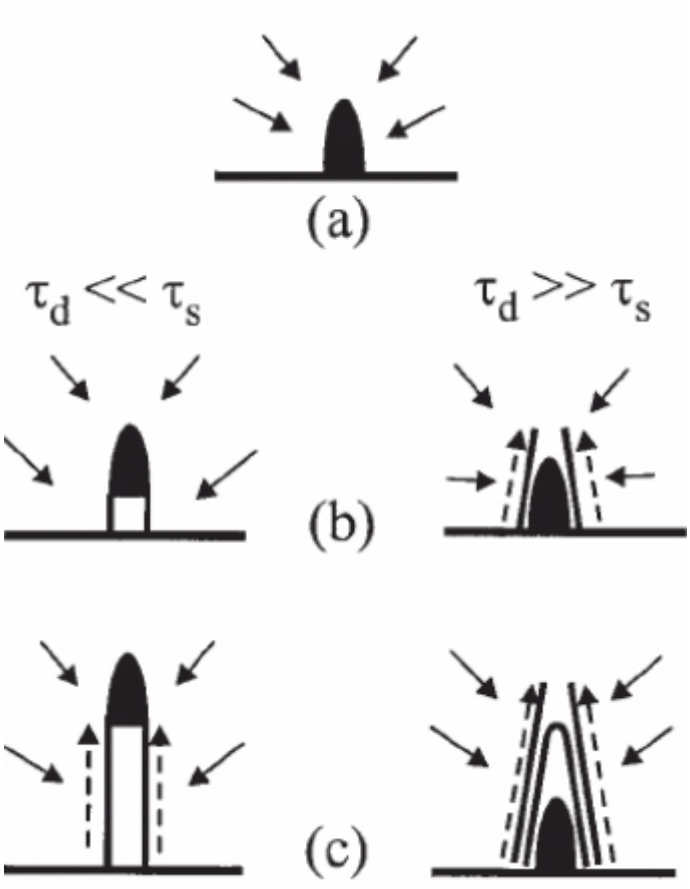

Figure 3.8 Schematic of CNTs growth mechanisms (a) saturation of catalytic nanoparticle with carbon, (b) carbon precipitation process, left: when $t_d << t_s$, right: $t_d >> t_s$, (c) tube growth process, left: tip-growth, right: root growth [68]

3.4.2 Synthesis methods

There are many methods of synthesizing controllable CNTs. The arc-discharge, laser ablation, and the chemical vapor deposition (CVD), which also includes the plasma enhanced chemical vapor deposition (PECVD), have been the main methods used for CNTs synthesis.

3.4.2.1 Arc-discharge method

CNTs are first produced by arc-discharge method in 1991 [36]. This method creates CNTs through arc-vaporization of two graphite rod placed end to end, separated

by approximately 1mm, in an enclosure that is usually filled with inert gas, normally helium and argon, at low pressure. The hardware setup is shown in Figure 3.9. During the arc-discharge, a deposit of randomly oriented MWCNTs with some by-products such as polyhedral particles and other graphitic particles forms on the cathode. The deposit growth rate is around 1~2 mm/min.

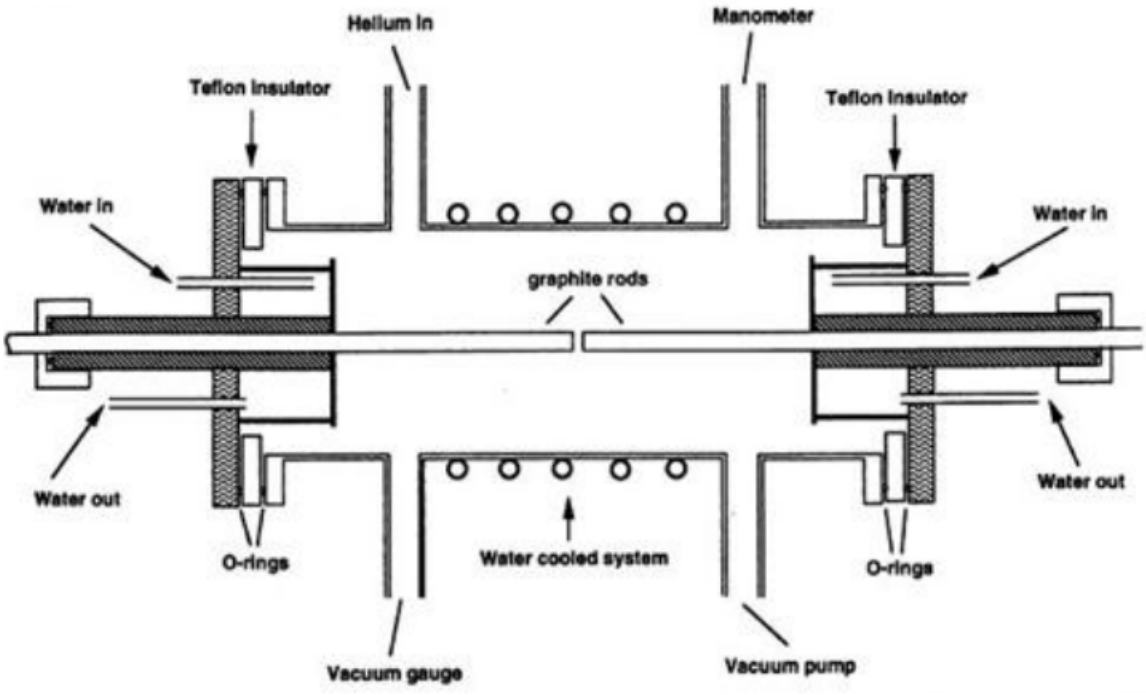

Figure 3.9 Schematic diagram of the Arc apparatus [69]

Large-scale synthesis of MWCNTs by arc-discharge has been achieved in helium atmosphere [70, 71]. It is found that the methane is the best gas for the synthesis of MWCNTs, due to the thermal decomposition of methane producing hydrogen that achieves higher temperature and activity compared to inert gases such as He or Ar [72]. The drawback of arc-discharge method is that the discharge conditions have to be

carefully controlled. Also, the CNTs produced with this method need to be purified before applications.

3.4.2.2 Laser ablation method

Carbon nonotubes can be synthesized by laser vaporization apparatus with an ablated pure graphite target located in an oven. This method is originally used as a source of metal clusters and ultrafine particles [73, 74], and then developed for fullerene and CNT production. Figure 3.10 shows a schematic of experimental setup of laser ablation method [75].

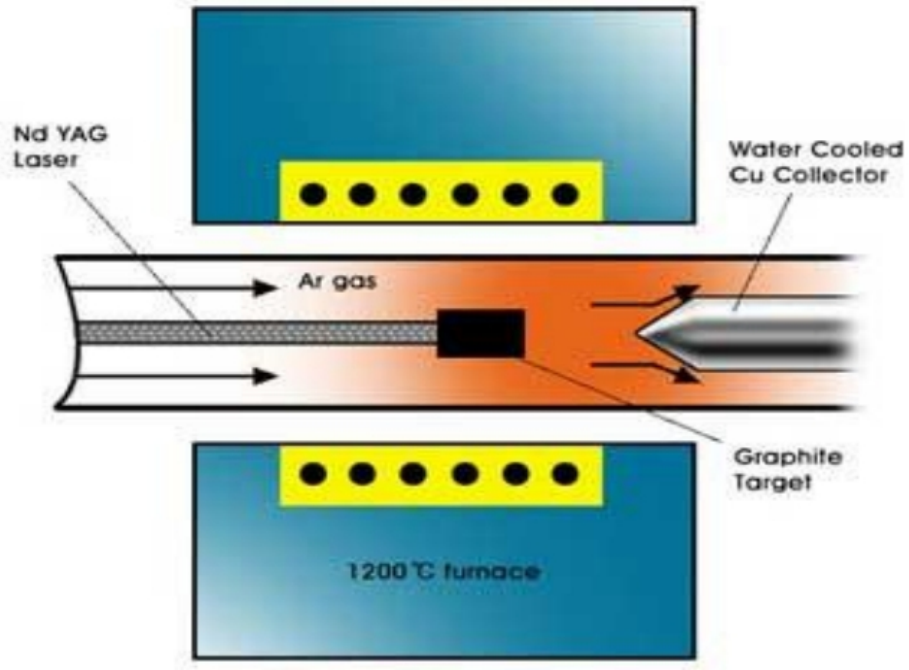

Figure 3.10 Schematic of laser ablation method [75]

The basic principle of this method is carbon target vaporization by laser ablation. A laser beam is introduced onto the carbon based target located in the centre of a quartz tube furnace. The target is vaporized in high-temperature argon atmosphere. The CNTs produced in the carbon vaporization process are conveyed by the gas to a special

collector. This method has several advantages, including high tube quality, and high yield. However, the large scale production of CNTs using this method is not as impressive as arc-discharge method.

3.4.2.3 Chemical vapor deposition (CVD) method

Chemical vapor deposition (CVD) is another widely used method to synthesize CNTs. It uses hydrocarbon vapor, such as methane, thermally decomposed in the presence of a metal catalyst. Chemical vapor deposition has several advantages, including simplicity, economic and controllable growth.

The CNTs synthesis process with CVD method essentially involves two steps: (1) catalyst preparation and (2) carbon nanotubes growth. In the first step, a transition metal such as Ni, Fe and Co is sputtered on to the substrate material. Then the catalyst coated substrate is subjected to either thermal annealing or chemical etching to induce catalyst particle nucleation. Nanotubes are achieved by changing the carbon source molecules into gas phase and depositing on the transition metals if the proper parameters are maintained. Parameters, such as type of hydrocarbon, type of catalyst, growth pressure, and temperature, are important for CNT growth in CVD method. Figure 3.11 shows a schematic of the CVD apparatus used in [76].

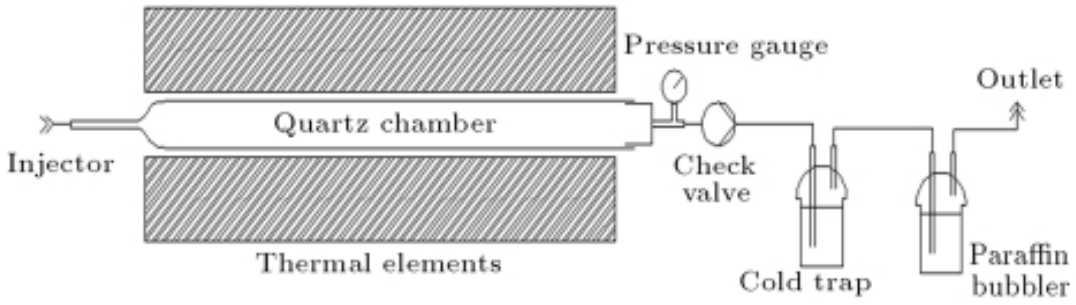

Figure 3.11 Schematic of CVD apparatus [76]

Apart from large scale production, CVD also offers the possibility of producing single CNT for use as probe tips in atomic force microscopy (AFM). The tips produced are smaller than mechanically assembled ones, thus significantly improving AFM resolution [77].

3.4.2.4 Plasma Enhanced Chemical vapor deposition (PECVD) method

Plasma enhanced chemical vapor deposition (PEVCD) is a type of CVD where chemical reactions involved in the deposition process occur after generation of plasma of the reacting gas through interactions in the plasma. Electrical (DC or RF) discharge is used to create the glow discharge which contains radicals, electrons, and ions, instead of the thermal lamp in the traditional CVD method. In a PECVD chamber, two parallel electrodes are mounted with substrate on the grounded one, as shown in Figure 3.12. The distance between two electrodes is adjusted in order to sustain the discharge. A separate heat source may be used to maintain the desired temperature of the substrate to enhance the nucleation density.

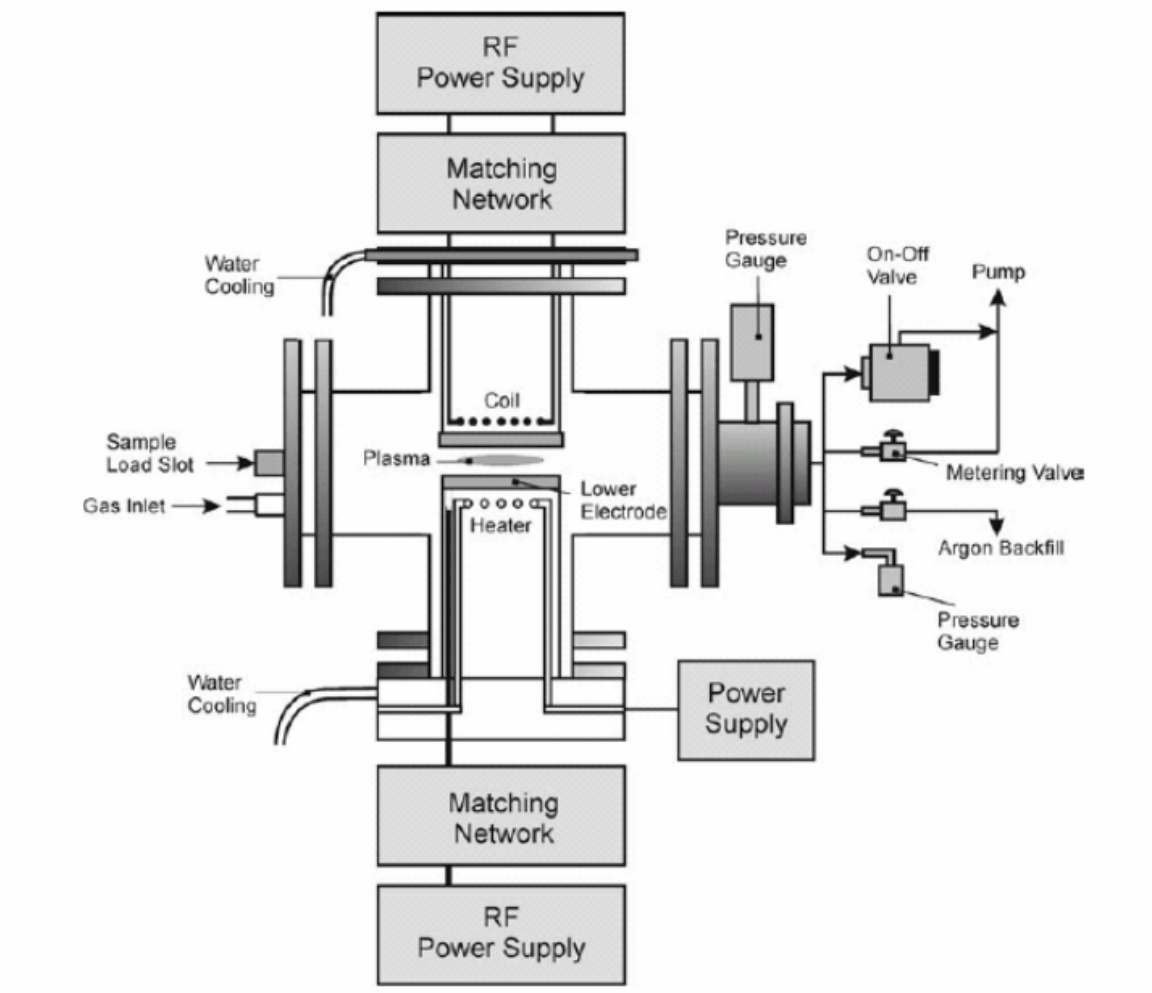

Figure 3.12 Schematic of PECVD [47]

CNTs are synthesized by the glow discharge in the chamber by applying a high frequency high voltage to electrodes. Sources such as DC, RF (13.56 MHz) or Microwave (2.45 GHz) are used to generate the plasma. The reaction gas, either C_2H_2, CH_4, C_2H_4, C_2H_6, or CO diluted with inert gas, is fed with operating pressure of 1 to 20 mTorr. The source carbon molecules are broken into reactive carbon atoms by the energy provided from the plasma. The carbon nanotubes are grown on metal catalyst particles which are already prepared on the substrate. The local electric field formed between the

plasma and the substrate holder allows CNTs to be grown extremely vertical with high density. Because heat is not needed for chemical reactions, this process is achieved at low temperatures.

The low operating temperature during the growth mechanism of carbon nanotubes is another advantage, which make it attractive for the integrating carbon nanotubes in semiconductor device fabrications.

3.5 Characterization Methods

In order to better understand the electronic and mechanical properties of CNTs, the morphological and structural characterizations need to be examined. There are many methods used for the characterization of materials depending on the desired property.

To test for defects, treatments, such as oxidation with nitric acids, can be performed to remove the caps at both ends [78]. This method reveals defects like carboxylic acid groups [78]. The determination of the concentration of these defects can be done by various methods. Calibrated energy dispersive X-ray and titration techniques with sodium bicarbonate are two methods which have been widely used [79].

In order to observe the photoluminescence phenomenon, the CNT bundles must be separated into individual tubes. Ultrasonication treatment with surfactants or using individual CNTs grown in channels of zeolite [80] is a good way to get individual tubes.

X-ray photoelectron spectroscopy (XPS) can be used to determine the chemical structure of CNTs. The scanning tunneling microscopy (STM) provides three-dimensional morphology information of samples. To use STM, CNTs must be deposited on a flat conducting substrate such as highly ordered pyrolytic graphite (HOPG) or Au. Infrared spectroscopy is often used to determine residual impurities from synthesis or

molecules capped on the CNT surface. It exhibits all the modification of the structure and reveals the nature of compounds added to the NTs and the catalytic properties [81].

The Raman spectroscopy is one of the most commonly used tools for structural characterization of CNTs. It is fast and also non-destructive [82]. The Raman line shape differs between metallic and semiconductor CNTs thus distinguishing these two types in a sample [83]. Many other characterization methods are also being studied. More information can be found in [84]

Chapter 4

Carbon Nanotubes Fabrication and Optimization

The primary objective of this research is to design and construct a pseudospark switch triggered by CNTs acting as cold cathode emitters. As mentioned, an appropriate trigger mechanism is very critical in pulsed power switches. Previous work has shown that CNTs have excellent field emission properties and can be used as electron emitter material in applications [35]. The high quality CNTs can emit milliamp current without degradation of field emission property in higher pressure than vacuum [86]. Therefore, if they are used in a plasma switch, they may offer improved switch performance. As a result, CNTs synthesis and optimization of the properties are the first step toward to the final goal of using them as trigger electrode in pseudospark switches.

In this research, CNTs, both randomly oriented, and vertically aligned, are synthesized with Chemical Vapor Deposition method (CVD). The CVD method has advantages of simple equipment setup, and excellent deposition uniformity over large area. Silicon wafers are used as the substrate for CNTs growth and iron (Fe) is coated on the silicon substrate as the catalyst using an ion sputtering system. Then the CNTs are synthesized in a CVD furnace under temperature range of 650°C to 700°C. The quality of CNTs is examined under scanning electron microscopy (SEM) and the electrical property is characterized with field emission measurements in vacuum. Synthesis parameters are

optimized by testing different CNT synthesis approaches. Three types of CNTs, randomly oriented, vertically aligned, and patterned are fabricated and tested.

4.1 Synthesis of Randomly Oriented CNTs

The synthesis process of CNTs mainly includes wafer preparation, catalyst sputtering deposition, and CNT growth in a CVD chamber.

4.1.1 Silicon wafer preparation

The silicon wafer preparation consists of wafer clean and wafer baking. Wafer is cleaned in the clean room and baked in vacuum. The cleaning process removes solvent, organic/ionic contamination, and hydrous oxidation from the surface. Baking process removes the moisture.

Details of the cleaning process are listed as below:

A. Solvent removal
    1. Immerse in boiling trichloroethylene (TCE) for 3 min.
    2. Immerse in boiling acetone for 3 min.
    3. Immerse in boiling methyl alcohol for 3 min.
    4. Wash in DI water for 3 min.

B. Removal of residual organic/ionic contamination
    1. Immerse in a (5:1:1) solution of H_2O-NH_4OH-H_2O_2; Heat solution to 75-80°C and hold for 10 min.
    2. Quench the solution under running DI water for 1 min.

C. Hydrous oxide removal
    1. Immerse in a (1:50) solution of HF-H_2O for 15 sec.
    2. Wash in running DI water with agitation for 30 sec.

The cleaned wafer is then transferred into a vacuum chamber with a heater attached on the top of the wafer holder for baking. The purpose of baking is to increase the adhesion between silicon and catalyst by removing the moisture on the wafer surface.

The baking procedure is listed as follows:

1. Bring the baking chamber to a vacuum of $1x10^{-6}$ Torr with mechanical and turbo pumps.
2. Turn-on the heater with 15% of the total power. Heater has controls to regulate the temperature increase rate.
3. Keep the wafer heated at 100°C for 5 min.
4. Cool down the wafer to room temperature and de-vacuum the chamber.

4.1.2 Catalyst sputtering deposition

The wafer is loaded into an ion sputtering deposition chamber when the wafer preparation process is finished. The ion sputtering system used in this research is schematically shown in Figure 4.1. The wafer substrate is mounted 15 cm above the plasma gun, also called as ion gun, is a filamentless ion source based on a microwave plasma discharge. A two-inch diameter Fe target, attached directly on the plasma gun, is used as the catalyst source. Argon is fed as the background gas and the pressure is maintained at 20 mTorr.

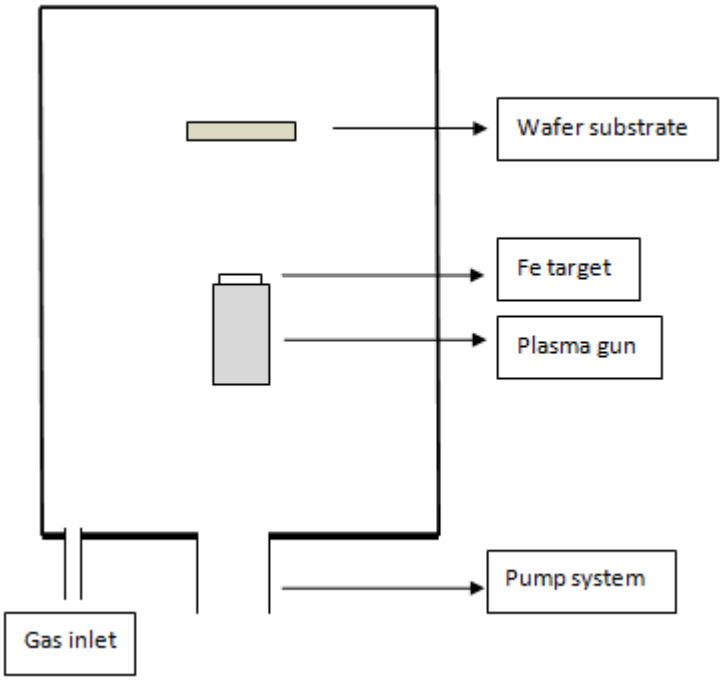

Figure 4.1 Schematic of ion sputtering system

Once the DC/RF power is applied to the plasma gun, plasma is generated. The ions are accelerated in the electric and magnetic field and bombard the target surface. The Fe atoms sputtered from the surface float to the wafer substrate and attach to the wafer surface. Eventually, a layer of Fe is deposited on the wafer surface. The typical sputtering times vary from 1min to 20 min, depending on the desired catalyst thickness. In order to examine the uniformity of the Fe distribution on silicon surface, a 800°C annealing process is done to break the Fe thin film into small “islands” before the SEM. Figure 4.2 are SEM pictures of silicon with Fe particles uniformly deposited on the surface.

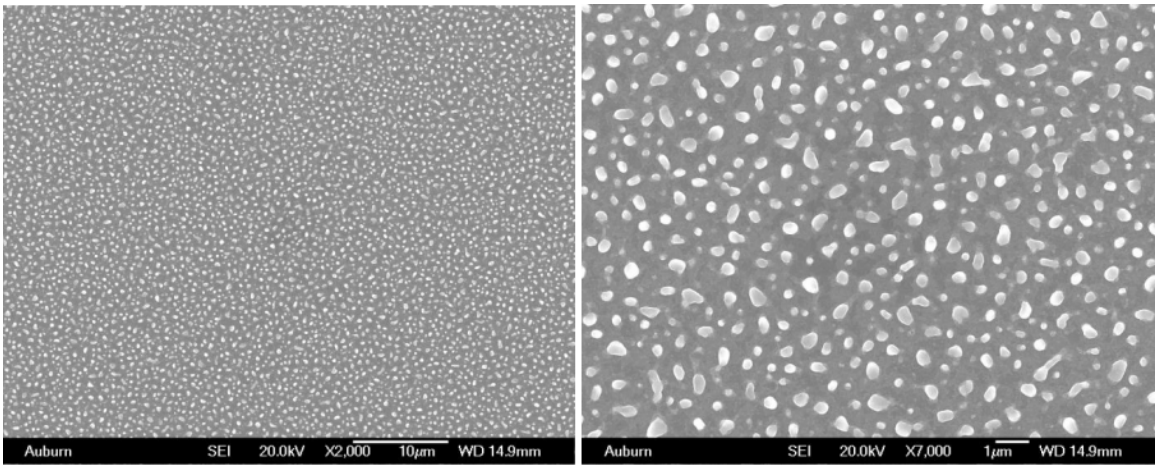

Figure 4.2 Fe sputtered silicon substrate.

4.1.3 Chemical vapor deposition

After the Fe catalyst layer is coated on the silicon, the silicon substrate is then transferred to the thermal CVD reactor. The quartz tube is the main chamber of the system, as shown in the Figure 4.3. A controllable resistive heater is used to heat the chamber to a desired reactive temperature. A thermocouple placed on the wafer holder is used to measure the process temperature. The flow of the gas into the chamber and the pressure are electrically controlled by flow meters and a set of valves between the pump and the chamber.

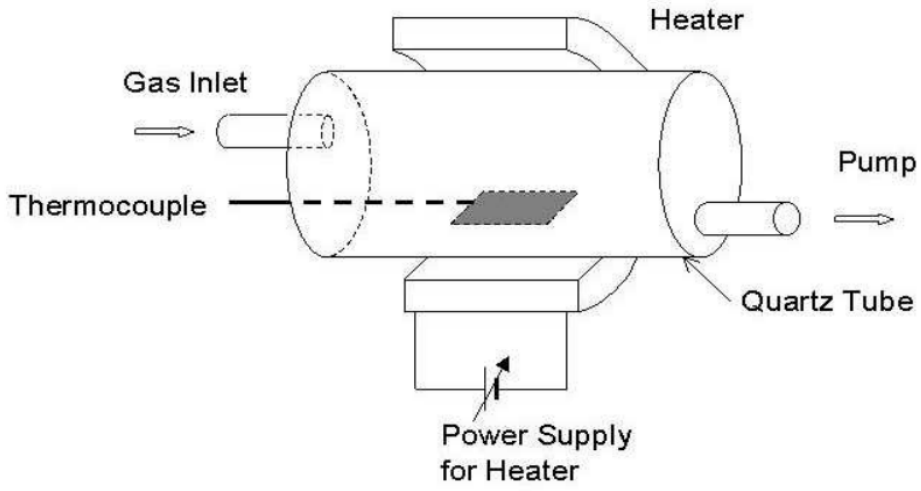

Figure 4.3 Schematic of CVD reactor [85]

Mixture of Acetylene (C_2H_2) and Argon (Ar) with flow rate of 20 and 75 sccm respectively, are used as the reaction gas maintaining a growth pressure of 70 Torr in the chamber. The CNTs are grown at a temperature of 650~750°C and the growth time is typically varied between 10~240 min depending on the desired tube density and tube length. Figure 4.4 shows the SEM pictures of a representative set of CNTs samples fabricated in this research.

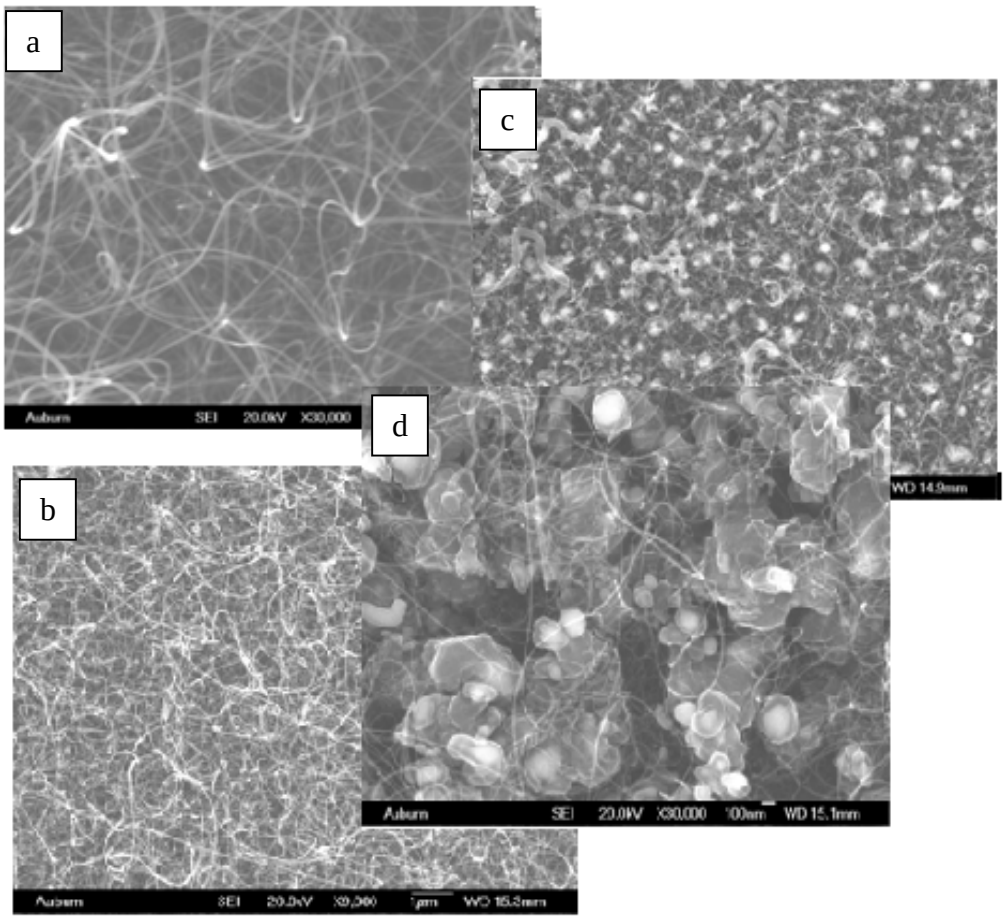

Figure 4.4 SEM pictures of CNTs (a: loose CNTs with good quality, b: dense CNTs with good quality, c: dense CNTs with bad quality, d: loose CNTs with bad quality)

As seen, the CNTs in Figure 4.4 vary dramatically. Some samples are good in term of tube length and tube density with very few carbon clusters and some are not. Some samples have clean tubes but low density. Some other samples contain very few tubes where the carbon clusters are dominant. Therefore, the CNT synthesis parameters are optimized in order to get high quality carbon nanotubes without clusters.

4.2 Optimization of CNT Synthesis Parameters

As stated earlier, high quality CNTs with low turn-on field is one of the important parameters of this research. Therefore, in this step, CNTs synthesis conditions using CVD method are thoroughly studied and optimized.

The previous work reveals that three variables, C_2H_2 concentration, CVD temperature, and catalyst thickness, are important for the CNTs synthesis [86, 87]. Therefore, different growth conditions are tested and the qualities in terms of tube length and density of resulting CNTs are investigated with SEM imaging system. The deposition procedure of the CNT synthesis is carried out firmly as outlined in section *4.1.3 Chemical vapor deposition*. The growth conditions and the SEM pictures of resulting CNTs are listed below.

Ratio of C_2H_2 to Ar:

Four different flow rate ratios of C_2H_2 to Ar, namely 10:75, 20:75, 30:75, 40:75, are used while keeping the CVD temperature of 700°C and catalyst thickness of 13 nm fixed. The SEM pictures of synthesized samples are shown in Figure 4.5. The sample with a ratio of 20:75 is concluded to have better morphology. Although carbon clusters present, the tube density is the highest.

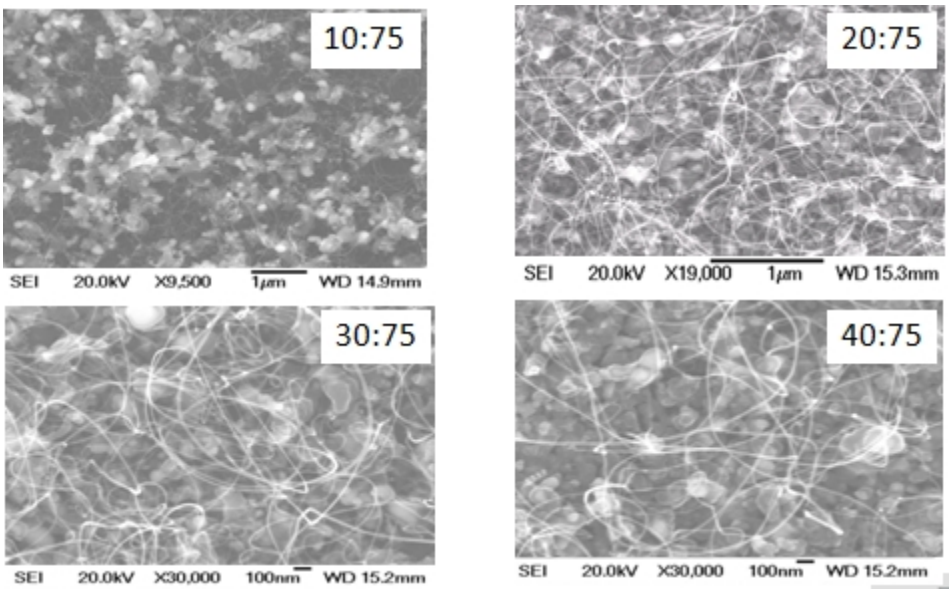

Figure 4.5 CNTs with different C_2H_2 concentration

Operation temperature:

Two temperatures of 700°C and 750°C are tested twice on different C_2H_2 to Ar ratio. First, 20:75 ratio is kept fixed and then the 30:75 ratio is kept fixed. The SEM pictures are shown in Figure 4.6 for these combinations. From these images, it is concluded that the samples grown in 700°C are better than the ones in 750°C.

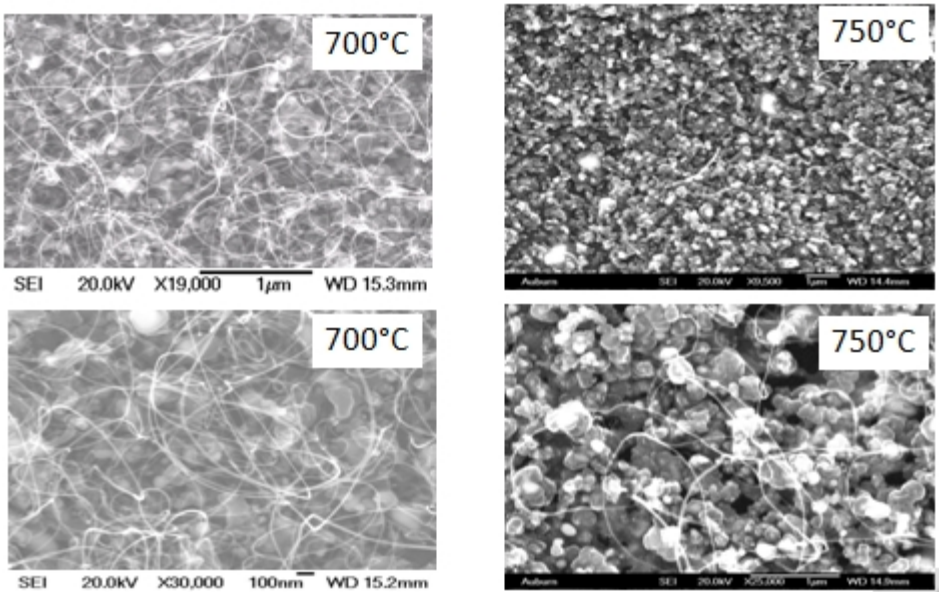

Figure 4.6 CNTs with different operation temperature (The upper two samples are grown at 20:75 ratio of C_2H_2 to Ar and the bottom two samples are grown at 30:75 ratio)

Catalyst (Fe) thickness:

Two catalyst thicknesses of 13 nm and 60 nm are also examined. First the C_2H_2 to Ar flow rate ratio of 20:75 is used and then the ratio of 30:75 is used for each substrate with different catalyst thickness. Temperature is set at 700°C for these growth processes. The SEM pictures are shown in Figure 4.7. The 13 nm catalyst thickness obviously results in growing better CNTs than the one with 60 nm thickness.

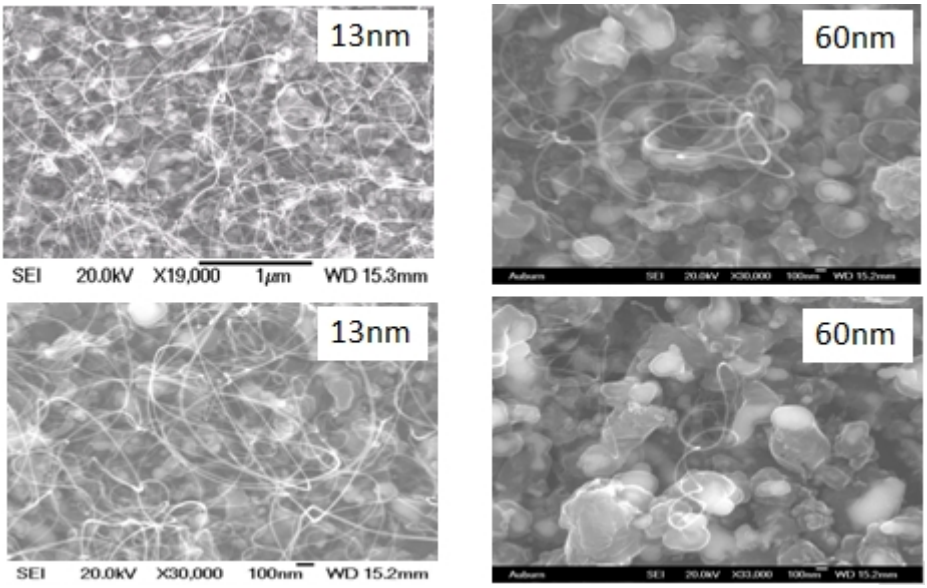

Figure 4.7 CNTs with different catalyst thickness (The upper two samples are grown at 20:75 ratio of C_2H_2 to Ar and the bottom two samples are grown at 30:75 ratio)

From these pictures, we see that some parameter combination produces CNTs with better morphology. Based on a series of fabrications, we set the optimized CNT synthesis parameters as, C_2H_2 Concentration of 20:75 ratio, CVD temperature of 700°C, and Fe thickness of 13nm. The first optimized and repeatable CNT sample is fabricated with this set of parameters and is shown in Figure 4.8.

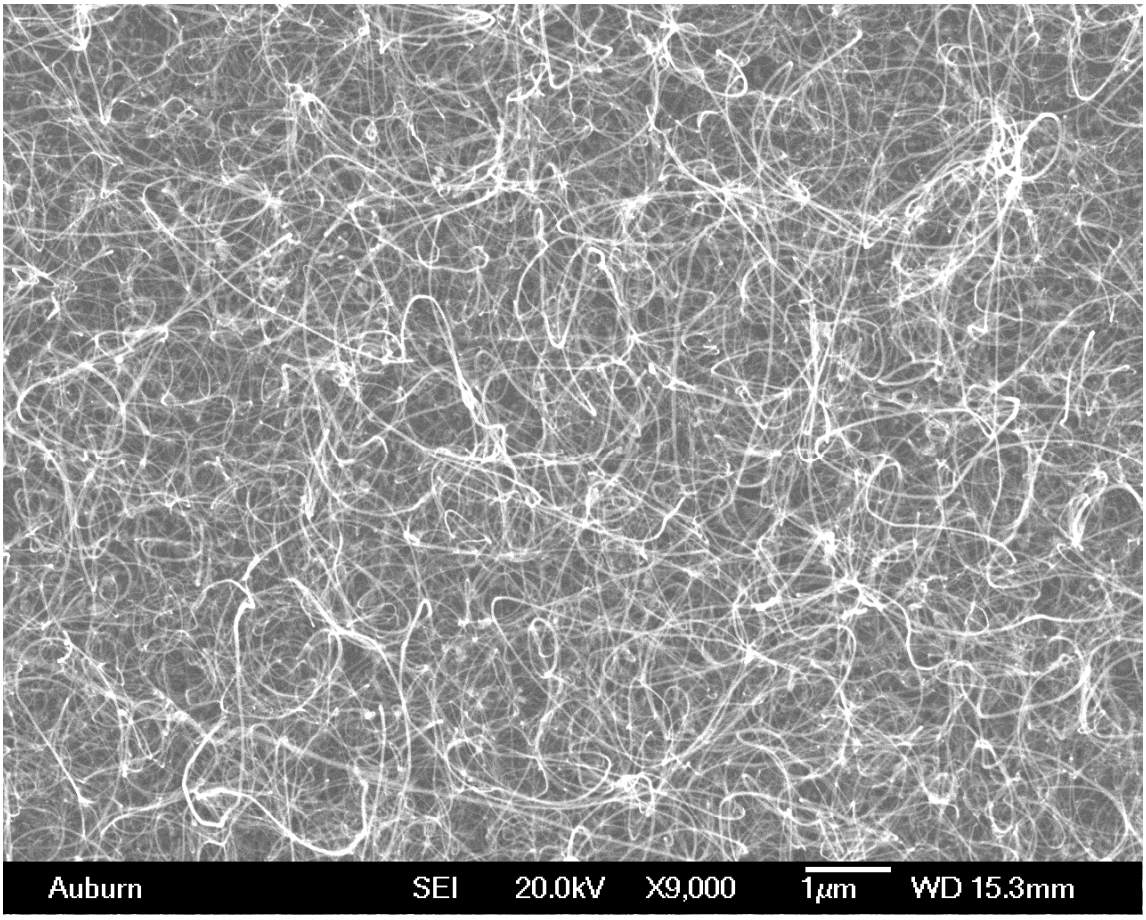

Figure 4.8 CNT sample fabricated with optimized CVD parameters

4.3 Aligned CNTs Synthesis

The aligned CNTs synthesis is also proposed and conducted using the knowledge of random CNTs growth. In the vertically aligned CNT synthesis, each tube needs the support from the surrounding tubes during the growth process. Two parameters that are important for the growth of vertically aligned CNTs are the uniformity and density of the catalytic Fe particle distribution on the substrate, and the catalytic Fe particle must be saturated with carbon to form a growth point.

In this research, the catalytic Fe particles are coated by the ion sputtering deposition described before. This method shows a very good uniformity and density of

the catalytic layer. The carbon saturation is achieved by a carbon treatment process in which carbon atoms are sputtered and attached to catalyst Fe particles on the silicon substrate. The carbon sputtering time is critical because the Fe particles cannot be saturated if sputtered too short, or the Fe particles get oversaturated by carbon atoms, leaving no seed for CNT growth, if sputtered too long.

In order to study the aligned CNT synthesis mechanism, four carbon sputtering time, 1 min, 5 min, 20 min, and 40 min, are tested. The substrate is cleaned and Fe sputtering deposited the same way as stated in the previous section. All CNTs are grown in the CVD furnace for 40 min. The CNT samples are shown in Figure 4.9.

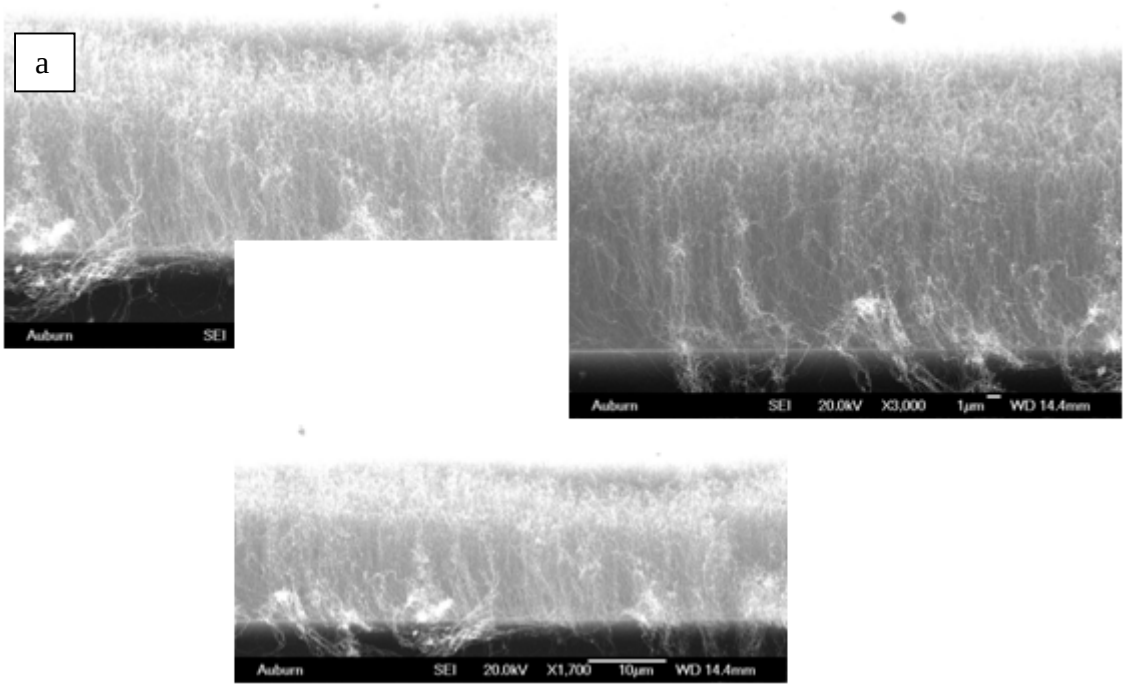

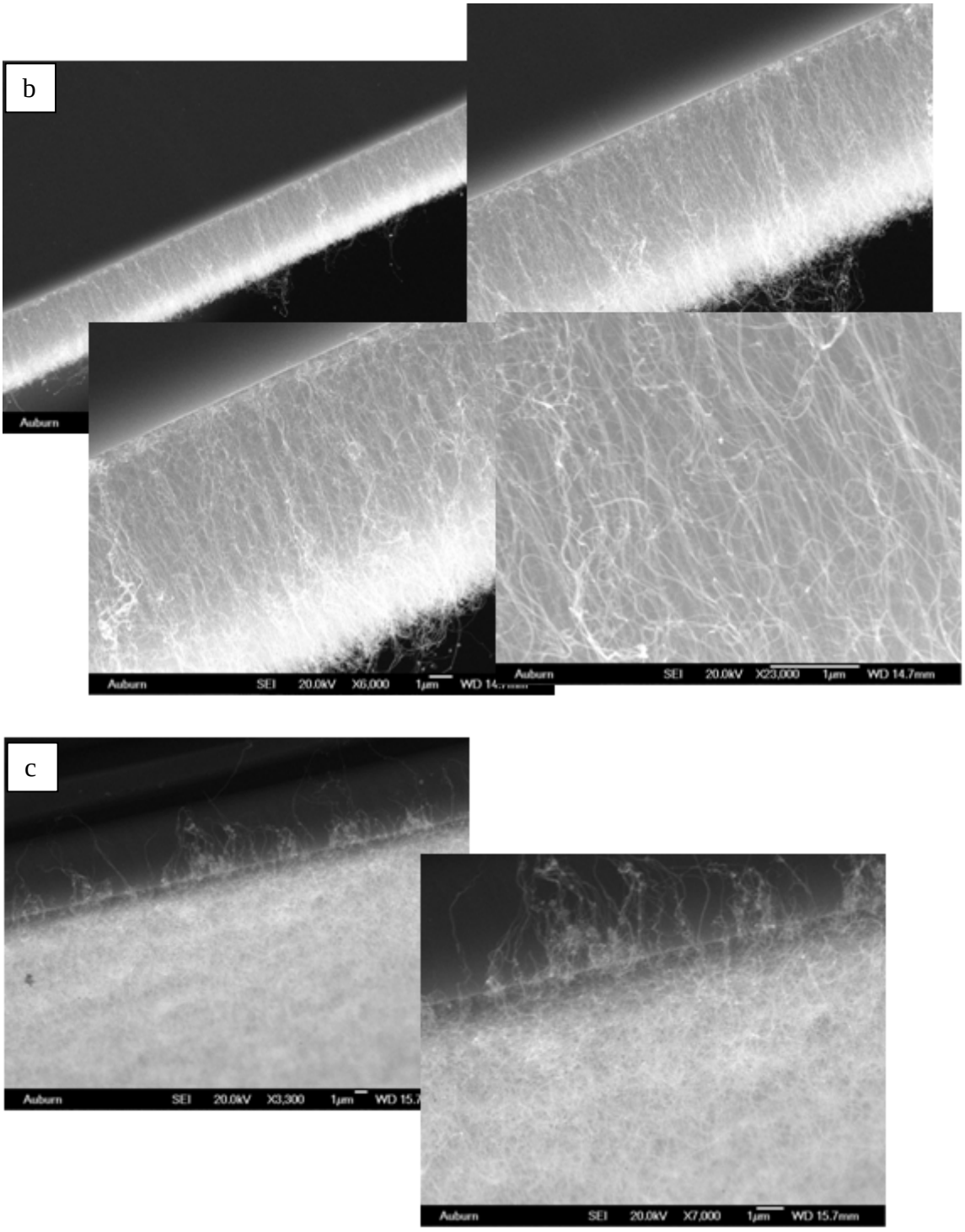

Figure 4.9 Aligned CNT samples (a) 1 min carbon pretreatment (b) 5 min carbon pretreatment (c) 20 min carbon pretreatment

The CNTs in sample (a) and sample (b) are well aligned with a relatively good tube density. Samples (c) looks more like the randomly oriented CNT. No CNTs are grown on the 40 min carbon sputtering deposited sample. This confirms that the catalyst gets oversaturated and no seed Fe catalytic particles exposed on the surface to support CNT growth.

Based on the results above, we consider the aligned CNT synthesis mechanism is illustrated in Figure 4.10. We believe that, if a Fe particle is saturated enough by carbon, a CNT growth point forms, which is represented with a red ball in the Figure 4.10. When the growth points are dense and uniform on top of the substrate, each tube receives supporting force from neighboring tubes because of proximity to each other. This allows all tubes grow in one direction, resulting in aligned CNT growth. When some of the growth points are not well formed, represented with black balls in the Figure 4.10, no tube grows on that spot, leaving a large gap distance. As a result, No support force exits in that area and the surrounding tubes have freedom to grow in random directions. This leads to more randomly oriented CNTs. When the Fe particles are oversaturated by carbon completely, no growth points form on the surface. Therefore, carbon clusters are formed on the surface instead of CNTs. This mechanism is confirmed with CNT samples synthesized in our lab (see Figure 4.11).

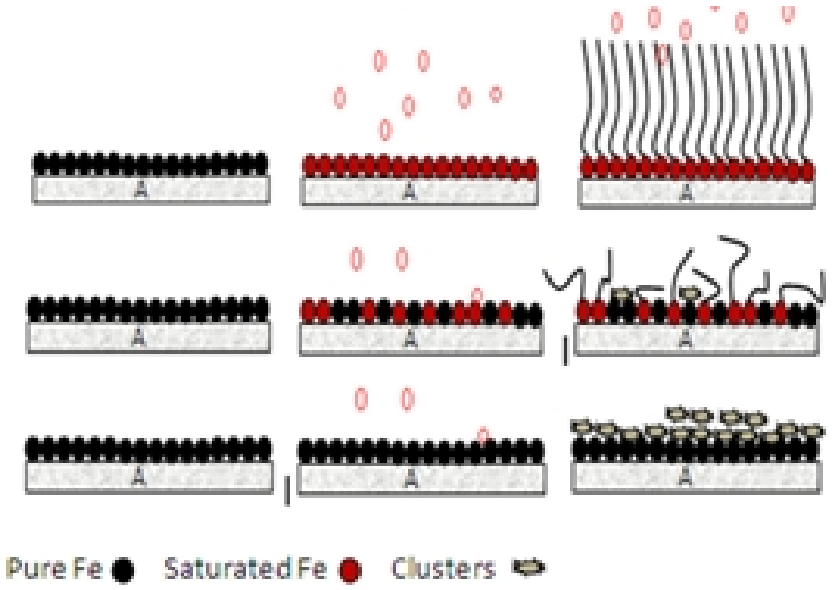

Figure 4.10 Mechanism of aligned CNT synthesis

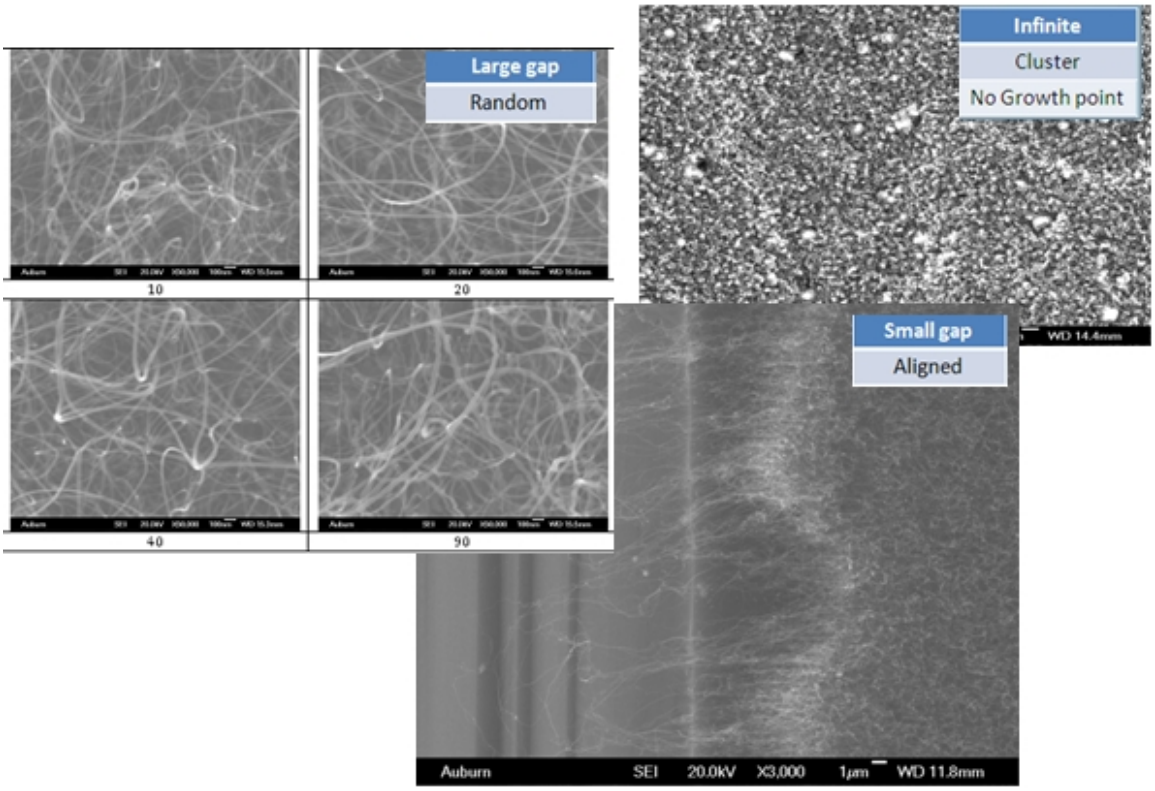

Figure 4.11 CNT samples with different growth point distance

4.4 Patterned CNT Synthesis

CNTs grown on a patterned silicon substrate with SiO_2 on top has also been performed using the photolithography technique adopted by the semiconductor microfabrication industry.

First, a 0.5 μm thick silicon dioxide (SiO2) layer, acting as the dielectric spacer, is formed on the top of the silicon substrate. The dielectric strength of SiO_2 layer has been tested both in vacuum and atmosphere, and maximum of 400 V can be applied without shorting the circuit. The test result is shown in Figure 4.12.

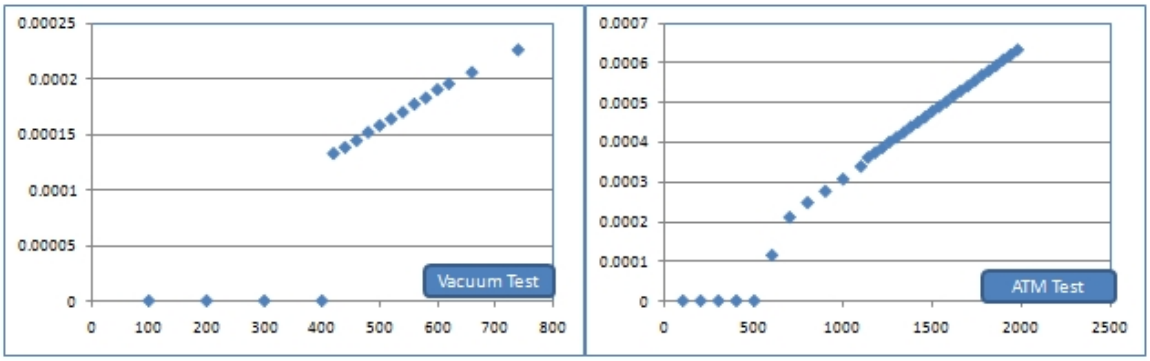

Figure 4.12 Dielectric strength test of SiO_2 (x axis is the applied voltage and the y axis is the emitting current)

Second, a set of 0.5 cm by 0.5 cm square holes with a depth of 60 μm is etched in the substrate by using wet and dry etching. Two masks are used in this step as shown in Figure 4.13. While the mask 1 is used to etch holes, the mask 2 is used to limit the catalyst area in the sputtering process. This is to restrict the CNT growth area small in the bottom of the holes, so the CNTs can grow without reaching the pattern edge. In this way, CNTs are only grown at the center bottom of the pattern and no tubes exit on the side wall. Desire not to have tubes on the sidewall is important because those tubes may cause

short circuits to the cathode body during testing the samples in the trigger electrode. Figure 4.14 shows a patterned square array on the substrate

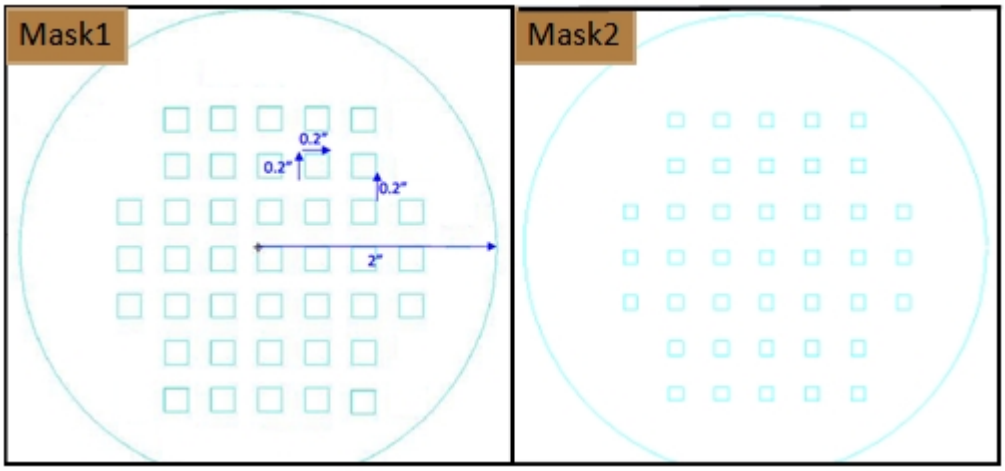

Figure 4.13 Masks of Photolithography, mask1 has 0.5 cm square holes and mask 2 has 0.35 cm square holes.

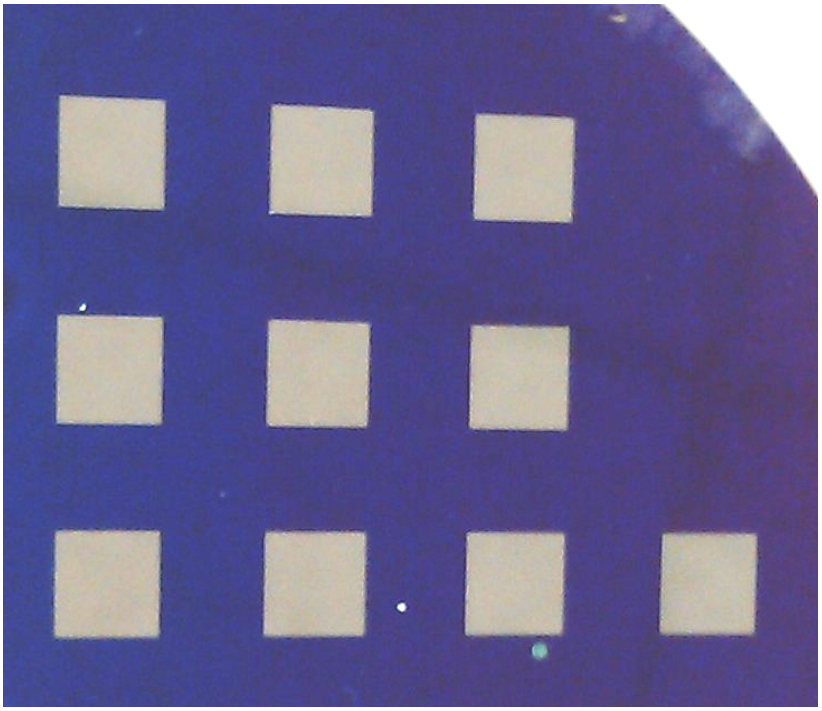

Figure 4.14 Patterned substrate

Last, the patterned substrate goes through the catalyst coating and CVD process. Similar to the one outlined earlier. A processing flow chart of the patterned CNT growth is shown in Figure 4.15.

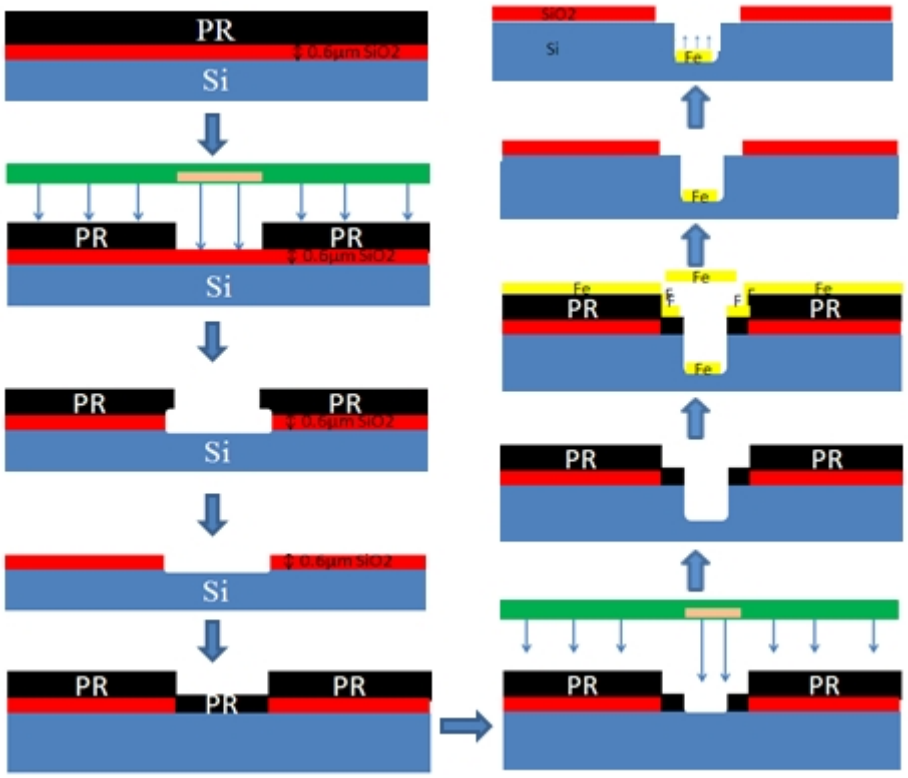

Figure 4.15 Flow chart of the patterned CNT fabrication process

Figure 4.16 shows the cross sectional view of one pattern hole. The profile of the etched wall is measured to be 60 μm and is shown in Figure 4.17. Figure 4.18 shows the CNTs inside the pattern, showing that randomly oriented CNTs have been successfully synthesized inside the silicon pattern.

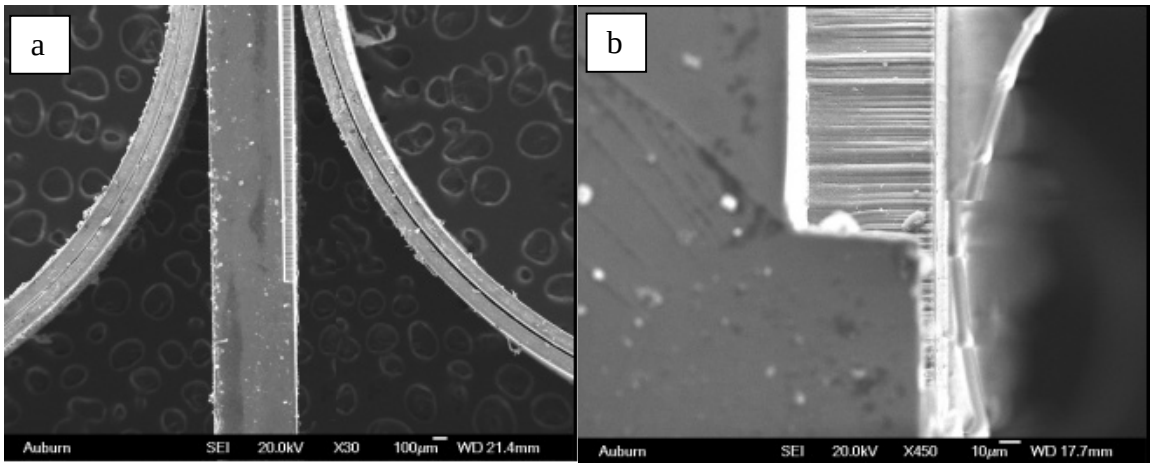

Figure 4.16 Cross sectional view of one pattern hole (a) one pattern square (b) enlarge view of the square edge

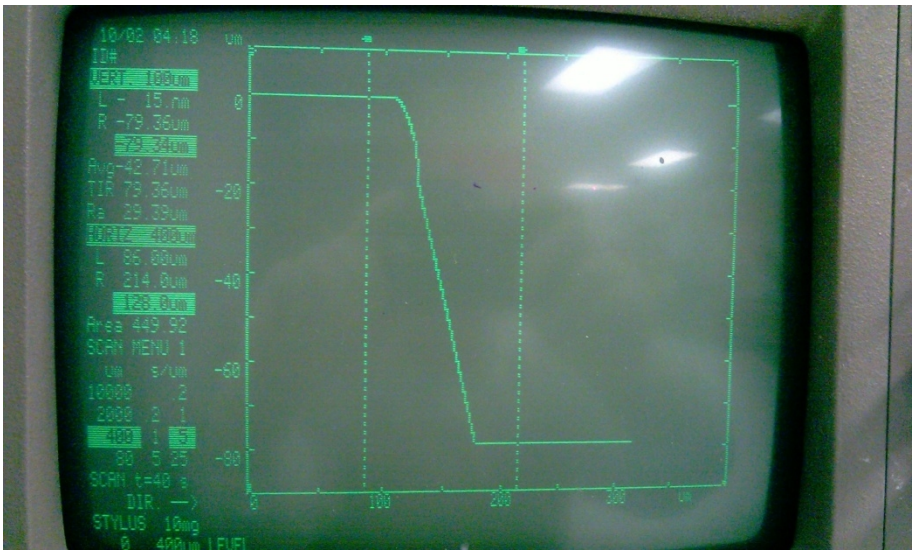

Figure 4.17 Profile of the pattern hole edge

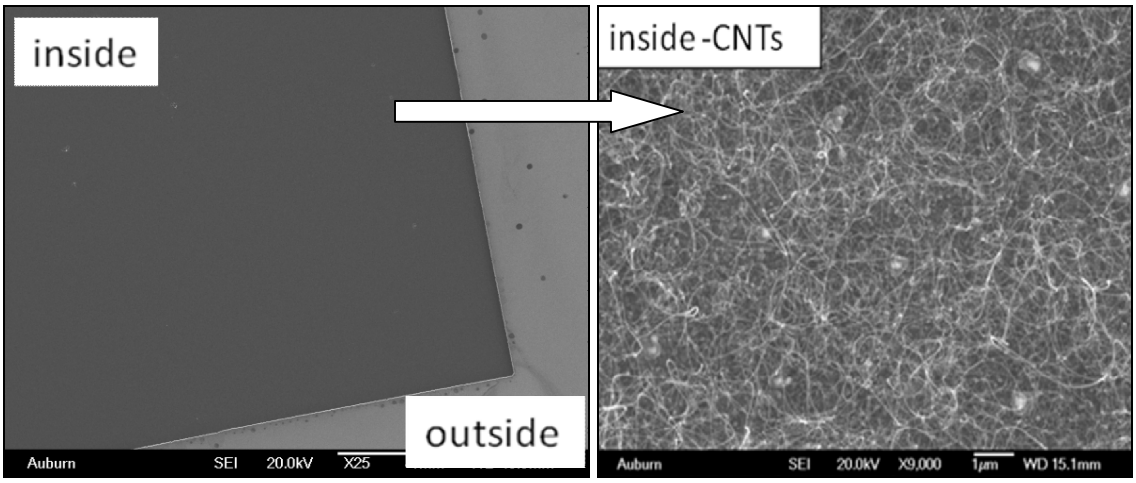

(a) (b)

Figure 4.18 Patterned CNTs (a) top view of the patterned CNTs (b) enlarge view of the CNTs inside the pattern

4.5 Electrical Properties of CNTs

4.5.1 Electron field emission

Electrical properties of CNTs are characterized through electron field emission measurements in vacuum. Electron field emission is the extraction of electrons from a solid, by tunneling through the surface potential barrier when a strong electric field is applied. The emission current, formed by the extracted electrons, represents the electrical ability of the material being tested.

In order to test the field emission properties of fabricated CNTs, a vacuum chamber equipped with ports for electrodes, pressure gauges, and other associate circuits is used in the experiment. The schematic test circuit is shown in Figure 4.19.

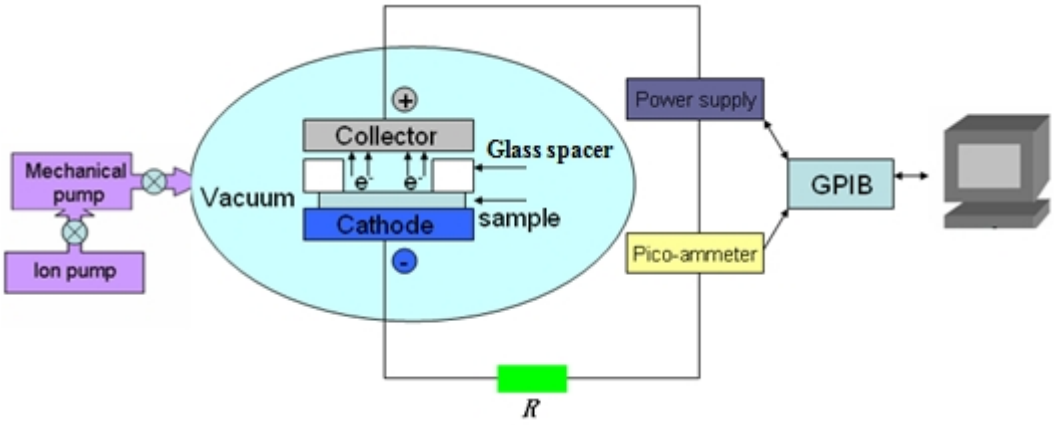

Figure 4.19 Schematic of the field emission test system [88]

By using the mechanical and turbo molecular pump, the pressure of the chamber is maintained at vacuum pressure of less than $1x10^{-6}$ Torr. The glass spacer placed between cathode and anode is 140 μm in thickness and the current limiting resistor is 3 MΩ. The glass spacer has two functions in this test. First, it works like a dielectric layer between anode and cathode. Second, it defines the electron emission area on the CNT surface. With the glass spacer, electric field and emission current density are calculated from the raw I-V data acquired from the oscilloscope. The applied voltages, ranging from 0~1200 V from a 5 kV high voltage power supply, are divided into three zones with three different increments. The first zone and the third zone are corresponding to the dark current emission stage, where electrons are not started to emit, and the saturated current emission stage, where the current stays at the maxim emission mode. The current in these two stages does not change much and the voltage increment is set at 80 V. In the second zone, the emission current experiences the transient from dark current to the saturated current, providing the turn-on field information. The increment in the second zone is set at 10 V so that more detailed information can be obtained.

When testing, a set of increasing biased voltages (0~1200 V) is applied between the cathode (the CNTs sample holder) and the anode (the electron collector) with controlled increments mentioned above. This results in an "up" I-V curve. Then, voltage gradually decreased back to zero following the same increments to get a "down" I-V curve. This process is repeated several times until the "up" and "down" I-V curves overlap. Current data are acquired from a pico-ammeter through the GPIB card and transferred to computer. Both the electric field and the current density data are calculated with the following equations,

$$E = \frac{V - IR}{d}$$

$$J = \frac{I}{S}$$

where R is the resistance of the current limiting resistor with a value of 3 MΩ, d is the gap distance of 140 μm, and S is the emission area of 0.0316 cm^2. The test data are displayed in a MATLAB based program. For each applied voltage, five current data with 1 second interval are recorded to assure the test accuracy. Figure 4.20 shows the MATLAB program interface and Figure 4.21 is a measured field emission characteristic of random CNT sample with 40 min growth time (a) and aligned CNT sample with 40 min growth time (b).

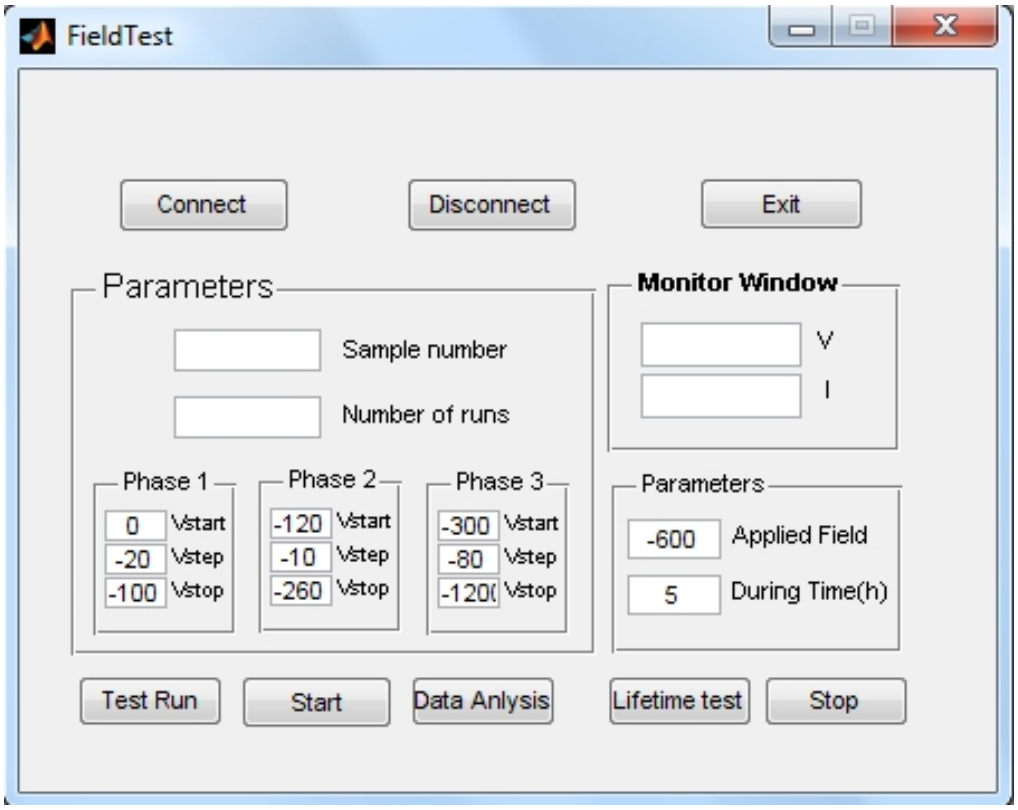

Figure 4.20 Interface of the test program

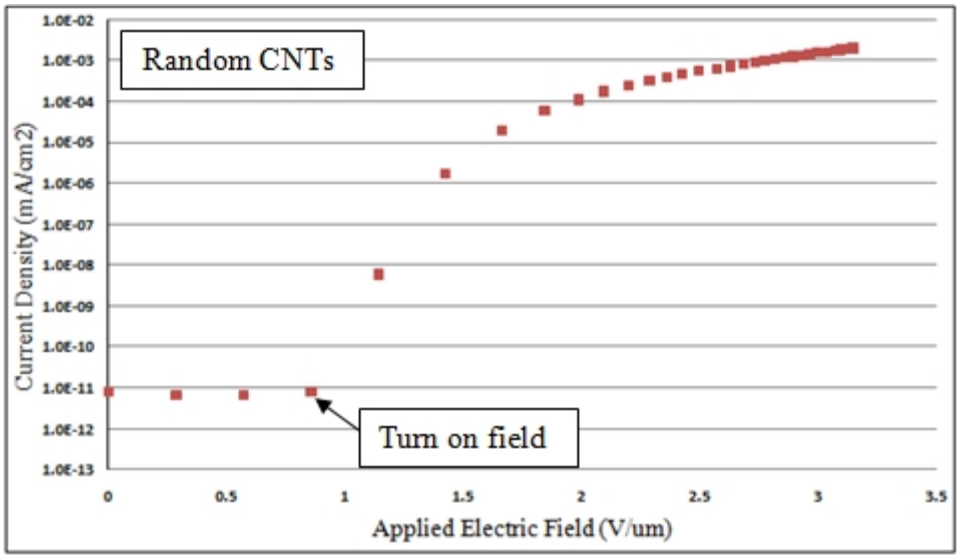

(a)

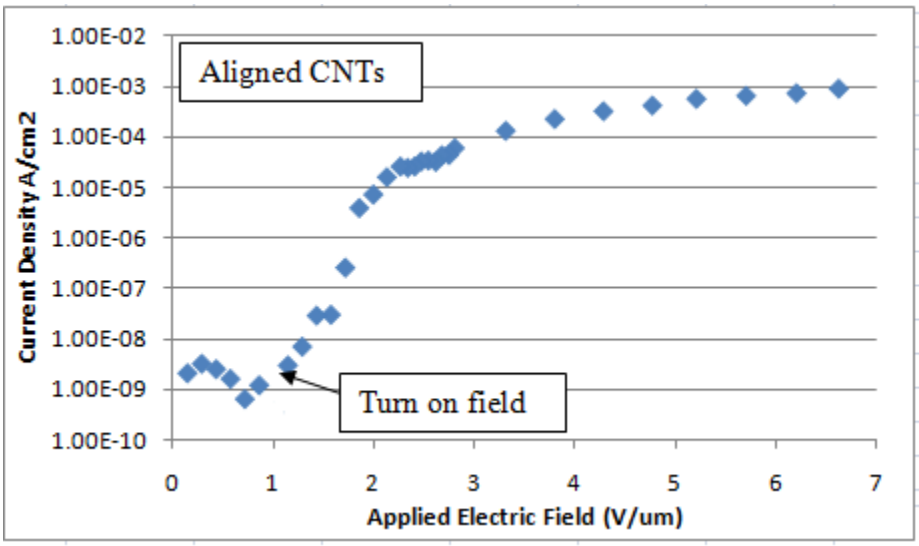

(b)

Figure 4.21 Field emission characteristic of random CNTs and aligned CNTs sample with 40 min growth time, (a) Random CNTs, (b) Aligned CNTs

In Figure 4.21, before the applied electric field reaches a certain point, the current density remains at the dark current level of 10^{-11} A/cm^2 for random CNTs testing and 10^{-9} A/cm^2 for aligned CNTs testing depends on the current noise level. This threshold electric field is termed as the "turn-on field" and is defined as the applied electric field where the current density is at least one order higher than the dark current density. For the data shown in Figure 4.21, the turn-on field is around 0.857 V/μm for random CNTs and 1 V/μm for aligned CNTs.

4.5.2 Turn-on filed and life time measurements

Compared to other electron emitter materials, CNTs exhibit low turn-on field and high saturation current density. There are very few studies interpreting the relationship between the low turn-on field and the length and density of the CNTs, which is related to the growth time in CVD. Understanding of this relationship is important in the

optimization of synthesis of CNTs and improves the cold-cathode emitter's performance.

For this, the CNTs are grown based on different growth time durations, namely, 10 min, 20 min, 40 min, 80min 120 min and 240 min, respectively. SEM imaging is used to examine the tube length and density. Field emission results are analyzed to investigate the CNTs growth time dependency of the turn-on field. Also, the CNTs life time is tested by repeating 100 consecutive runs of field emission tests.

Figure 4.22 shows the SEM images of the six CNTs samples mentioned above. Randomly oriented CNTs grow in all directions and tubes twine up, which leads to the difficulties on quantitative measurements of CNTs density. But, it can be qualitatively seen from the SEM images that the tube length and tube density increases with the growth time. Comparing the sample growth time of 240 min to 10 min sample, the 240 min sample clearly contains more tubes. Figure 4.22 also shows that all of CNTs samples used in this study have good quality with very few clusters.

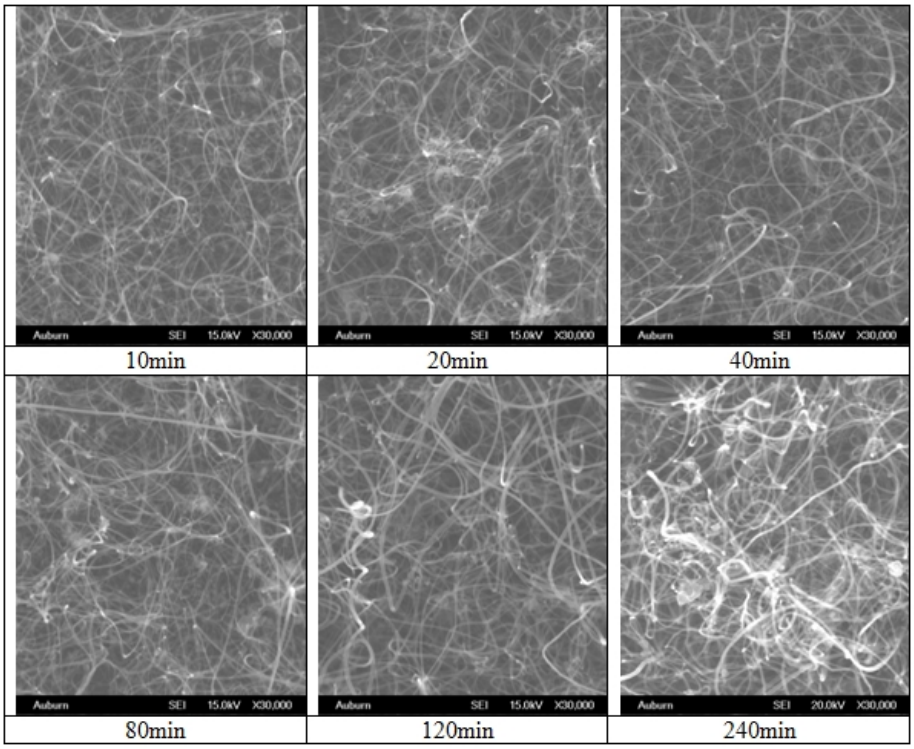

Figure 4.22 SEM images of CNTs samples under 30k magnifications

Field emission characteristics of these six CNT samples are tested and the results are shown in Figure 4.23. As seen in this figure, field emission characteristic curves are orderly arranged in a way that as the growth time increases, the turn-on field decreases. Thus indicates that the CNTs sample with longer growth time has lower turn-on field. The lowest turn-on field is 0.5 V/μm belongs to the 240 min growth time sample and the highest turn-on field is 1.02 V/μm belongs to the 10 min growth time sample.

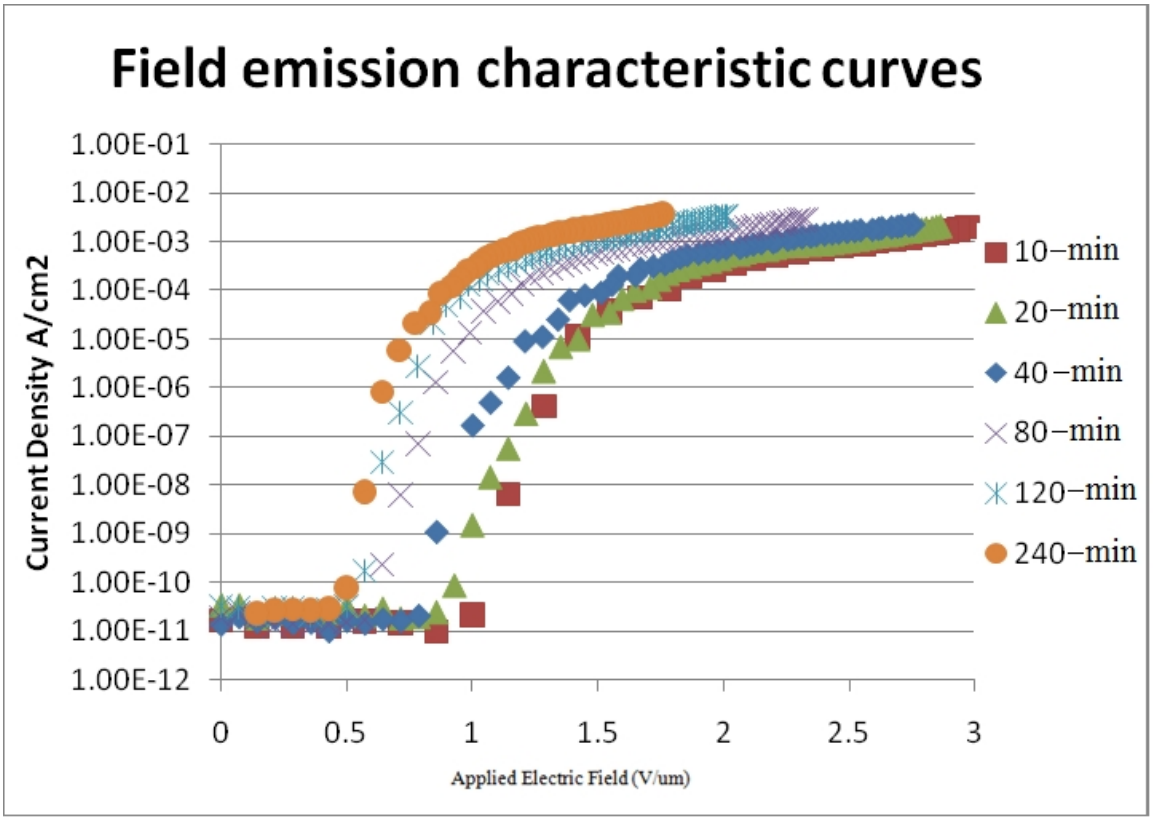

Figure 4.23 Field emission characteristics of CNTs samples

The turn-on fields for all six samples are listed in Table 4.1 and plotted as a function of growth time in Figure 4.24. An exponentially decreasing curve is observed. The turn-on field drops dramatically at the beginning, and stabilizes between 0.5~0.6 V/m after the growth time is longer than 80 min. Increasing the growth time further does not decrease the turn-on field substantially.

When the growth time is short, i.e. 10 min, the CNTs are short in length and loose in density, which means there are less electron emitting spots. As the growth time increases, CNTs become longer and denser, raising more electron emitting spots. As a result, the turn-on field decreased. However, increasing the tube length and tube density reaches a limit of the turn-on field. In this case, the field enhancement on the surface is

not as efficient. When the CNT density is high, the tubes form almost a flat surface and "Screen Effect" occurs. The screening effect is due to the close proximity of the tubes and it is known that it could seriously affect the emission current [89]. This leads to the fact that the current density remains almost the same no matter how long and how dense the tubes are.

Table 4.1 Turn-on field of the tested CNT samples

Growth time (min)	10	20	40	80	120	240
Turn-on field(V/μm)	1.02	0.91	0.78	0.6	0.53	0.5

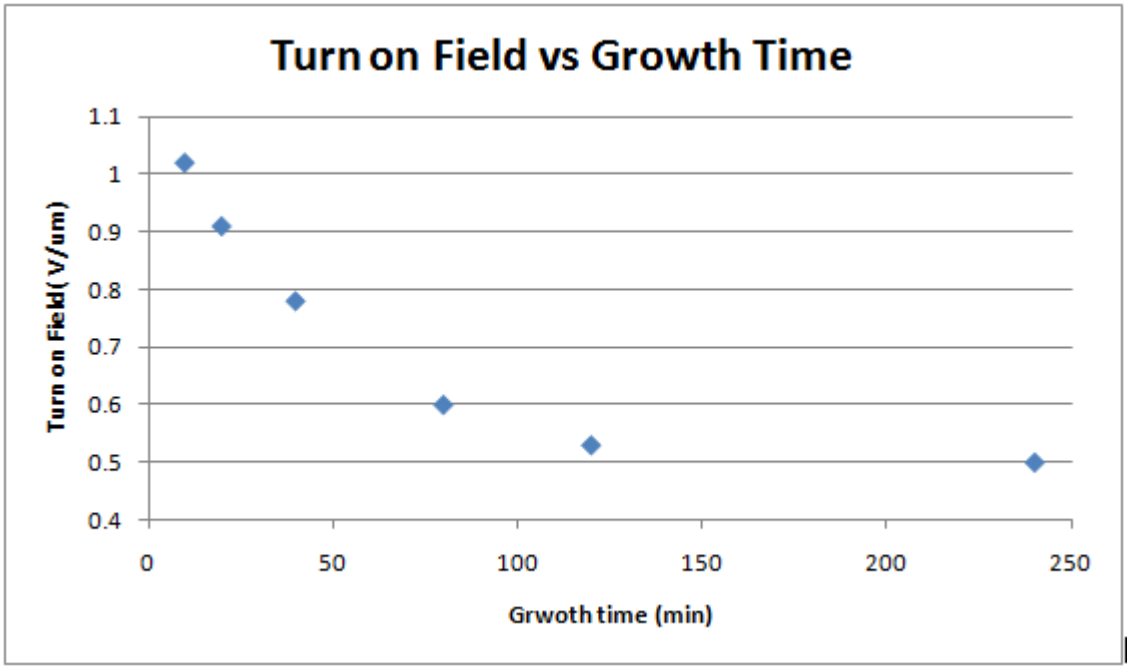

Figure 4.24 Turn-on field vs. growth time

Life time test of CNTs as cold cathode emitter is also examined by repeating 100 consecutive field emission tests for samples with 10 min and 240 min growth time only. The turn-on fields are shown in Figure 4.25. For the 10 min growth time CNT sample, the turn-on field starts at 1.02 V/μm at first and stabilizes at 1.14 V/μm after 30th run. The

turn-on field of 240 min growth time sample starts at 0.5 V/μm and stabilizes at 0.57 V/μm after 50th run. Both turn-on fields increase about 0.1 V/μm for repeating the test for 100 times. This data show a good working life time for both samples after several conditioning runs. Comparing these two samples, 240 min growth time sample needs more conditioning runs, which is reasonable because 240 min sample emits more electrons, which generates more heat. We speculate that the heat accumulates in the CNTs and damages weak tubes until a balance is reached.

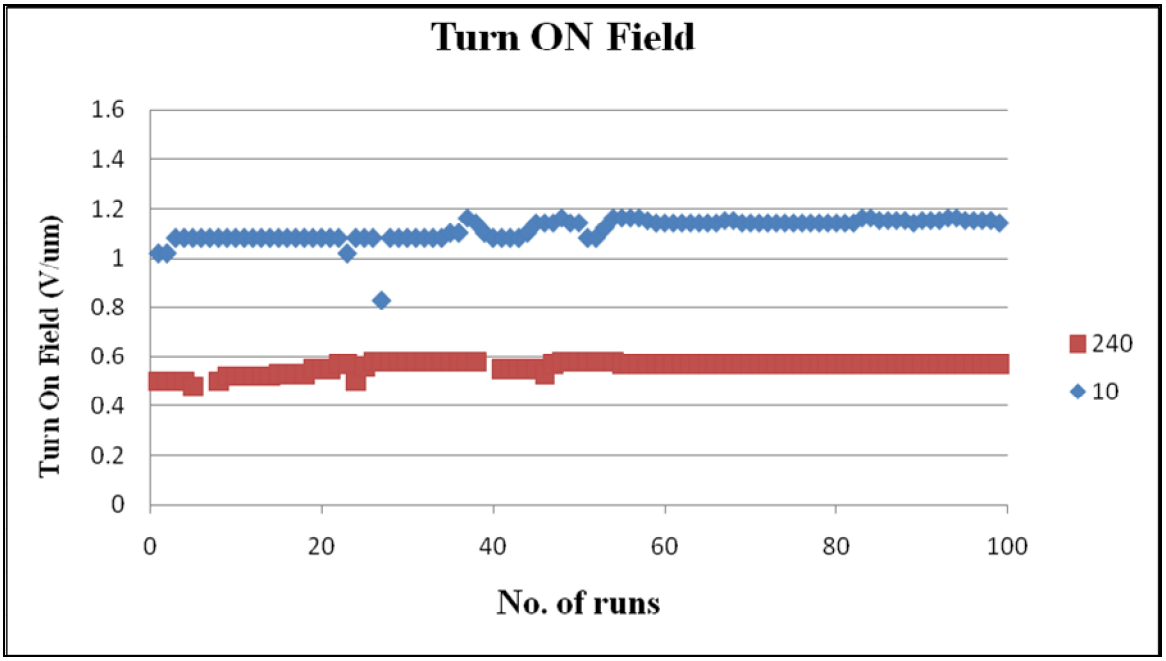

Figure 4.25 CNTs life time test

Chapter 5

Triggered Pseudospark Switch Construction and Test

5.1 Switch Body Construction

The hollow cathode effect is a crucial point in the pseudospark switch design. In this project the hollow cathode effect is implemented in the switch hardware configuration shown in Figure 5.1. The designed pseudospark switch consists of a U-shaped hollow cathode, planar anode, CNT coated trigger electrode, and periphery circuitry. A quartz tube, 8 cm long and 2 cm in diameter, is used as the switch enclosure forming the vacuum chamber. The U-shape electrode is pre-machined with a 2 mm diameter bore hole drilled on the front surface, and the planar anode, made out of a circular copper plate with a diameter of 1.8 cm, is placed 3 mm away from the cathode front surface. The CNTs electron emitter coated trigger electrode is held on a specially machined alumina holder, and placed at the open-end side of U-shape cathode, where the CNTs are fully exposed to the electric field. The overall switch is shown in Figure 5.1 and the CNTs holder is shown in Figure 5.2. The switch is well sealed in a vacuum chamber that can be kept in vacuum of $1x10^{-6}$ Torr when not operated.

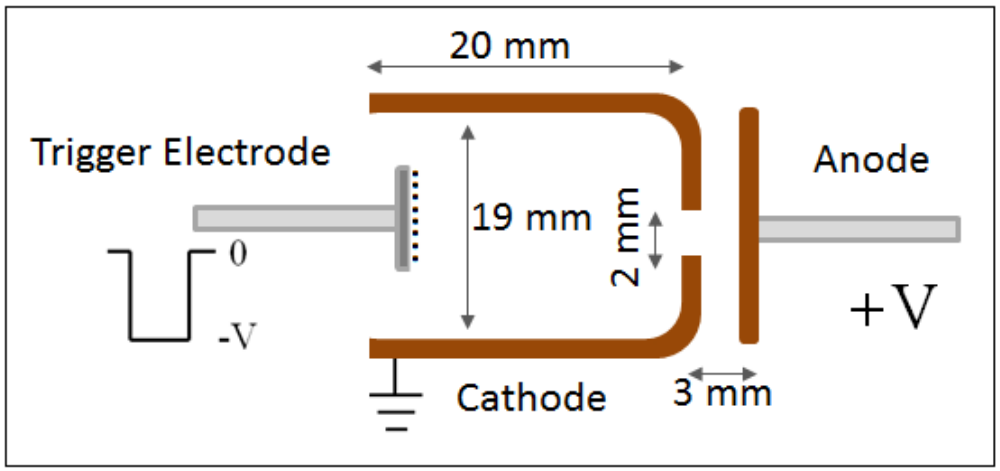

Figure 5.1 Sketch of pseudospark switch

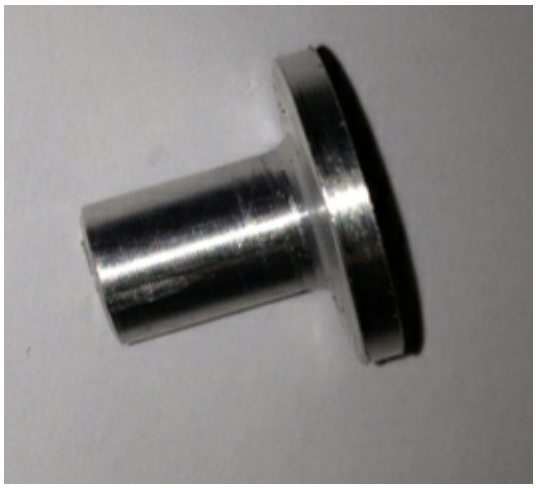

Figure 5.2 Sample holder serving as part of the trigger electrode

The switch is designed to operate from a few mTorr to 100s of mTorr pressure by using a combination of a mechanical pump and a turbo pump. A gas inlet system is connected to the switch enclosure to which different inert gas, such as Helium, Argon, or Nitrogen, is selectively fed. The anode is connected to a 35 kV DC power supply through a 22 MΩ current limiting resistor, and the hollow cathode is grounded. The trigger electrode is connected to a negative pulse generator where negative pulse up to 1000 V

and current up to 50 A can be generated. In a single pulse, the trigger pulse rise time is less than 100 ns with a pulse width in the range of 0.5 to 1 ms. Different pulse width can be obtained by changing the resistance in the discharging circuit of the pulser. The assembled switch chamber is shown in Figure 5.3.

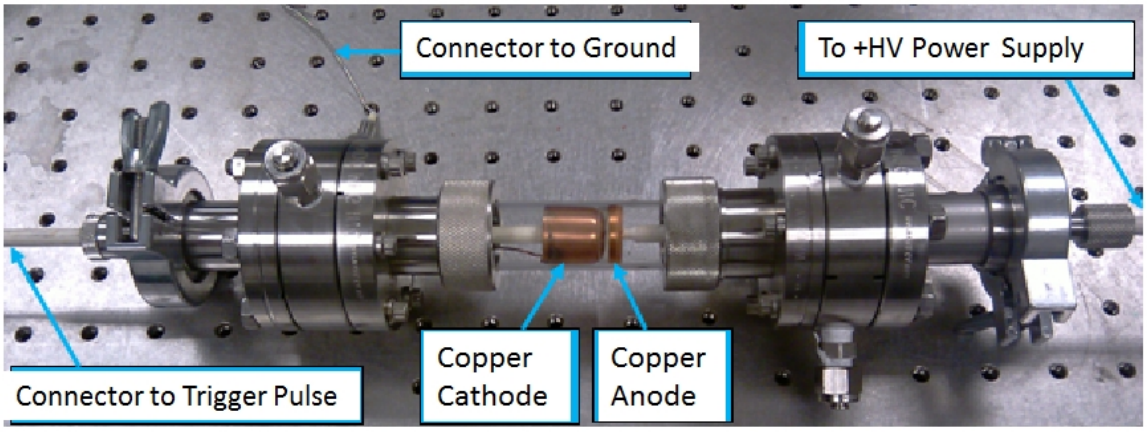

Figure 5.3 Assembled PSS Switch Chamber

5.2 Test Experimental Setup

In the experiments, hold-off voltage, trigger delay, and jitter are measured. Figure 5.4 shows the schematic of the experimental setup with the diagnostics. The hold-off voltage is measured through a high-voltage probe with 2000 attenuation, and the pulse voltage is measured with another high-voltage probe with 1000 attenuation. The current data is measured through a Rogowski current transformer in which the current is converted into voltage. Both voltage and current data are collected by an oscilloscope through a USB cable and recorded by a computer. Data is analyzed once each experiment set is completed. Two small holes on the cathode wall are made and a high speed camera is set to capture the visual information of the plasma formation in the cathode cavity.

Consecutive frames of the video images can be obtained to examine the transit plasma formation.

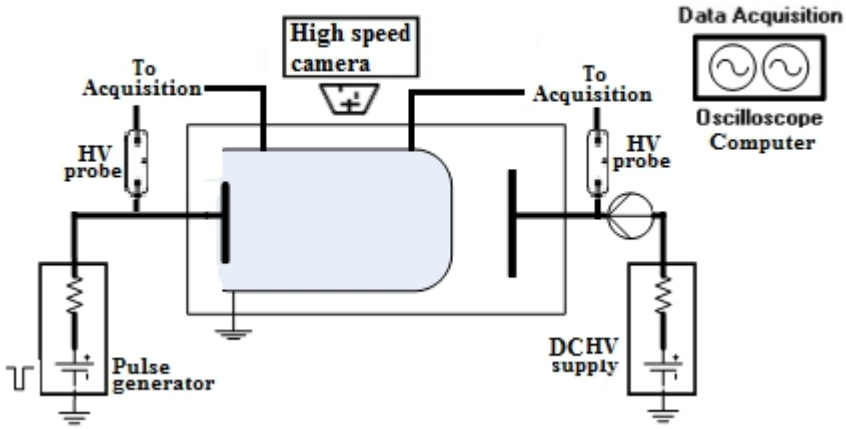

Figure 5.4 Schematic of the test experimental setup with diagnostics

The switch is first tested without triggering to determine the maximum breakdown voltage at a given background pressure. This determines the hold off voltage of the switch. Then it is tested with CNTs triggering to analyze the switch performance, such as the delay time and jitter. Five trigger electrodes are fabricated with different types of CNTs. The switch operating characteristics are analyzed for each trigger electrode having different CNTs. Switch performance comparisons are made based on these trigger electrodes. The test procedure is listed as follow:

1. Hold off voltage test in different pressures
2. Trigger delay time test with different trigger voltages
3. Conduction current and current rise time test with different trigger voltages
4. Jitter calculations based on delay tests.

5. Repeat of trigger delay test time for the remaining trigger electrodes having different CNTs, namely, random CNTs, aligned CNTs, and CNTs with different growth time

5.3 Switch Hold-off Measurements

The switch is first tested without triggering to determine the maximum self-breakdown voltage by gradually increasing the anode voltage until a breakdown event is captured and the breakdown voltage is recorded. The Plasma formation is inspected visually by a video camera. One frame-image is shown in Figure 5.5. It clearly shows that the plasma is formed inside of the hollow cavity of the cathode and bridges the two electrodes through bright plasma.

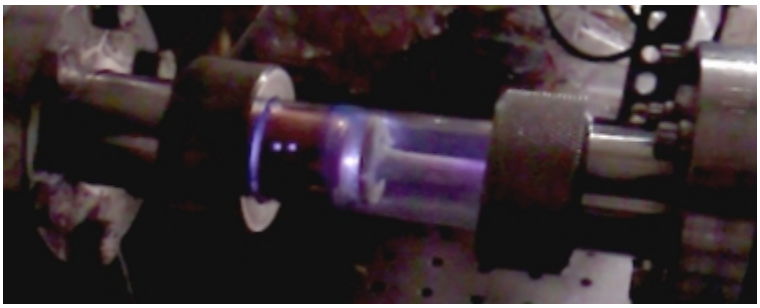

Figure 5.5 Hollow cathode breakdown event

In order to get the breakdown statistic for different pressure, a pressure sweep test is carried out. Helium is fed as the background gas and the pressure varied from 5 mTorr to 100 mTorr for the fixed electrode geometry, as described in Figure 5.1. All breakdown voltages are collected and plotted in Figure 5.6. The breakdown voltage is around 24 kV at 5 mTorr and exponentially decreased to 15 kV at 100 mTorr, showing the switch is operating in the “left side of the Paschen curve” which is the traditional operating pressure region for pseudospark switches [2]. Based on our experimental conditions, 100

mTorr is selected as the switch operation pressure and 12 kV is set as the switch hold off voltage to test the triggered mode operation. Higher hold off voltage can be obtained by decreasing the switch pressure.

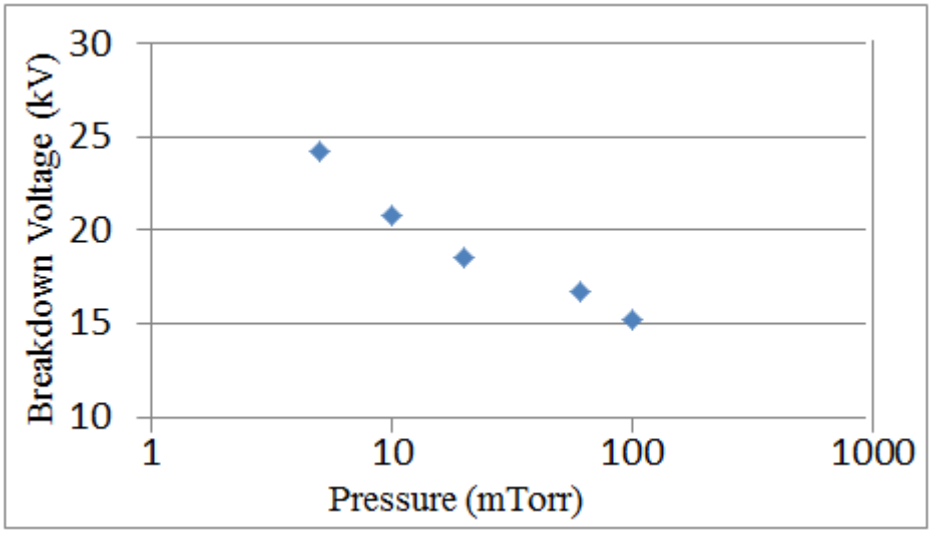

Figure 5.6 Self breakdown voltages of non-triggered switch as a function of pressure

5.4 Switch Operation-Trigger Mode

Once the operation pressure and the hold off voltage are determined, the switch is then tested under trigger mode. Five trigger electrodes based on different types of CNTs are used. These different CNTs are one vertically aligned and four randomly oriented samples fabricated under different growth conditions. The SEM images are shown in Table 5.1 and named as:

Aligned-40: vertically aligned CNTs with 40 min growth time

Random-20: randomly oriented CNTs with 20 min growth time

Random-40: randomly oriented CNTs with 40 min growth time

Random-80: randomly oriented CNTs with 80 min growth time

Random-120: randomly oriented CNTs with 120 min growth time

Table 5.1 SEM images of tested samples

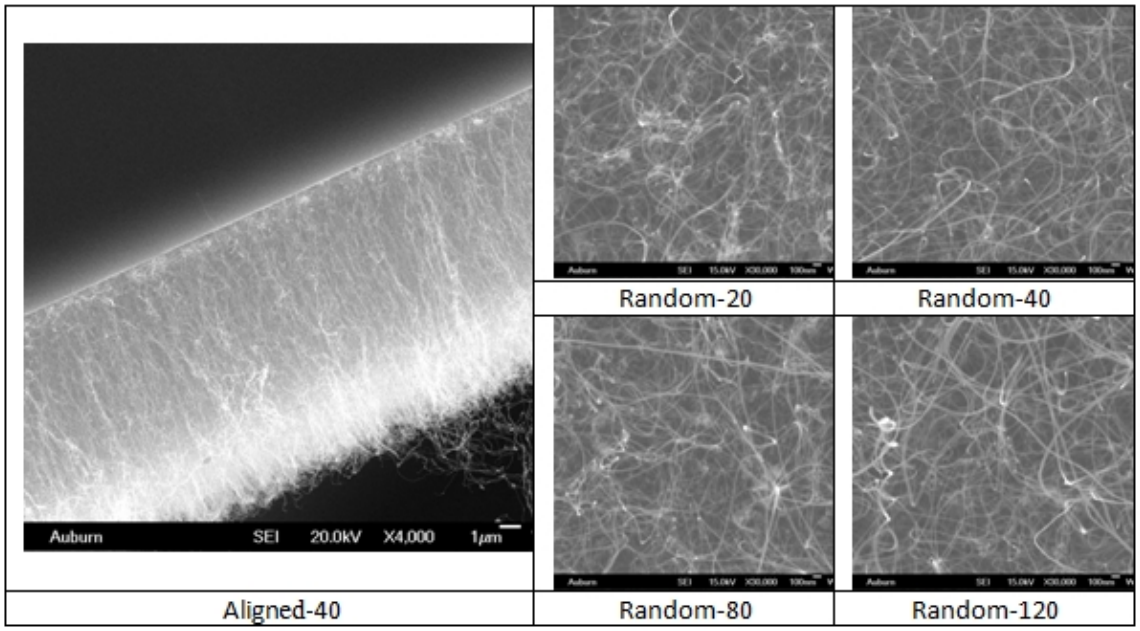

When triggering, the anode is set to 12 kV by the main power supply, and the cathode is grounded as shown in Figure 5.1. The operation pressure is fixed at 100 mTorr. A set of negative trigger pulses, ranging from 200 V to 800V is used to provide the negative bias on the CNTs where the seed electrons are emitted. In a single pulse, the trigger pulse rise time is less than 100 ns with a pulse width in the range of 0.5 to 1 ms. A recorded pulse shape is shown in Figure 5.7.

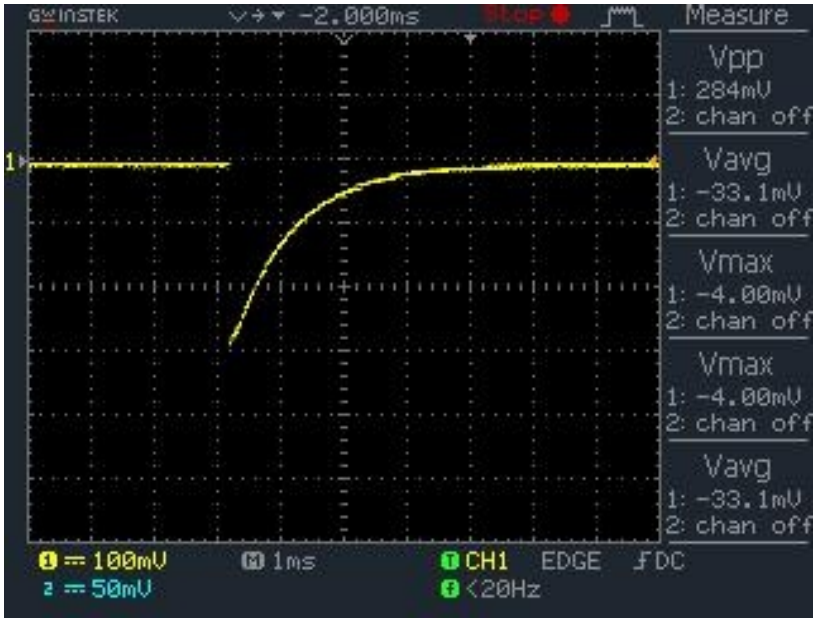

Figure 5.7 Trigger pulse shape

Once the trigger voltage is applied, the plasma forms in the hollow cathode instantly, filing the cathode cavity with bright light. Meanwhile, it propagates towards the anode rapidly, bridging the two electrodes in a very short time. The image of the triggered breakdown event is shown in Figure 5.8, and the triggered breakdown waveforms are shown in Figure 5.9. The upper curve is the hold off/applied voltage, and the bottom curve is the trigger voltage. It can be seen that the applied voltage drops dramatically and almost simultaneously when the pulse trigger applies. The voltage across the cathode and anode gradually recovers to where plasma is formed momentarily within the switch, and to the value to maintain glow-discharge mode for a very short time. The pseudospark switch is designed to operate in a non-self-sustaining mode so the whole discharge and plasma event takes place in about 3 to 4 ms. Once the breakdown occurs, the stored energy is fully discharged until the external circuit is charged again

bringing the two main electrodes back to the hold off voltage through the 22 MΩ current limiting resistor.

It should be noted that the emphasis in this dissertation is put on the initiation of the plasma and the operating characteristics of CNTs field emitted electron triggering information, such as the delay time and jitter. Other information, such as the discharge operation, and maximum peak power are not in the scope of this work.

Figure 5.8 Triggered breakdown event

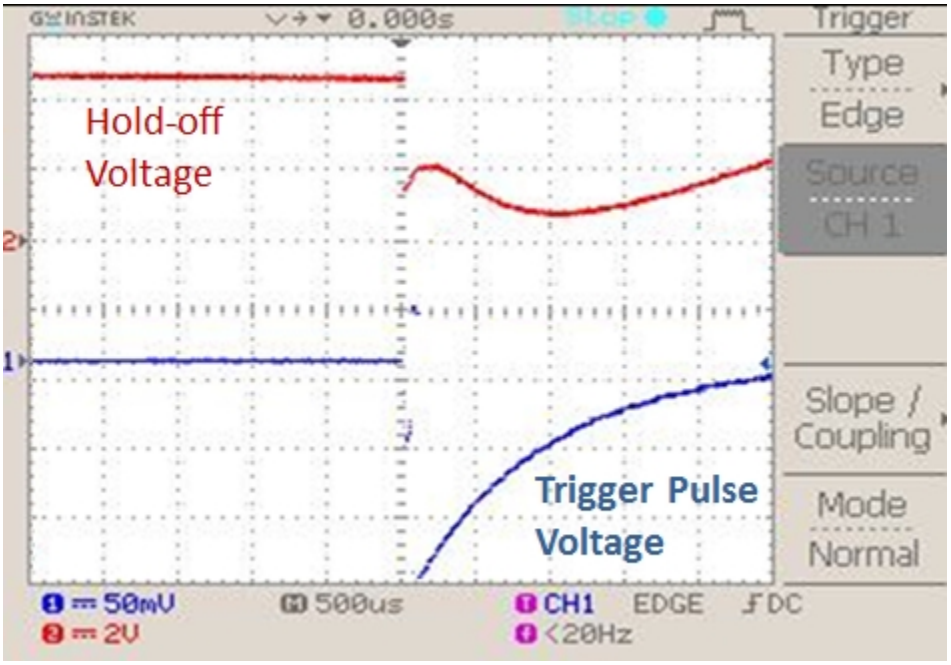

Figure 5.9 Triggered breakdown waveforms

5.4.1 Delay time measurements and analysis

Second step of the experiments is to examine the delay time variation as a function of the trigger voltage for a fixed trigger electrode. Five trigger pulse voltages, namely 200 V, 400 V, 600 V, 700 V and 800 V, are used in this test. The trigger sample is selected and fixed at the random CNTs with 40 min growth time. The SEM image of this sample is shown in Figure 5.10.

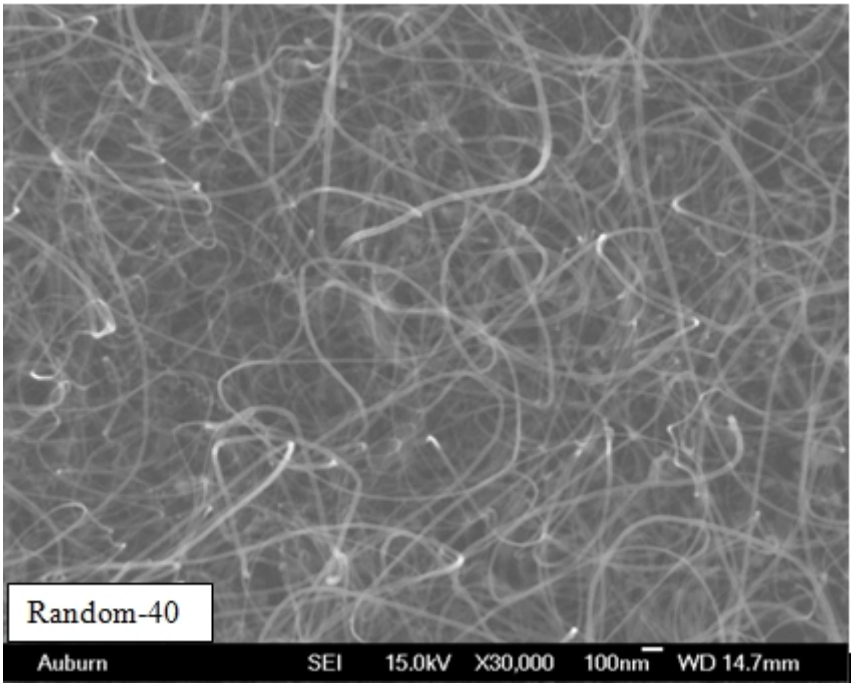

Figure 5.10 SEM image of CNTs used as the trigger electrode

In this dissertation, the delay time is defined as the time difference between the initial drop points of both the trigger and the hold off voltage, as illustrated in Figure 5.11. For each trigger voltage, the delay time is recorded and calculated as defined. This process is repeated for several times and the delay time is averaged for each designated trigger voltage. The overall delay time as a function of trigger voltage for Random-40 CNTs sample is shown in Figure 5.12. As can be seen, the lowest delay time is for 800 V

trigger pulse voltage with 3 μs, where the longest delay is for 400 V trigger pulse voltage with 9 μs. The trigger pulse voltage of 200 V did not trigger the switch. This result can be seen by the field emission data of this CNT sample shown in Figure 5.13. The 200 V triggering voltage is below the turn-on voltage of the CNTs where no emission current is detected. As a result, the switch failed to trigger. The trigger pulse voltage of 400 V is above the turn on voltage of the CNTs and produces almost 2 μA current. Although the switch can be triggered by the field emitted electrons, the delay time is relatively long due to the low level of the current emission. When the trigger voltage is above 600 V, the emission current reaches 10~100 μA, which results in a steady decrease in the delay time from the previous case. Figure 5.13 also shows that the field emission current continues to increase for trigger pulse voltage of 700 V and 800 V. The corresponding delay times of these two voltages triggering decrease as the trigger pulse voltage increase. Based on this trend, shorter delay time is possible for larger trigger voltage. This phenomenon can be explained that when the trigger voltage increases, the electric field on the CNTs increases as well. As a result, electron emission increases. Moreover, the emitted electrons are further accelerated in the cathode cavity by the higher electric field and plasma can be initiated easier with shorter delay time.

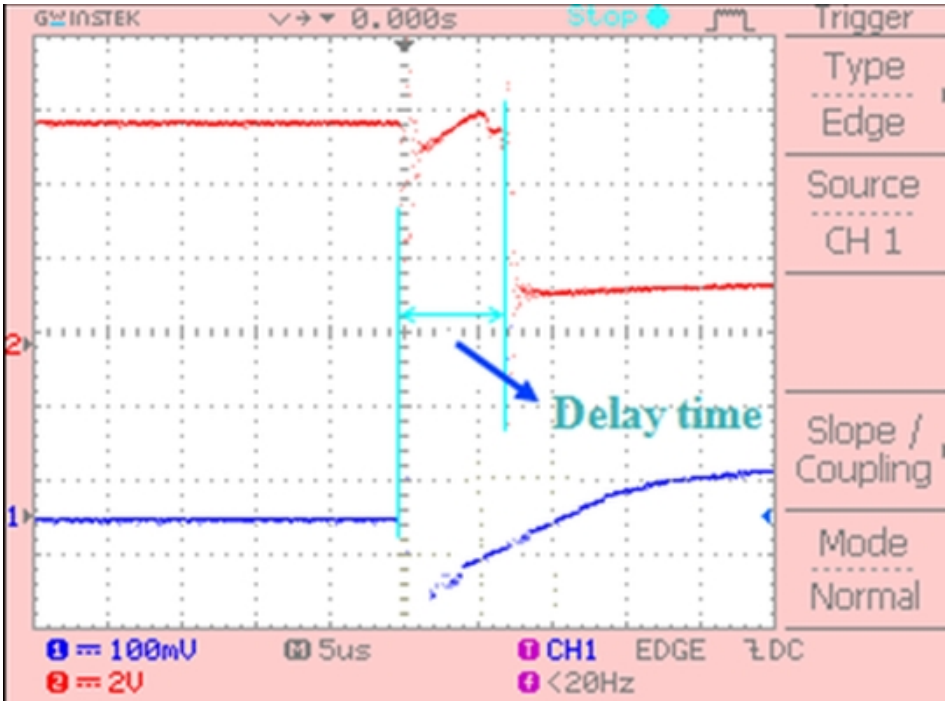

Figure 5.11 Delay time

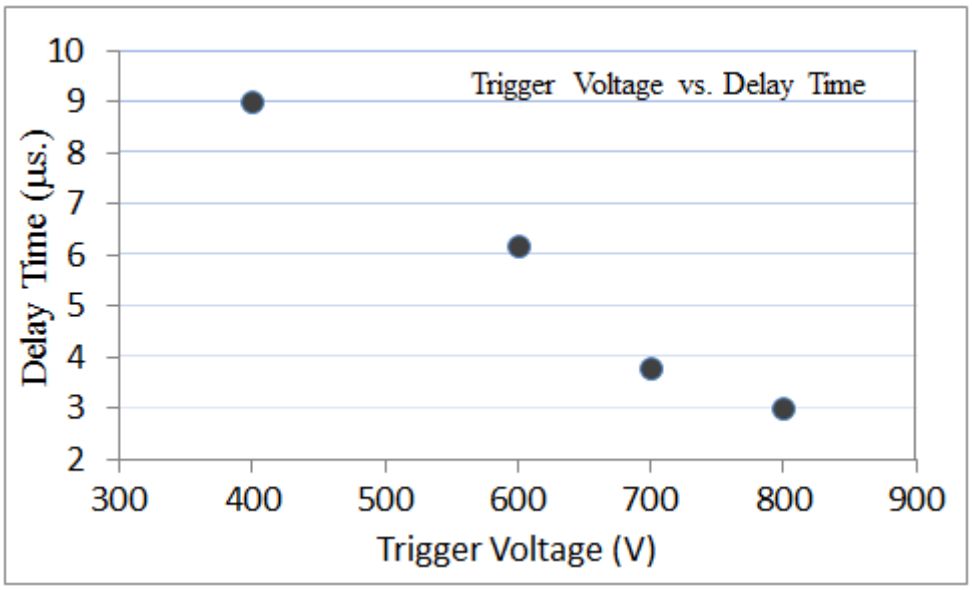

Figure 5.12 Delay time variation

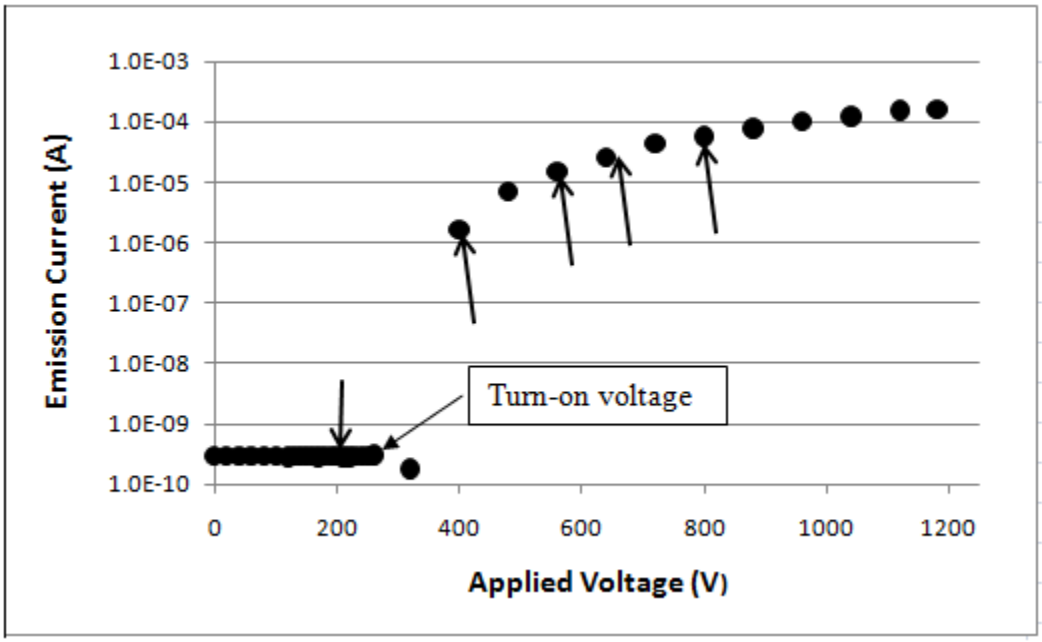

Figure 5.13 Field emission characteristics of Random-40 CNT sample

5.4.2 Conduction current and current rise time

The conduction current is measured through a Rogowski current transformer. Figure 5.14 is a representative of the current waveform of a breakdown event from these measurements. The current rise time for each trigger is calculated. The peak current in these experiments ranges from 0.6 A to 1 A depending on the applied trigger pulse voltage. Although pseudospark switches are operated at kA ranges, in our experiments, we are only interested in the feasibility of triggering by use of CNTs. Therefore, a current limiting resistor is used to limit the conduction current in the order of 1 A range in the switch.

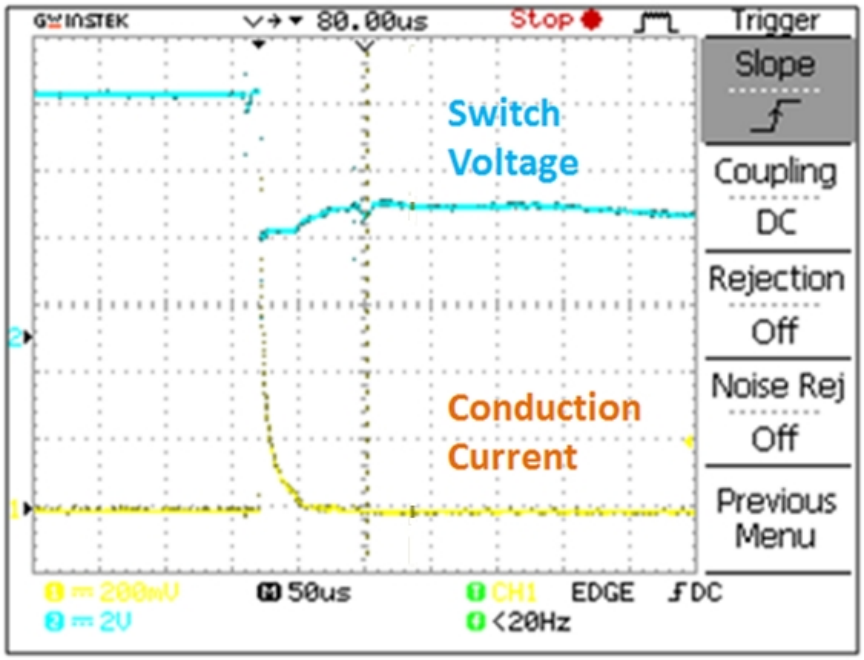

Figure 5.14 Screen shot of current waveform at switch closing

Similar to the definition of the delay time, the current rise time is measured as the time difference between the trigger voltage drop and the maximum peak current. Shorter current rise time is a desired parameter in a switch operation. The test results for different triggering voltages are plotted and shown in Figure 5.15. Similar to the delay time, the current rise time is also inversely proportional to the applied trigger pulse voltage. The current rise time is 520 ns for trigger pulse voltage of 400 V and decreases to 240 ns for trigger pulse voltage of 800 V.

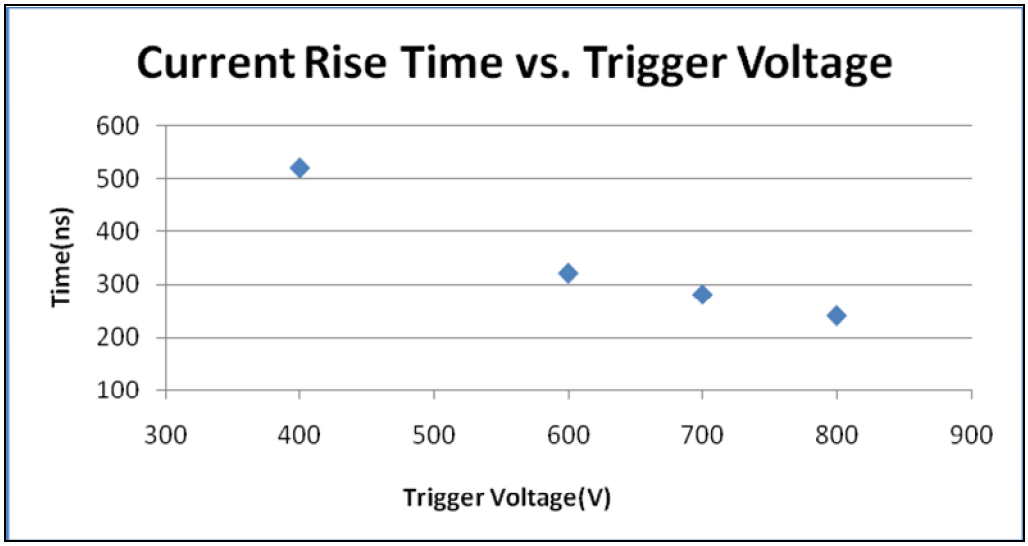

Figure 5.15 Current rise time variation as a function of trigger pulse voltage

5.4.3 Jitter time calculation

In this dissertation, the jitter time is defined as the standard deviation of delay time for the successive switch closing and is calculated using Equation (1) based on twenty repetitions of the switch trigger.

$$s = \sqrt{\frac{\sum (x_i - \bar{x})^2}{n}} \tag{1}$$

where the $\bar{x}$ is the average value of the twenty delay times, n is the total repetition number. Experimental conditions are kept identical throughout repetitions and the delay times for four different trigger voltages for number of tests are plotted in Figure 5.16. The calculated jitter time is shown in Table 5.2. The results show that hundreds of ns jitter time is achieved in this triggering method.

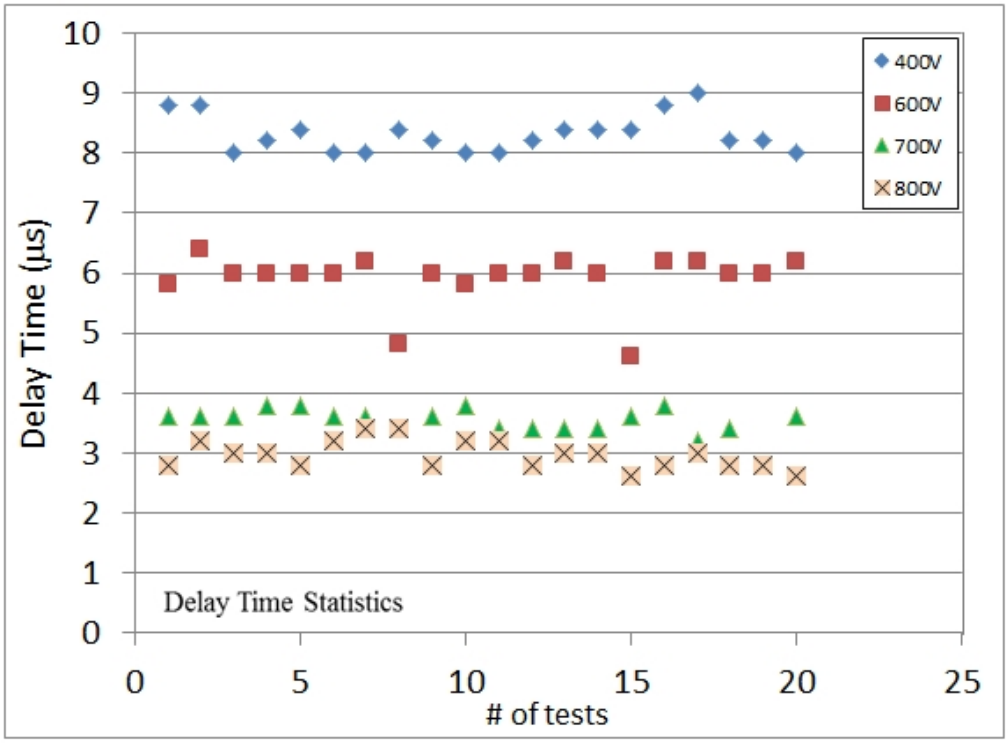

Figure 5.16 Statistics of delay time

Table 5.2 The jitter variation

Trigger voltage	400V	600V	700V	800V
Jitter	314ns	442ns	238ns	236ns

5.5 Switch Operation under Different CNTs as Trigger Electrode

The switch operating characteristics are examined based on the remaining four different types of CNTs trigger samples and the switch performance comparisons are made in terms of delay time. The field emission data of all the randomly oriented CNTs is shown in Figure 5.9, whereas the field emission data of vertically aligned sample shown previously in Figure 4.21 (b). The delay time for the random CNT samples are processed as outlined in the previous section and presented in Figure 5.17. The random-20 min sample has the longest delay time, while the random-120 min sample has the

shortest delay time, for all trigger voltages. Similar to the previous case, the trigger pulse of 200 V pulse can not trigger the switch except for the random-120 min sample. The data is consistent with the electron field emission abilities of each sample.

As introduced earlier, the delay time of the switch depends on the performance of the trigger material. Therefore, the CNT electrical property, characterized as the electron field emission characteristics, play a significant role in the switch operation and the delay time. If the CNT sample has longer and denser tubes as a result of longer growth time, the turn-on field is decreased. Therefore, the delay time is predicted to be shorter. This is confirmed by the field emission data in Figure 5.18, where the random CNTs with 20 min growth time have a turn-on field of 0.89 V/μm while the random CNTs with 120 min growth time have a turn-on field of 0.56 V/μm. As a result, random-120 sample has the lowest delay time over all, while random-20 sample has the longest delay time for all the different trigger pulse voltages.

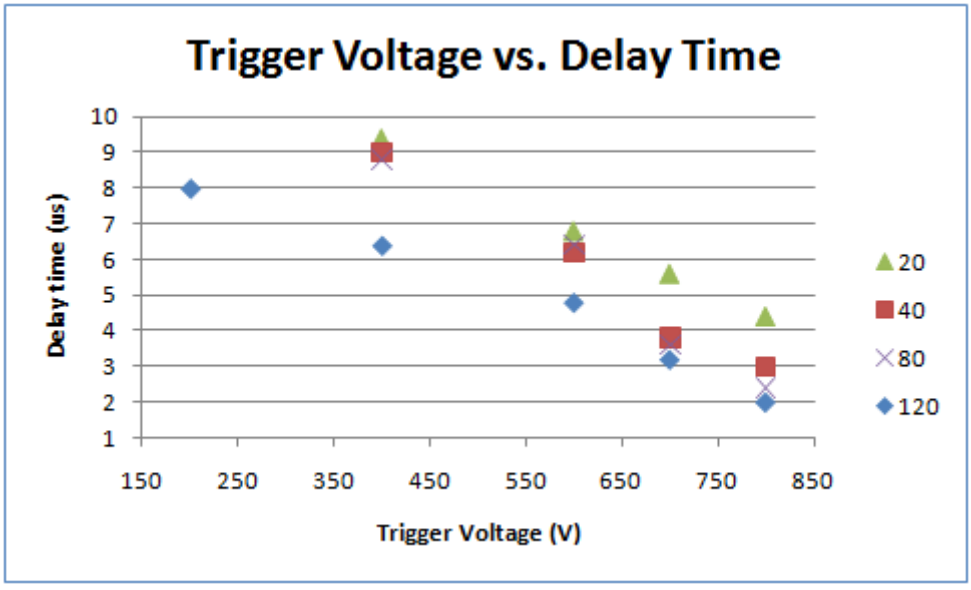

Figure 5.17 Delay time of different CNTs samples

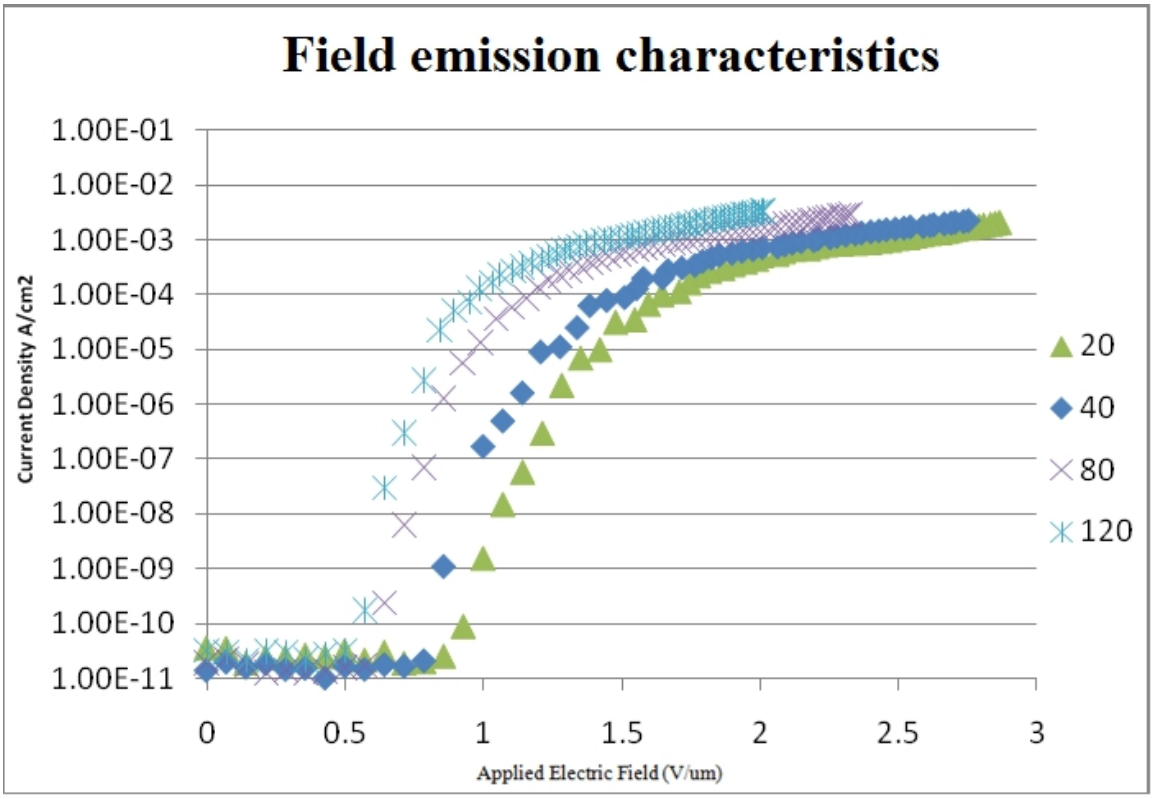

Figure 5.18 Field emission characteristics of random CNT samples

The aligned CNT sample with 40 min growth time is also used to trigger the switch. Figure 5.19 compares the turn-on field of both aligned and random CNTs samples in different pressure. In both case, the turn-on field of the samples increases with the pressure. In vacuum, the turn-on field is around 0.98 V/μm for the aligned-40 sample, which is larger than the turn-on field of random CNT sample with 40 min growth time in the same vacuum condition. On the other hand, the turn on fields of random-40 and aligned-40 are 2.5 V/μm and 3.8 V/μm in 20 mTorr pressure, respectively.

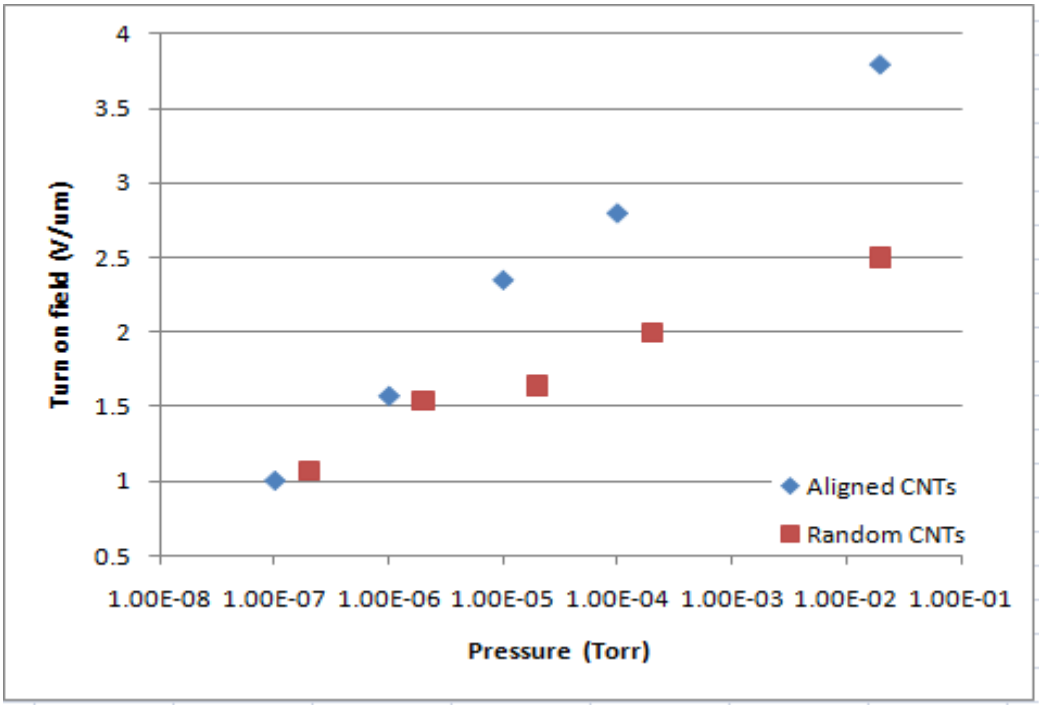

Figure 5.19 Field emission results of rand and aligned CNTs in partial vacuum

Figure 5.20 compares the delay time for aligned and random CNT samples in the condition of 40 min growth time. The result shows that the delay times triggered by these two samples are comparable and the delay time based on the aligned CNT triggering is a little bit smaller, which seems to conflict with the field emission test results mentioned above. A further study reveals that these two samples have different emission area. The aligned CNT sample has a large area, which compensates the disadvantage of higher turn-on field. The turn-on fields and the sample area are listed in Table 5.3.

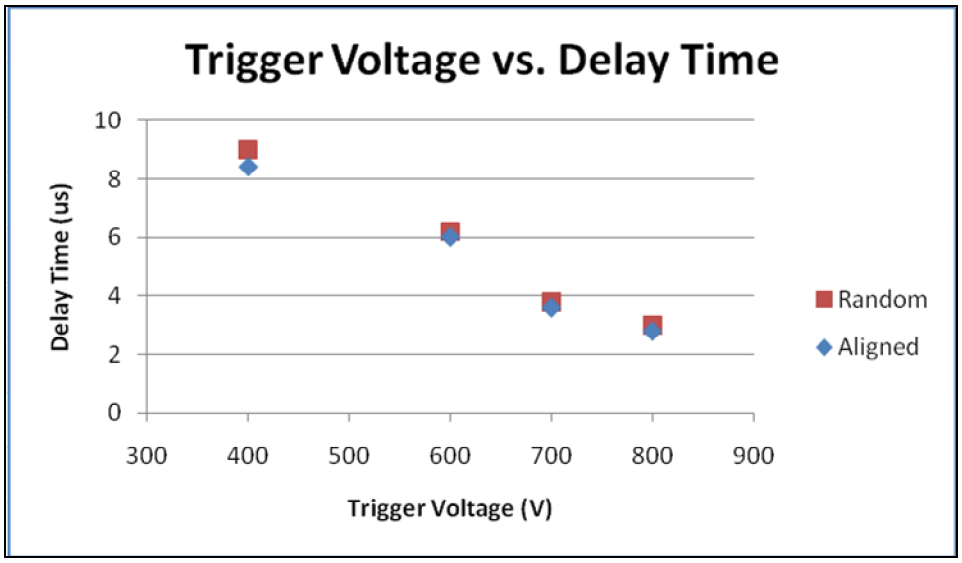

Figure 5.20 Delay time for random and aligned CNTs with 40 min growth time

Table 5.3 Random and aligned samples

Growth time (min)	Rand(40)	Align(40)
Turn-on field(V/μm)	0.78	0.98
Turn-on field(V/μm) in 20 mTorr	2.5	3.8
Area(cm^2)	1.17	1.26

Chapter 6

Summary and Conclusions

Triggering system is one of the important parts of a pseudospark switch. At least 10^9 seed electrons are needed to initiate a breakdown for switch closing with low jitter. Several mechanisms can provide these seed electrons, such as thermionic emission, field emission, or photoemission. In this research, the electron field emission is selected as the trigger method. The efficiency of the electron field emission determines how well the plasma switch operates.

This project presents the design and construction of a CNT triggered pseudospark switch that is easy-to-construct, compact, and has the ability of over 10 kV hold off voltage and nanosecond jitter time. The switch is triggered by electron field emission mechanism in which the CNTs coated cold cathode is used as the trigger electrode.

The designed pseudospark switch is constructed with a hollow cathode, a planar anode, a trigger electrode, and periphery circuits. A quartz tube, 8 cm long and 2 cm in diameter, is used as the switch enclosure (the vacuum chamber). The u shape electrode, located in the center of the chamber, is pre-machined and works as the hollow cathode. A cupper planar anode is placed 3 mm away from the cathode. Helium at 100 mTorr pressure is used as background gas in the chamber. CNTs are used as the cold cathode

electron emitter material. Electrons are emitted from the CNTs surface, get accelerated in the electric field and initiate the breakdown.

CNT synthesis mechanism and property optimization have been thoroughly studied. Random, aligned, patterned CNTs have been synthesized with high quality and the electrical properties have been tested in term of the field emission ability. CNT samples with turn-on fields as low as 0.5 V/μm are obtained for the 240 min growth.

The CNT synthesis study also reveals the relationship between turn-on field and the sample growth time. The turn-on field decreases exponentially with the sample growth time, and eventually stabilizes at certain points. Increasing the growth time further does not decrease the turn-one field substantially. When the growth time is short, the CNTs are short in length and loose in density, which means there are less electron emitting spots. As the growth time increases, CNTs become longer and denser, raising more electron emitting spots. As a result, the turn-one field decreased. However, the screen effect prevents a further decrease no matter how long and how dense the tubes are. Understanding of this relationship benefits the optimization of synthesis process of CNTs and improves the cold-cathode emitter performance.

The lifetime of the trigger sample is also tested by repeating 100 consecutive field emission tests. Test results show a relatively good life time of CNT samples after several conditioning runs without obvious degradation is. The sample life time and the stability are very important as in many applications.

The designed pseudospark switch, triggered with CNTs, is tested in different conditions and results are presented. The switch operates at 100 mTorr pressure with a

hold off voltage of 12 kV. The applied trigger voltage varies from 200 V to 800 V. The current rise time is about hundreds of nanosecond.

The delay time for a set of trigger voltages, namely 400 V, 600 V, 700 V, 800 V, ranges from 2.97 to 8.32 μs. A decreasing trend of the delay time with trigger voltage is observed. When the trigger voltage increases, the electric field on the CNT samples increases. As a result, more electron emission takes place from the sample surface. Moreover, the emitted electrons get further accelerated in the higher electric field and plasma can be initiated easier. Therefore, higher trigger voltage has a shorter delay time. The jitter time is expressed as the standard deviation of delay time for the successive switch closing. Hundred of nanosecond jitter time has been obtained.

The triggering tests based on different types of CNT samples confirm that the delay time depends on the performance of the trigger material, represented as the electron field emission ability. The random 20 min sample with a largest turn-on field of 0.89 V/μm, has the longest delay time, while the random 120 min sample with a lowest turn-on field of 0.56 V/μm, has the shortest delay time, for all trigger voltages. The data is consistent with respect to the electron field emission characteristics of each sample.

The switch is triggered when a trigger voltage as low as 400 V applied to the CNT cold cathode emitter. This result is one of the differentiating characteristic of our switch to the ones in the literature. That means it provides several advantages in the switch design and fabrication. Low trigger voltage can be sassily supplied with less isolation requirements, leading to a possibility of switch size reduction and simpler peripheral circuitry. By use of lower than 1 kV trigger voltage, one can avoid unwanted discharge in the switch chamber and subsequent reduction in wear and increase switch stability.

In this project, the pseudospark switch has been successfully triggered with carbon nanotubes. This is the first reported results in the literature. But, several issues still need to be investigated, for example, electron emission mechanism, the transient plasma property, and the variation of the switch performance in different background conditions and the electrode materials. Further studies, including the switch optimization, trigger under different conditions, such as pressure, trigger pulse shape, and CNTs with different characteristics, need to be investigated to better understand the exact behavior of CNT triggered pseudospark switches.

References

[1] K. Frank, "The Fundamentals of the Pseudospark and Its Applications", *IEEE Transactions on Plasma Science*, vol. 17, pp. 748-753, 1989.

[2] M. Gundersen, G. Schaefer, "Physics and applications of Pseudosparks", *NATO ASI Series B. Physics*, vol. 219, 1990.

[3] M. Legentil, C. Postel, "Corona-Plasm Triggered Pseudospark Discharges", *IEEE Transactions on Plasma Science*, vol. 23, No.3, 1995.

[4] R. Tkotz, "Triggering of Radial Multichannel Pseudospark Switches by a Pulsed Hollow Cathode Discharge", *IEEE Transactions on Plasma Science*, vol. 24, pp. 53-54, No.3, 1996.

[5] H. Bluhm, "Pulse Power Systems Principles and Applications", *Springer;* 1 edition, June 15, 2006.

[6] E. Schamiloglu, R.J.Barkwer, M.Gundersen, and A.A.Neuber, "Modern Pulsed Power: Charlie Martin and Beyond", *Proceeding of the IEEE*, vol. 92, pp.1014-1020, 2004.

[7] J.Christiansen and C. Schultheib, "Production of High Current particle Beams by Low Pressure Spark Discharge", *Z. Phys*. A 290, pp 35-41, 1979.

[8] G. Schaefer and K. H. Schoenbach, "Basic Mechanisms Contributing to the Hollow Cathode Effect", *Physics and Applications of Pseudosparks*, vol.219, M. A. Gundersen and G. Schaefer, Eds. New York: Plenum Press, 1990.

[9] A.D. White, "New Hollow Cathode Glow Discharge", *Journal of Applied Physics*, vol. 30, No. 5, 1959.

[10] K. Frank, E. Boggasch, J. Christiansen, A. Goerter, W. Hartmann, C. Kozlik, G. Kirkman, C. Braun, V. Dominie, M. A. gundersen, H. Riege, and G. Mechterscheimer, "High-power pseudospark and BLT switches", *Plasma Science, IEEE Transactions on*, vol. 16, pp. 317-323, 1988.

[11] R. Tkotz, A. Gortler, J Cristiansen, S. Dollinger, K Frank, "Pseudospark Switches-Technological Aspects and Applications", *IEEE Transactions on Plasma Science*, vol. 23, No. 3, June 1995.

[12] E. Schamiloglu and R.J. Barker, "Special Issue on Pulsed Power: Technology and Applications". *Proc.* IEEE, 92(7), 2004.

[13] G. Stockhausen and M. Kock, "Proof and analysis of the pendulum motion of beam electrons in a hollow cathode discharge", *Journal of Physics D: Applied Physics*, vol. 34 pp. 1683-1689, 2001.

[14] A. Gortler, J. Christiansen, R. Dotzer, and K. Frank, "Investigations of pulsed surface flashovers for the triggering of pseudospark high-power switches", *Plasma Science, IEEE Transactions on*, vol.17, pp. 762-765, 1989.

[15] V.D. Bockov, V.M.Dyagilev, V.G.Ushich, O.B.Frants, Y.D. Korolev, I.A. Sheirlyakin, and K. Frank, "Sealed-off pseudospark switches for pulsed power appliacations (current status and prospects)", *Plasma Science, IEEE Transactions on*, vol. 29, pp. 802-808, 2001.

[16] M. Legentil and C. Postel, "Corona-Plasm a Triggered Pseudospark Discharges", *IEEE Trans on Plasma Science*, vol. 23, No. 3, 1995.

[17] G. Mechtersheimer, "High repetition rate, fast current rise, pseudo-spark switch", *J. Phys. E: Sci*, vol. 19, No. 6, 1986.

[18] C. Jiang, A. Kuthi, and M.A.Gundersen, "Toward ultracompact pseudospark switches", *Applied physics letters*, vol. 86, 2005.

[19] C Jiang, "Photocathodes for Compact Optical Triggering of Back-Lighted Thyratrons", *IEEE IPMHVC conference, Proceedings of 2008*, pp. 477-479, 2008.

[20] M. Chung, "Novel Trigger Mechanism High-Power Switch: The Electrostatic Plasma Injection Switch", *IEEE Transaction on Plasma Science*, vol. 34, No. 5, 2006.

[21] Y.K. Kwon., "Characterization of a Pulse-Charge-Mode Multigap Pseudospark Device as an Enhanced Electron Beam Source", *The Japan Society of Applied Physics*, 2003.

[22] T.J. Sommerer. "Cathode heating mechanisms in pseudospark plasma switches", *Journal of Applied Physics*, Issue 8, 1992.

[23] A. Kuthi., "Advanced Multi-gap Pseudospark Switch", *14th IEEE International Pulsed Power Conference*, Dallas TX, 2003.

[24] K. Frank, I. Petzenhauser, U.Blell, "Critical assessment of multistage pseudospark switches", *Proceedings of the 26th International Power Modulator Conference*, pp. 584-587, 2004.

[25] J. Urban and K. Frank, "Time Resolved Spectroscopic Characterization of the Plasma of a Pseudospark Dischage", *IEEE Transactions on Plasma Science*, vol. 32, 2004.

[26] A. Naweed, "Lifetime and switching characteristics of a high-current multichannel pseudospark", *Journal of Applied Physics*, vol 86, 1999.

[27] G. Mechtersheimer and R. Kohler, "Multichannel pseudo-spark switch (MUPS)", *J. Phys. E: Sci.*, vol. 20, pp. 270-273, 1987.

[28] W. Neff and J. Kiefer, "Requirements for simultaneous ignition of all channels in a high current radial multichannel pseudospark switch", *IEEE Trans. Plasma Sci.*, pp 347-352.

[29] T. Mehr, "Trigger Devices for Pseudospark Switches", *IEEE transactions on Plasma Science*, vol. 23, 1995.

[30] J.Y. Shim, E.J. Chi, H.K Baid,"Field emission characteristics of amorphous carbon and diamond emitters", *Vacuum microelectronics conference*, 1996. IVMC'96, 9th international' 10.1109/ivmc.1996.601827

[31] W.Y Huang., "Field emission characteristics of polymethyl methacrylate polymer thin film", *Vacuum nanoelectronics conference*, 2006 and the 2006 50th international field emission symposium., IVNC/IFES 2006 10.1109/IVMC.1996.601827

[32] A.N. Ionov, E.O. Popov, A.A.Pashkevich, "Field emission from metal covered by film of polymer insulator", *vacuum electron sources conference*, 2004, proceedings. IVESC2004. The 5th International; 10.1109/IVESC.2004.1414142

[33] J. Deng, B. Zhang, "Field Emission from Metal-coated Nano-Crystalline Graphitic Films", *Vacuum Nanoelectronics Conference*, 2006 and the 2006 50th International Field Emission Symposium,. IVNCIFES 2006 10.1109/IVNC.2006.335469

[34] R.D. Underwood and D. Kapolnek, "Field Emission From Selectively Regrown GAN pyramids", *Device Research Conference*, 1996.Digest. 54th Annual, 10.1109/DRC.1996.546417

[35] S. Li, "Cold Cathode Materials for Pseudospark Switches", *Master thesis*, Auburn University, 2008

[36] S. Iijima, "Single-shell carbon nanotubes of 1-nm diameter", *Nature*, vol. 354, 56, 1991.

[37] S. J. Tans, A. R. M. Verschueren, and C.Dekker, "Room-temperature transistor based on a single carbon nanotube", *Nature (London),* vol.393, 49, 1998.

[38] A. Javey, J. Guo, Q. Wang, M. Lundstrom, H.J. Dai, "Ballistic carbon nanotube field-effect transistors", *Nature*, vol. 424, pp. 654-657, 2003.

[39] C. Lu, Q. Fu, S. Huang, and J. Liu, "Polymer Electrolyte-Gated Carbon Nanotube Field-Effect Transistor", *Nano Lett*, vol 4, pp.623-627, 2004.

[40] S.J. Tan, M.H. Devoret, H.J. Dai, A.Thess,R.E.Smalley, L.J.Geerligs, and C.Dekker, "Individual single-wall carbon nanotubes as quantum wires", *Nature(London)*, vol. 386, pp. 474-477, 1997.

[41] M. Bockrath, D.H.Cobden, and P.L.McEuen, Science 290,1552,2000.

[42] H.J. Dai, J.H. Hafner, A.G. Rinzler, D.T. Colbert, and R.E. Smalley, "Nanotubes As Nanoprobes in Scanning Probe Microscopy", *Nature (London),* vol. 384, pp.147-150, 1996.

[43] W.A. deHeer, A. Chatelain, and D. Ugarte, "A carbon nanotube field-emission electron source", *Science*, vol. 270, pp.1179-1180, 1995.

[44] J. Kong, N.R. Franklin, C. Zhou, M.G. Chapline, S. Peng, K. Cho, and H. Dai, "Nanotube Molecular Wires as Chemical Sensors", *Science* vol. 287, pp.622-625, 2000.

[45] M. Endo, T. Hayashi, And Y. A. Kim, "Large-scale production of carbon nanotubes and their applications", *pure Appl. Chem,.* vol.78, No.9, pp.1703-1713, 2006.

[46] T.W. Ebbesen, Editor, "Carbon nanotubes: preparation an dproperties", *CRC Press*, 1997.

[47] M. Meyyappan, Editor, "Carbon nanotubes science and applications", *CRC press* (2004)

[48] R.C. Batra, A. Sears, "Continuum models of multi-walled carbon nanotubes", *International Journal of Solids and structures*, vol. 44, pp. 7577-7596, 2007.

[49] W. Wang, J.Y. Huang, D.Z.Wang, Z.F.Ren, "Low-temperature hydrothermal synthesis of multiwall carbon nanotubes", *Carbon,* vol. 43, Issue: 6, pp. 1328-1331, 2005.

[50] N.J. Coville S.D. Mhlanga, E.N. Nxumalo, "A review of shaped carbon nanomaterials", *South African Journal of Science*, vol. 107, No. ¾, 2011.

[51] Z.J. Chang, X. Zhao, Q.H. Zhang, D.J. Chen, "Nanofibre-assisted alignment of carbon nanotubes in macroscopic polymer matrix via a scaffold-based method", *EXPRESS Polymer letters,* vol. 4, No. 1, pp 47-53, 2010.

[52] T.W. Ebbesen, H. Lezec, H. Hiura, J.W. Bennett, H.F. Ghaemi, and T. Thio, "Electrical conductivity of individual carbon nanotubes", *Nature,* vol. 382, pp. 54-56, 1996.

[53] F. Kreupll, "Carbon Nanotubes in Interconnect Applications", *Microelectronic Engineering,* vol. 64, pp. 399-408, 2002.

[54] B. Q. Wei, et al., "Reliability and Current Carrying Capacity of Carbon Nanotubes," *Appl. Phys. Lett.,* Vol. 79, No. 8, pp. 1172-1174, 2001.

[55] A. Naeemi and J. D. Meindl, "Carbon nanotube interconnects". ISPD '07: *Proceedings of the 2007 international symposium on Physical design,* ACM Press, New York, NY, USA. pp. 77-84., ISBN 978-1-59593-613-4.

[56] S. Wind, J. Appenzeller, and P. Avouris, "Lateral scaling in CN field effect transistors", *Phys. Rev. Lett.*, vol. 91, pp. 058 301-1-058 301-4, 2003.

[57] S. Niyogi, M. A. Hamon, H. Hu, B. Zhao, P. Bhowmik, R. Sen, M. E. Itkis, and R. C. Haddon, "Chemistry of Single-Walled Carbon Nanotubes", *Acc. Chem. Res.,* vol. 35, pp 1105–1113, 2002.

[58] H. Dai, "Carbon Nanotubes: Synthesis, Integration, and Properties", *Acc.Chem. Res.*, vol. 35, pp. 1035-1044, 2002.

[59] H. TA, and J. Hill, "Modeling the Loading and Unloading of Drugs into Nanotubes", *Small*, vol. 5, pp. 300-08, 2009.

[60] N. W. S. Kam, M. O'Connell, J. A. Wisdom, H. Dai, "Carbon nanotubes as multifunctional biological transporters and near-infrared agents for selective cancer cell destruction", *PNAS*, vol.102, pp.11600, 2005.

[61] H. Muguruma, Y. Matsui, Y. Shibayama, "Carbon Nanotube-Plasma Polymer-Based Amperometric Biosensors: Enzyme-Friendly Platform for Ultrasensitive Glucose Detection", Jpn. J. Appl. Phys. Vol, 46, pp. 6078, 2007.

[62] J. Clendenin, J. Kim, S. Tung, "An Aligned Carbon Nanotube Biosensor for DNA Detection", *Proc of 2007 2nd IEEE conference on Nanotechnology,* pp.1028, 2007.

[63] A.J. Cheng, "Cold Cathodes for Applications in Poor Vacuum and Low Pressure Gas Environments: Carbon nanotbues versuszinc oxide nanoneedles", *Master Thesis*, Auburn University, 2006.

[64] A. Thess, R. Lee, P. Nikolaev, H.Dai, P.petit, J. Robert, C. Xu, Y.H. Lee, S.G. Kim, A.G. Rinzler, D.T.Colbert, G.E.Seuseria, D.Tomanek, J.E.Fischer, and R.E. Smalley, "Crystalline Ropes of Metallic Carbon Nanotubes", *Science*, vol. 273, pp. 483, 1996.

[65] L. Christiansen, and C. Schultcheiss, "Production of high current particle beams by low pressure spark discharges", *Z. Phys.A,* vol. 290, pp. 35, 1979.

[66] R.T. K.Baker, and P.S. Harris, *Chemistry and physics of carbon*, Chap 2, pp 83-165 New York , 1978.

[67] R.T.K. Baker, and P.S. Harris, R.B. Thomas, and R.J. Waite, J. Catal., "Formation of filamentous carbon from iron, cobalt and chromium catalyzed decomposition of acetylene", *Journal of Catalysis*, vol. 30, pp. 86-95, 1973.

[68] O.A. Louchev, Phys, "Formation Mechanism of Pentagonal Defects and Bamboo-Like Structures in Carbon Nanotube Growth Mediated by Surface Diffusion", *Physica status solidi (a),* vol. 193, pp. 585-596, 2002.

[69] R. Saito, G. Dresselhaus, and M.S. Dresselhaus, editors, "Physical Properties of Carbon Nanotubes", *Imperial College Press,* 1998.

[70] T. W. Ebbesen, P. M. Ajayan, "Scale synthesis of carbon nanotubes", *Nature,* vol. 358, pp. 220-222, 1992.

[71] D. T. Colbert, J. Zhang, S. M. Mcclure., "Growth and sintering of fullerene nantobues", *Science,* vol. 266, pp. 1218, 1994.

[72] X. Zhao, M. Ohkohchi, M. Wang, S. Ilijima., "Preparation of high-grade carbon nanotubes by hydrogen arc discharge", *Carbon*, vol. 35, pp. 775, 1997.

[73] D.E. Powers, S. G. Hansen, M.E. Geusic, A.C. Puiu, J.B. Hopkins, T.G. Dietz., Langridgesmith P R R. Smallley R E, *J Chem Phys,* vol. 86, pp. 2556, 1982.

[74] E. R. Bernstein, "Atomic and molecular clusters", *Elsevier Science B V.,* New York, 1990.

[75] M. Daenen, R. D. deFouw, B.Hamers, P.G.A. Janssen, K.Schouteden, M.A.J. Veld, "The Wondrous World of Carbon Nanotubes", *Project,* 2003.

[76] N. Arjmandi, P. Sasanpour and B. Rashidian, "CVD synthesis of Small-Diameter Single-Walled Carbon Nanotubes on Silicon", *Transactions D: computer science and engineering and electrical engineering, scientia iranica*, vol. 16, No.1, pp 61-64.

[77] J.H. Hafner, C.L. Cheung, C.M. Lieber, "Direct Growth of Single-Walled Carbon Nanotube Scanning Probe Microscopy Tips", *J. Am. Chem. Soc*, vol. 121, pp. 9750-9751, 1999.

[78] H. Hu, P. Bhowmik, B. Zhao, M.A.Hamon, M.E.Itkis, R.C.Haddon, "Determination of the acidic sites of purified single-walled carbon nanotubes by acid–base titration", *Chem Phys Lett*, vol. 345, pp. 25-28, 2001.

[79] T. Belin, F. Epron, "Characterization methods of Carbon nanotubes", Materials Science and Engineering: B, vol,119, issue2, pp.105-118, May, 2005.

[80] J. Guo, C. Yang, Z.M. Li, M. Bai, H.J. Liu, G.D. Li, E.G. Wang., "Efficient Visible Photoluminescence from Carbon Nanotubes in Zeolite Templates", *Phys Rev Lett*, vol 93, pp. 17402, 2004.

[81] M. Pereira, J. Figueiredo, J. Orfao, P. Serp, P. Kalck, Y.Kihn, "Catalytic activity of carbon nanotubes in the oxidative dehydrogenation of ethylbenzene", *Carbon*, vol. 42, pp. 2807, 2004.

[82] S. Arepalli, P. Nikolaev, O. Gorelik, V. Hadjiev, W. Holmes, B. Files, L. Yowell, "Protocol for the characterization of single-wall carbon nanotube material quality", *Carbon*, vol. 42, Issues 8-9, pp. 1783, 2004.

[83] A. Jorio, M. Pimenta, A. Souza-Filho, R. Saito, G. Dresselhaus, M. Dresselhaus, "Characterizing carbon nanotube samples with resonance raman scattering", *New. J. Phys*, vol. 5, pp. 139, 2003.

[84] A. Merkoci, "Review Carbon nanotubes in Analytical Sciences", *Microchim Acta*, vol. 152, pp. 157-174, 2006.

[85] Y. Tzeng, C. Liu, C. Cutshaw and Z. Chen, "Low-Temperature CVD Carbon Coatings on Glass Plates for Flat Panel Display Applications", *Mat Res. Soc. Proc*, vol. 621, 2000.

[86] R. Bokka, H. Kirkici; "Degradation of Field Emission Characteristics of CNTs" *proceedings of 2010 IEEE International Power Modulators and High Voltage Conference,* 2010.

[87] H. Zhao, H. Kirkici, "Effects of Impurity Ratios on Field Emission of Carbon Nano-tubes". *proceedings of 2010 IEEE International Power Modulators and High Voltage Conference*, 2010.

[88] S. Li, H. Kirkici, "Field emission characteristics of carbon nano tubes under varying background pressure conditions", *IEEE Pulsed Power Conference*, pp. 693-696. 2009

[89] H. Yuan, “Computer simulation of the field emission properties of multiwalled carbon nanotubes for flat panel displays” , *Journal of vacuum science & technology. B, Microelectronics processing and phenomena*, volume 21, issue 4, page 1648.